The University of Sheffield

Remotely Actuated Magnetic Motors for Unrestrained Machines in the Body

---

Cameron Duffield

A thesis submitted for the degree of Doctor of Philosophy

7th January 2024

Version: Final

Remotely Actuated Magnetic Motors for Unrestrained Machines in the Body

BY

Cameron Duffield

A thesis submitted to

The University of Sheffield

Department of Automatic Control and Systems Engineering

in partial fulfilment of the requirements for the degree of

Doctor of Philosophy

7th January 2024

Cameron Duffield

Remotely Actuated Magnetic Motors for
Unrestrained Machines in the Body

PhD Thesis, 7th January 2024

Supervisors: Dr Shuhei Miyasita
Dr Roderich Gross

The University of Sheffield
Department of Automatic Control and Systems Engineering
Amy Johnson Building
Portobello Street
Sheffield, S1 3JD

Acknowledgements

I'd first like to thank my supervisor, Dr Shuhei Miyashita, for his consistent support and feedback throughout the project. He has given me an insight into the world of academia, for which I will be forever grateful. I would also like to thank my second supervisor, Dr Roderich Groß, for being available to support me when needed.

I would like to thank all my colleagues within the Sheffield Micro and Biomedical Robotics Laboratories. I would in particular like to thank Quentin Lahondes, Marco Pontin, Joanna Jones, and Abigail Smith who were there throughout. I would like to thank the ACSE technical staff, including Richard Wilkinson for keeping us safe especially through the COVID-19 pandemic, and the ACSE PGR support staff including Keira Sweet and Professor Ivan Minev.

I'd like to thank my parents for their unwavering support and for their emphasis on education when I was growing up. I'd like to thank my friends Joanna Jones and Daniel Barry for keeping me sane. Thank you to Trefor Jones for helping with proofreading this thesis.

Lastly this would not have been possible without funding from The Engineering and Physical Sciences Research Council and The University of Sheffield.

Declaration

I, Cameron Duffield, declare that the work presented in this thesis is my own. All material in this thesis which is not of my own work, has been properly accredited and referenced.

Sheffield, 7th January 2024

Cameron Duffield

Abstract

Small scale robotics is hampered by the need to power electronic actuators and sensors, with batteries often forming a significant proportion of the mass and volume of the robot. One approach to overcome this is to use magnetic fields to actuate magnetic robots.

Typically, to achieve a rotating motion within a magnetic robot, a magnetic field needs to be rotated, rotating a permanent magnet. This applies a net torque to the entire robot, causing it to roll, even if the magnet is connected to a moving part connected to the main body. This is because some torque is transferred to the body through friction, and in the absence of any resistive forces the torque causes the body to rotate. If a mechanism is to be driven independently from a stationary main body, the body needs to be securely anchored to prevent it also rotating with the mechanism.

In this thesis, magnetically actuated motors are developed using two main principles. The first approach uses a magnetic field gradient to apply a force to a magnet, which is then converted to a rotational motion using a crank. This is oscillated by an alternating magnetic field; this alternating motion is converted to a continuous rotation by a double ratchet mechanism. The second uses the torque applied to a magnet by a magnetic field to create a rotational motion; by having a pair of magnets at 45° to each other and using the interaction between them, an alternation magnetic field can be converted to a continuous rotation. A system is developed to independently control a robot's pose using a ferromagnetic sheet; allowing a mechanism within the robot to be driven without affecting the pose by counteracting the torque applied to the motor by the magnetic field.

This new approach allows mechanisms within a robot to be driven by a magnetic field, while still allowing the robot body to be unconstrained within its environment. This opens up the possibility of devices, such as capsule robots, which need to be able to move within their environment, while also performing

tasks requiring moving mechanisms.

Nomenclature

α	Angle between magnet and magnetic field
β	Angle from the axis of the magnet dipole
$\ddot{\theta}$	Angular acceleration
$\dot{\theta}$	Angular velocity
ϵ	Crank arm angle
η	Efficiency
γ	Angle a crank passes through each stroke
μ_0	Vacuum permeability
∇B	Magnetic field gradient
ω	Angular velocity
ρ	Density
τ	Torque
τ_{ext}	External torque
τ_{int}	Internal torque
τ_{mot}	Output motor torque
τ_{soft}	Torque acting on a soft magnet
θ	Angle of the motor

$\vec{\tau}$ Torque vector

$\vec{B}$ Magnetic flux density vector

$\vec{F_m}$ Force acting on a magnet

$\vec{m}$ Magnetic moment

$\vec{P}$ Position vector

$\vec{p}$ Position vector

$\vec{r}$ Position vector

B Magnetic flux density

B_r Residual flux density

B_x Magnetic field perpendicular to the dipole creating it

B_z Magnetic field parallel to the dipole creating it

c Constant of integration, initial angle of a crank

d Diameter

F Implant force

f Frequency

f_a Actuation frequency

f_{so} Step-out frequency

Fr Friction

h Height between the crank axis and the crank arm guide

I Moment of inertia

k Empirical constant for soft magnetism

L Load

l Magnet edge length

m Magnetic moment

m_z Vertical component of magnetic moment

N Normal force

n Gear ratio

P Pitch

p Distance from centre of magnet dipole

R Radius

r Distance between magnet centres

T Time

V Volume

v Velocity

W Width

x Cartesian co-ordinate axis

y Cartesian co-ordinate axis

z Cartesian co-ordinate axis

Contents

Chapter 1

Introduction and Motivation

Micro-robotics is an active area of research with robots being developed for a variety of applications. One use of micro-robots is for in-vivo medical applications, where they have great potential to reduce the invasiveness of surgeries. There is significant work developing capsule endoscopes (covered in Section 2.1.1). These reduce the need to anaesthetise the patient, as is the case for conventional endoscopy, reducing the risk of complications. Capsule endoscopes can travel passively, moving through the digestive tract by peristalsis, this approach is limited by the inability to actively control the position and orientation of the capsule. Where the capsule is magnetically controlled this adds the ability to control the position and orientation of the capsule to allow a particular area of interest to be more closely inspected. Further developments being investigated are the addition of further capabilities to these controlled capsules to allow for targeted drug delivery, biopsies to be taken, and foreign objects to be removed from the gastro-intestinal tract.

Micro-robotics also has applications outside of medicine. Micro-robots can be used for inspection within small pipe networks, in a similar way to how capsule endoscopy can be used for inspection of the human digestive tract. The ability to inspect pipes using micro-robots has the potential to reduce the need for excavation work and disruption. Micro-robotics also have applications in micro manufacturing. Micro-actuators are needed where space is at a premium, such as within smart phones. Precise manipulation is required for the assembly of micro-electronics, this can be achieved using high precision manipulators in pick and place machines. Self-assembly presents an alternative method for assembling micro-scale components, reducing the need for precision manipulators.

For the further development of micro-robots it is desirable for suitable motors to be developed so that torques and rotational motion can be produced within the robot. Rotational motion can easily be converted to either continuous or reciprocating linear motion, making it useful for a wide variety of mechanisms. These motions can be used in robots for tasks including locomotion, manipulation of objects, or reconfiguring the robot layout to make it more suited for different tasks.

Micro-robots can either be wirelessly controlled, or tethered, with wireless robots having a number of advantages. Tethered robots need to have an uninterpreted route back to the controller for the wire to pass along, making

them unsuitable for use in enclosed spaces. The wires in the tether are also vulnerable to damage, making the robot less robust. To make a robot wireless it needs to either store the energy onboard, for example by using batteries, or have a means of wireless power transfer from an external source. Stored energy is finite, limiting the operating time of the robot. In order to have an acceptable operating life batteries end up being both heavy and bulky, this is especially pronounced in small scale-robotics where the energy source can end up making up the majority of the robot. These factors combine to make wireless power transfer highly desirable for micro- and milli-robots.

One option to wirelessly transmit power to a robot is through the use of magnetic fields to apply a force or torque to magnetic material within the body of the robot. Magnetic fields are able to safely pass through most materials, including human tissue, making them suitable for use in a medical setting. The manipulation of magnetic micro-robots using a coil system, an arrangement of one or more electromagnetic coils controlled by a computer or microcontroller, is established and it is possible to accurately control the magnetic field and field gradient across a workspace, many of these existing systems in research laboratories could easily be adapted to drive a magnetic motor. It is possible to make all of the components of a magnetically actuated robot biocompatible, this is made easier because there is no need to have any electronics onboard the robot. Magnetic actuation is easily scalable, so designs can be easily reduced in size from use in milli-robots to micro-robots. The parts needed for magnetic actuation are both lightweight and low cost.

Existing magnetic control techniques rely on accurately controlling the orientation of a magnetic field to apply a torque to a robot body, or the magnetic field gradient to apply a force to it for translation. This means an overall force or torque is applied to the robot, making it move as a single rigid or deformable body. This gives five degrees of freedom, x, y, z, pitch, and yaw, and it is not possible to actuate mechanisms within the robot without the whole body experiencing a net force or torque acting on it from the magnetic field. Adding in magnetically actuated motors allows for the main body of the robot to be stationary while a mechanism within it is driven, adding in an extra degree of freedom to the system. Magnetic motors also allow for multiple motors to be actuated within the same workspace while rotating about different axes on the same plane; existing approaches would require all robots in the workspace to rotate together in the same direction. It is possible to

create a uniform magnetic field, with no gradient, or a magnetic field gradient with no magnetic field at the workspace. By having two designs of magnetic motor, one relying on magnetic force from the field gradient and the other relying on magnetic torque from the field, there can be addressable control of two sets of motors within a single workspace. This gives another degree of freedom, bringing the total up to seven.

1.1 Research Objectives

The project's overarching aim will be accomplished through the following list of objectives:

a) Develop magnetically actuated motors capable of being actuated by a simple input of an alternating magnetic field so that multiple motors can be operated simultaneously in the same workspace. The behaviour of these motors should be modelled and experimentally validated.

b) The motors should be suitable for use in medical devices such as implants and capsule robots. For this they need to be safe to operate in the human body by not incorporating toxic materials or requiring magnetic fields which could be harmful to the patient.

c) To be suitable for capsule robots, a method of orientating a magnetically actuated robot incorporating a motor is needed. This is necessary so that mechanisms within the device can be actuated, while the body of the device itself remains steady in the desired pose.

1.2 Research Contributions

The prime contributions gathered throughout the development of this project are summarised below:

a) The primary contribution of the project is the development of wireless magnetic motors capable of giving a continuous rotation and torque output, while being driven by an alternating magnetic field, while modelling their performance and experimentally verifying these

models.

b) A further contribution of this work is to demonstrate the capabilities of these motors in their target application of being used in medical robotics. The motors were demonstrated in a robotic implant for the treatment of long gap oesophageal atresia, and a capsule robot for the removal ingested button batteries.

c) An additional contribution is the proposal and implementation of magnetically orientating the robot while the motor is actuated by the same magnetic field. This allows a magnetic motor to be operated independently from the pose of the robot.

1.3 List of Publications

In this section the three publications relating to this thesis are outlined. The contributions of each of the authors on the publications is outlined.

Magnetic Force Driven Wireless Motor

Cameron Duffield and Shuhei Miyashita, 'Magnetic Force Driven Wireless Motor, In: Annual Conference Towards Autonomous Robotic Systems, published [2020], [Springer]' Reference [1].

This publication form the basis of Chapter 3.

The author contributions are:

- Cameron Duffield proposed the concept for the motor, designed and made the motor, conducted experiments, and carried out the mathematical modelling.
- All authors reviewed and edited the text.

Wirelessly Magnetically Actuated Motor for Tissue Regeneration Robotic Implant

Cameron Duffield, Abigail F Smith, Daniela Rus, Dana Damian and Shuhei Miyashita. 'Wirelessly Magnetically Actuated Motor for Tissue Regeneration Robotic Implant'. In: IEEE International Conference on Intelligent Robots and

Systems (IROS). IEEE. 2022, pp. 465–471 Reference [2].

This publication forms the basis of Chapter 4.

The author contributions are:

- Cameron Duffield designed the motor, carried out experiments, and performed the mathematical modelling
- Abigail F. Smith assisted with the experiments using biological tissue
- The implant was developed based on [3]
- All authors reviewed and edited the text

Remotely Actuated Magnetic Motor for Unconstrained Robotic Capsule

Cameron Duffield, Jialun Liu, Yuqi Zhang, George Ashton, Daniela Rus, Dana D. Damian, and Shuhei Miyasita 'Remotely Actuated Magnetic Motor for Unconstrained Robotic Capsule' Journal submission under review.

This publication forms the basis of Chapter 5.

The author contributions are:

- The working mechanism of the motion was developed by Shuhei Miyashita, Daniela Rus, and Etienne Perroux
- Cameron Duffield designed the implementation of the motor and the capsule, carried out the mathematical modelling, proposed and designed the pose control system, carried out all experiments except for those for the button battery detection and to measure the torque on the soft magnetic element, designed the experiments fro measuring the torque on the soft magnetic element
- The work on button battery detection in this section was carried out by Yuqi Zhang as part of his MRes project
- Jialun Liu developed the sensor array used for the button battery detection and assisted Yuqi Zhang with his work
- George Ashton carried out the experiments to determine the magnetic

moment of the soft magnetic element as part of his MEng project

- All authors reviewed and edited the text

1.4 Thesis Outline

This thesis is presented as:

- Chapter 1: Introduction
- Chapter 2: Background and related works
  - An overview of the existing work relating to this thesis and providing context for the work done
- Chapter 3: Magnetic force driven wireless motor
  - A new concept for a magnetically actuated motor driven by an alternating magnetic field gradient
  - The output torque of the motor through its cycle was modelled, and the effect of scaling the design investigated
  - The motor was prototyped and the model for torque was experimentally validated by measuring the output torque of the motor
- Chapter 4: Wirelessly magnetically actuated motor for tissue regeneration robotic implant
  - The motor concept from Chapter 3 is further developed to simplify the design, reduce the size, and increase the torque output
  - The maximum speed of the motor is modelled
  - The speed and output torque of the motor are experimentally investigated, validating the models
  - The motor is presented in an implantable robot for tissue regeneration therapies for conditions such as long gap oesophageal atresia, or short bowel syndrome

- Chapter 5: Remotely Actuated Magnetic Motor for Unconstrained Robotic Capsule
  - A second novel concept and design of a magnetic motor, utilising magnetic torque instead of magnetic force, is demonstrated
  - The torque output of the motor were modelled an experimentally verified
  - A novel system for controlling the pose of a robot using the motor independently from the actuation of the motor is presented
  - The motor and pose control system are presented in a capsule robot for retrieving ingested button batteries from a patient's stomach
- Chapter 6: Discussion
  - The potential to have multiple motors actuated within the same workspace, and methods for individually controlling them are discussed
  - The relative merits of the three motors presented and two from the literature are compared
  - Potential applications of magnetic motors are discussed
- Chapter 7: Conclusion and future work
  - This chapter concludes the thesis and discusses its limitations
  - Potential directions for future work are outlined

Chapter 2

Background and Related Works

This chapter looks at the background of the project and the existing work related to it. It begins by looking at how small scale robots are used in the medical field, both in capsule endoscopes and other less established fields. It then looks at micro-robots more generally, looking at the actuation methods and methods of locomotion. The chapter finally looks at magnetic control approaches and the current state of the art for magnetic control. From this the gap in the literature is found to guide the work presented in this thesis.

2.1 Ingestible robots

An emerging field within robotics is ingestible medical devices. These have potential to be used for a variety of applications in the gastro-intestinal tract. Devices have been developed for visual inspection of the gastro-intestinal tract, in a similar manner to an endoscope, and there is potential for further development to allow for more advance procedures to be carried out with these devices.

2.1.1 Capsule Endoscopy

Flexible endoscopy is widely used, however, some patients have difficulty with it, and the required anaesthetic has side effects. Some areas, such as the small intestine are also difficult to reach. Capsule endoscopy was developed to overcome some of these difficulties, using peristalsis to travel through the digestive tract. There is, however, a lack of control-ability and the process is slow, so several attempts have been made to develop methods of controlling the motion of the capsule endoscope.

Lien et al. present a capsule endoscope with a permanent magnet in it, allowing the location and pose to be controlled. It is controlled using an external permanent magnet on a stepper motor. It has a variable speed rotation mode for rolling locomotion, and a 1.8° step mode to allow for fine control of the pose. Equations for the torque on the magnet are presented. Experiments were carried out to validate the equations [4].

Lee et al. propose using a helical motion up the inner wall of a tubular organ. Pushing the capsule against the inner wall of the organ can aid with accurate diagnosis. The system was tested with a water filled stomach mock-up. The frequency response was analysed, and the stable range of rotation and

precision was determined. The system used to generate the required magnetic fields used both Helmholtz and Maxwell coils. Helmholtz coils consist of two parallel electromagnetic coils, where the distance between them is equal to the radius. When two equal currents are applied a uniform magnetic field is generated. For a Maxwell coil the distance between the coils is equal to $\sqrt{3}$ times the radius. When equal currents, with reversed directions, are applied a magnetic field gradient is produced. [5] One area not addressed by the paper was potential methods to make the system autonomous, through either sensors on the capsule or through the use of external localisation techniques.

Nokata et al. developed a magnetically driven capsule designed to operate in the abdominal cavity using a long narrow piece of ferromagnetic material within the capsule. This was actuated using solenoids external to the body, when tested in a rabbit's body. The capsule was successfully manoeuvred through the abdominal cavity, by a surgeon, to the rabbit's liver; this was verified using x-ray imagery [6].

Ye et al. made a similar capsule robot for biopsy [7] capable of navigating to the site to be sampled using permanent magnets within the capsule body and a coil system consisting of four pairs of electromagnetic coils. To deploy the biopsy needle a fifth coil acts on a piece of paramagnetic material to push the needle out of the capsule body; the needle is retracted back into the capsule using springs.

An alternative to using magnetic fields to directly move capsules is to use vibro-impact propulsion. This approach utilises a mass-spring-damper system resonating and impacting against the main body of the capsule to drive it forwards [8]. One challenge of this kind of motion is how it is able to pass obstacles it encounters, such as circular folds within the small intestine. The oscillating mass can be magnetic, allowing it to be excited by a sinusoidal external magnetic field to drive the capsule with sufficient force to overcome the obstacles [9]. A mathematical model was also developed to describe the resistance forces experienced by a capsule as it encounters a circular fold in the small intestine and the force produced by the vibro-impact drive to predict the motion of the capsule. The results of this model were compared to finite element analysis and experimental data to validate the approach [10].

2.1.2 Other medical applications

Ingestible robots have applications beyond simple visual inspection using capsule endoscopes. Work has been done to develop robots which can be ingested for a variety of applications such as targeted drug delivery, wound treatment, and biopsy.

Miyashita et al. developed a micro-robot which is capable of delivering drugs directly to a wound in the stomach, such as that caused by an ingested button-cell battery. The robot is folded and contained within a capsule of ice for easy swallowing, once the ice is melted it unfolds to its deployed form using a shape memory polymer system. It is then able to walk to the wound site using an asymmetric friction motion. This robot is also actuated by a neodymium magnet controlled by an external magnetic field and located using three hall effect sensors. A realistic model oesophagus and stomach, including roughness and selection of a material with properties similar to those found in the body, was constructed to test this robot [11].

Miyashita's group also developed an indigestible robot which has been designed to patch stomach ulcers. The robot has demonstrated it is capable of travelling to the site of an ulcer and patching it. After the robot is swallowed, it travels to the wound site by a rolling motion. It is controlled by an external magnetic field acting on a neodymium magnet in the robot. The patch is folded based on the principles of origami such that when activated its area is ten times that when folded. The patch is made from a shape memory hydrogel, and is deployed on contact with water drunk by the patient [12].

Chemical adhesion is widely used for medical applications, however, there is a trade off between the bio-compatibility and the adhesive properties. Iwasaki et.al. present a reversible adhesion using suction cups for use in the stomach. Suction cups work based on a pressure differential between the inside and the outside of the cup. A force is required to adhere and detach the cup, but once adhered no force is required, and the system is fully reusable. The suction cups were moulded from Ecoflex 30 with a neodymium magnet to allow them to be remotely operated using a magnetic field. The system was tested in dry and wet conditions, and under water and oil. The future work includes testing the system on rough surfaces and scaling down the design to be used for in-vivo applications [13].

Hoang et al. developed a capsule endoscope with a retractable biopsy punch. The punch is magnetically actuated to extend and retract, meaning it uses no energy from the capsule endoscope. A magnet spins the punch, causing it to move along a screw thread and protrude from the capsule to take a sample. It is then rotated in the reverse direction to retract back within the capsule. The system was tested in porcine intestine [14]. This work is interesting as well as using a magnetic field to manoeuvre and position the capsule endoscope the magnetic field to extend and retract a biopsy needle.

Steerable needles can be used to target specific areas of tissue, while avoiding sensitive areas. One challenge is how to achieve tight curvatures, Sperry et al. addressed this by adding a magnet into the needle tip to allow it to be steered using the magnetic field from a permanent magnet outside of the body. The needle is driven forwards by its screw head, rotated using a length of soft tubing connected to a stepper motor [15].

2.2 Milli-robots and mechanisms

Ingestible medical robots are on the millimetre to centimetre scale, which is on the larger end of the field of micro-robotics. To fully appreciate what could be possible for medical robotics it is necessary to consider the achievements in the wider micro- and milli-robotics field.

2.2.1 Milli-robots with Locomotion

The small size of micro- and milli-robots allows them to access areas which are difficult to reach with larger robots for purposes such as inspection; one example is the small pipe inspection robot developed by loi et al. Existing robots used piezo-electric actuation; this requires a high voltage amplifier and power cable, which both restrict motion. Two coreless motors spin eccentric masses to produce a centrifugal force. This is transmitted to the surface by elastic brush fibres. The motion is two part: the first part the brushes are not in contact with the surface, for the second they are in contact with the surface. The robot exhibited unusual turning characteristics. When the masses are at the front increasing the angular velocity of the right motor causes the robot to turn to the right. When the masses are at the back of the reverse is true, meaning increasing the angular velocity of the right motor makes the robot

turn to the left [16].

Legged locomotion has the advantage of increased stability, ability to traverse rough terrain with obstacles, and improved traction on steep inclines when compared to wheeled robots. Hoover et al. developed a robot with a body made from a smart composite microstructure: it has rigid composite links and flexible polymer hinges fabricated in one go using layering of composites and laser-cutting. The number of joints does not affect the manufacture cost. Multiple parts can be manufactured in parallel, limited only by the size of the laser cutter bed. At the small scale surface forces, such as friction, dominate inertial forces. Flexible joints are a way of avoiding friction, however, continuous rotation is not possible. Off axis loads must be minimised and the elastic limit of the material not exceeded. Actuators are expensive in weight and power, so are minimised in the design. Shape memory alloy (SMA) wire was used as it has a high power density and direct line of pull. Return springs were used in conjunction with the actuators. There are two degrees of freedom: rotation into and away from the body, and forward and backward leg rotation. The robot moves with a tripod gait which is programmed into the mechanism using four bar linkages [17].

Jafferis et al. developed an insect scale flapping robot for un-tethered flight. One difficulty associated with untethered flight on this scale (90 mg) is the energy source, with commercially available batteries having insufficient specific power. To overcome this the authors used a small solar array receiving light of an intensity of several suns from a combination of halogen and LED bulbs to power piezoelectric actuators [18]. James et al. used a similar approach for their laser powered flying robot. With a robot mass of 104mg the authors used a 976 nm laser on a photo-voltaic cell to power two piezoelectric actuators [19].

Wnag et al. developed a micro fish inspired by the fins of squid and cuttlefish, with an overall length of 150 mm. The fish had a tail with an SMA wire down each side to actuate it using an electrical current [20].

2.2.2 Micro and Precision Actuation

Micro manipulation, the manipulation of parts with micrometer precision, is used for both micro assembly, such as in pick and place machines, and for actuation of compact devices, such as as mobile phone lenses.

Disturbance signals become more significant on the micro scale. Piezoelectric actuators do not guarantee a precise step, so precision sensors are required; this increases the size of the actuator. A motor with micro gears can achieve the same resolution, but smaller. A micro harmonic drive (10 mm diameter or less) gives reductions between $160 : 1$ and $1000 : 1$ with only six moving components. They are backlash free and give the same position accuracy as large scale harmonic drives. Being backlash free means the motor encoder can be multiplied by the transmission ratio to give the end effector position. The miniaturised robot Parvus was analysed to find the greatest cause of position error. It was found that the absolute position error was 10 to 30 times higher than the repeatability error. It was hypothesised that this was due to the relatively low stiffness of the drives ($0.6 - 6.13$ Nm rad^{-1}). Friction in the bearings prevents gears from returning to their neutral position, this leads to elastic hysteresis. Kinematic and dynamic compensation strategies for transmission error were investigated and tested and were able to reduce the absolute position error by 50 % [21].

Smartphone cameras are required to fit within a compact space while retaining high levels of precision to achieve high image qualities. For optical zoom one of the lenses needs to be moved, Kim et al.propose a smart polymer actuator is used to drive an optical zoom lens. They used a diametric elastomer to move the lens, these require high voltages to actuate, however, have a faster response time and have well established repeatability compared with conducting polymers. The system was used to actuate a biomimetic silicone lens [22].

Micro-robots have the potential to be used collectively as modular reconfigurable robots. In [23] Campbell et al. demonstrate a method for combining the power of eight individual robots to form cells of greater collective strength. The authors simulate the strategy systems with many cells and propose a strategy for low complexity control by distributing the control between the elements. They demonstrate the system to a limited extent with a prototype using two cells.

2.2.3 Self-assembly

Self-assembly is a potential method for making micro-scale structures. Self-assembly removes the need for manipulators by using properties of the

components themselves for the assembly. It also opens up the possibility of having a large robot disassembled to allow it to pass through a small gap, before reassembling on the far side to make a larger and more complex robot than would have been possible to fit though the constriction.

In Nakagawa et al. Mn_3O_4 crystal nano-blocks were self-assembled using evaporation of a dispersion. They assemble at the air-liquid interface. They are brought together by capillary action and the evaporation of the liquid media. The direction of the crystals relative to the substrate is controlled by changing the polarity of the substrate. Changing the medium changes the evaporation rate [24].

Bowden et al. demonstrated the self-assembly of hexagonal elements at a perfluorodecalin (PFD)/ water interface using capillary forces. Each edge was selectively coated to give either a positive or negative meniscus. They found that like menisci attract, while opposites repelled. This phenomena was used to give different attraction and repulsion forces to form the desired pattern [25]. This work was further developed in [26] to self-assemble $10\,\mu m$ scale units to mimic the way molecules and crystals assemble.

Integrated circuits can consist of multiple wafers stacked to make a system in packing (SIP). The accurate positioning of these wafers is currently done with dies, which is a slow process. The new approach presented in [27] uses liquid surface tension to position the chip. The wafer is treated to give hydrophilic and hydrophobic areas, droplets of liquid are put on the hydrophilic areas. The chips are positioned above, then placed on the liquid droplets. As the liquid evaporates the chip is placed on the wafer. The chips are bonded after being deposited. Hydrogen fluoride dissolved in the liquid etches the oxide layer on the silicon wafer. The factors which affect misalignment are: chip size, liquid volume, initial miss-alignment, surface tension, and the contrast between the hydrophilic and hydrophobic areas. This still relies on an external manipulator, so is more of a hybrid approach, rather than true self-assembly.

Programmable matter is a structure which changes its physical properties in response to an external influence or autonomy. In [28] Yim et al. look at self-assembling soft modular matter. There is a structure which can be disassembled into a flexible string, then reassemble autonomously. There are a series of cubes connected by strings, each contains magnets so the structure

self-assembles into the programmed shape. Two different strategies are used to calculate the connection pattern: the inner connection method, and the boundary connection method. The individual layers are moulded, then glued together.

In biology 1D protein strings fold to form 3D structures. Cheung et al. investigated an approach to determine folding sequences for 1D strings to fold into 2D and 3D shapes. They proposed an algorithm for determining the folding sequence using strings composed of very simple robotic modules, and simulated it. The authors proposed that it could be used for self-assembling and self re-configurable system [29].

In [28] a string of soft cubes are self-assembled and can be disassembled into a continuous string using tension. Once in a string the soft nature of the cubes makes the string highly flexible. Once the tension is released elastic and magnetic forces reassemble the string to its previous shape.

2.3 Origami Robots

Origami is the art of folding paper to create a structure from a flat sheet. This approach can be used to create robots using folds in a flat sheet, folds in the final structure can then be actuated to provide the functionality required of the robot.

2.3.1 Origami for robot fabrication

Origami can be used as a method to fabricate a robot body from a flat sheet of material using a sequence of folds. This can simplify the manufacture, especially in the case of self-folding origami, by reducing the number of components and manufacturing steps.

Any pattern is theoretically possible using a pattern composition algorithms for foldable joints. Folding can be used to create a shape changing robot that optimises itself for a given task. Using flat sheets to make 3D structures by folding simplifies manufacture and can minimise manual assembly by the use of smart materials. Flexible electronics allow for circuitry on the robot body and the addition of components without wires. Layering of sheets can give a robot

both stiff and flexible parts. They can be made into pills before unfolding within the body to allow for incision free surgery. Traditional actuators do not suffice for smaller robots, due to the difficulties of making hinge parts at a small scale, and the added complexity of adding many degrees of freedom [30].

Miyashita et al. proposed a system of interchangeable origami exoskeletons for a permanent magnet robot to provide different functionality for individual tasks. The exoskeletons were manufactured using a three layer system; when heated the middle layer shrank, forming folds based on the width of cuts made in the outer two, non-shrinking, layers. The exoskeletons were designed to fold around the magnet, connecting with water soluble arms so the exoskeleton can be shed by submerging in water. Exoskeletons were made to facilitate, rolling, floating, pushing obstacles, and gliding [31] [32].

One difficulty encountered with self folding origami is the ability to sequence the order of the folds. Liu et al. developed a system of addressable folding where each hinge is a different colour, so absorbs a different wavelength of light. When exposed to the correct wavelength of light the coloured strip heats a polymer layer, causing it to shrink. The colours and corresponding lights used are: yellow, Blue LED; cyan, red LED; magenta, green LED. This can be used for sequential folding. By using two opposing folds of different colours the fold can be reversed once [33].

Tachi et al. covered the principle of making any shape by origami using standard "molecules". These consist of surface polygons, edge tucking molecules to bring the edges together, and vertex tucking molecules to bring the vertexes together. The unfolded sheet must be topologically equivalent to a disk. Each vertex has a segment on the inside, called a tuck box; an iterative approach is needed to ensure they do not interfere [34].

2.3.2 Folding as a form of actuation

Folding is also used as a form of actuation in some robots; to achieve this a number of challenges need to first be overcome. The folds need to be reversible to allow repeated motions to be carried out by an actuator, where multiple individually controlled actuators are required a method of addressing the individual folds is needed.

Boyvat et al. used wireless electromagnetic power transmission to heat spring shaped shape memory alloy (SMA) actuators. The resistor capacitor inductor (RCL) circuit in the receiver for each actuator is tuned to have a different resonant frequency by changing the capacitor. Different stimulation frequencies can be used to change to folding order, multiple frequencies can be used to achieve simultaneous folding. The system was demonstrated on a robotic arm and gripper [35]. This system has potential for addressable wireless actuation, however, the system is currently too large for micro-robotics. Using SMA actuators has the disadvantage that energy is needed to hold the actuator in a given position, regardless of the force.

To be effectively used as an actuation method the folding needs to be reversible. Several methods have been developed to address this challenge. Baker et al. used ionoprinting of hydrogels to create a reversible fold. A redox reaction is used, causing the hydrogel to change volume and fold. The iron ions are caught by the hydrogel and reacted with a weak reducing agent to release two protons [36].

Na et al. used a heat actuated system for reversible folding. The middle layer of a three layer system expands/ contracts depending on temperature. It takes ten minutes to fold, and two to unfold. Once folded it doesn't return to a completely flat shape [37].

Programmable matter refers to active materials with controllable stiffness and geometry. Hawkes et al. present a network of triangles which can be folded into a predetermined shape using embedded actuation using a universal crease pattern origami concept. The structure is made from a tiled sheet consisting of a thin foil actuator, semi-rigid tiles, and flexible electronics. The tiles were made from an epoxy fibre composite and laser micro-machined to make slot for magnets before curing and after curing to create the tiled structure. Elastomers are used for the flexural hinges with SMA foil actuators. To span the hinges the flexible electronics also need too stretch as well as bend; this was achieved using pattern tracing and cutting to produce a grid to it can stretch [38].

Origami can also be used to make conventional robots more compliant. Salamanderbot has two rigid sections with the drive joined by a deformable origami section to allow it to negotiate narrow passage ways and tight bends. It has low profile wheels with factor three rotational symmetry, making it

resistant to rolling. They tested both belt drive and geared drive, finding that geared drive is faster and can climb steeper inclines [39].

Origami has potential to simplify the manufacture of small scale robots through self-folding, where the number of folds does not add to the difficulty of manufacture. Having origami in the construction can also be used to add compliance to larger structures, the slight compliance is each hinge sums to give a compliant structure. Alternatively origami hinges can be actuated to replace the need for conventional hinges, allowing for more joints with out adding cost to the manufacture of the mechanism.

2.4 Magnetic Control

One method of wirelessly controlling micro-robots is with a magnetic field. Actuation using magnetic fields has the unique potential for actuating micro-robots in enclosed geometries, such as within the human body, due to their ability to pass harmlessly through many materials, including human tissue [40].

2.4.1 Magnetic Robots

There is usually an attractive force between any two permanent magnets with near magnetic fields as one magnet aligns with the field of the other and experiences a magnetic field gradient. By continuously rotating the controlling magnet to induce a lag angle between it and the controlled magnet Mahoney et al. induced a lateral force action on the controlled magnet. This was used to push it across a surface and levitate it. The controlling magnet was separated from the driven magnet by a surface [41].

Soft magnets are made from a ferromagnetic material, but have no permanent magnetisation. When subject to a magnetic field of sufficient strength they develop a magnetic dipole with the direction dependant on the field and the geometry of the soft magnetic body. Abbott et al. model the force and torque applied to a soft magnetic body by an arbitrary field, then experimentally validate the method. They include field strengths from weak to saturating [42].

The majority of coil systems are small devices intended for research, for use in

medical applications it would be necessary to scale them up to a size useful for acting on a person. A coil system of a clinical scale was developed by Rahmer at al. [43] using an array of 18 oil cooled copper coils. The authors used this system to demonstrate remote operation of magnetic drills through gel and tissue samples.

Zhang et al. utilised a bi-stable carbon fibre laminate to make a venus flytrap inspired gripper. Two compliant fingers were constructed from carbon fibre, each had a magnet positioned on the end. To actuate the gripper a force was applied to the magnets using an external magnetic field. The use of snap-through stability of compliant fingers allowed the gripper to close, however, the gripper had to be manually reset to the open position before it can be reused [44].

Magnetic actuation has applications in internal surface finishing for tubes and manifolds, which are difficult to reach using conventional polishing techniques. Zhang et al. used a spherical magnet with abrasives inside a manifold to polish the internal surface. The magnet is rotated using a bar magnet external to the tube. The bar magnet is rotated, while also moving axially along the tube as the tube is being rotated, to ensured all internal surfaces were evenly polished to achieve the desired surface finish. The authors reported an 86 % improvement in surface finish for the section polished [45].

Son et al. used an alternative method to coil-systems for controlling a tissue penetrating robot. A cylindrical array of permanent magnets was made such that there is a stable point for a magnet in the centre; by moving the magnet array the micro-robot is moved away from this centre point, the further from this point it is the greater the force pushing it back towards the centre point. By actuating the magnetic array the position of the magnetic micro-robot within the workspace can be controlled [46].

To have a magnet which can be switched on or off, an electromagnet is conventionally used. This has the disadvantage, compared with a permanent magnet, of requiring a continuous current supply while a magnetic field is required. Rochat et al. describe an alternative switchable permanent magnet. A cylindrical permanent magnet is positioned between two u-shaped iron parts. In one position the flux passes through the iron, such that externally it appears to have no magnetic field. When rotated 90° the flux is

able to leave the iron, so the system behaves as a permanent magnet. This has the advantage over an electromagnet that it requires no energy to remain in the same state, giving it potential applications in docking drones, and robots climbing magnetic surfaces [47].

Conventional magnetic control is limited to five degrees of freedom, because torques can't be applied around the axis of magnetisation. Work has been done by Diller et al. to add a sixth degree of freedom by using non-uniform magnetisation to act as a moment arm of the micro-robot [48].

One medical application for magnetism is using magnetic nanoparticles to tag and trace cells. Mechanical stimulation using magnetic nanoparticales can be used to facilitate cell proliferation and differentiation of stem cells. They consist of an iron oxide core with a biocompatiable polymer coating. This has uses in regenerative medicine to restore and regenerate the function of damaged cells [49].

Hong et al. [50] developed a millimetre scale gear box, actuated using a magnet. A permanent magnet was connected to the input shaft of the gearbox and actuated using a rotating permanent magnet. The gearbox is used to increase the output torque from the magnet, allowing it to be used to drive mechanisms which would otherwise be impossible. Elastic elements are used to store potential energy from the magnetic input and release it rapidly to allow for brief high power motions, such as jumping.

Magnetic actuation can be used to create a wide variety of motion in milli and micro-robots. Systems of electromagnetic coils can be used to create any orientation and strength of magnetic field; alternatively permanent magnets can be used to create the magnetic field, with its position and orientation controlled to create the desired magnetic field at the workspace. The forces and torques applied to the the robots by the magnetic field are applied to the entire body, making it difficult to actuate mechanisms within the robot without the entire body moving, unless it's anchored to the surroundings.

2.4.2 Soft Magnetic Robots

Hard micro-robots are generally a single rigid object, and are only capable of moving in a limited number of ways. Because of their rigid nature it is difficult for them to fit through small gaps with limited clearance, or they may cause

damage when interacting with soft objects, such as human tissue.

Existing small-scale robots are limited by their ability to negotiate obstacles and varied terrain. Soft robots have more degrees of freedom, giving them great potential for multimodal locomotion. Hu et al. present a millimetre scale soft magnetic robot that can swim in and on the surface of liquids, climb menisci, walk, roll, jump over obstacles, crawl in tunnels, and pick and place objects. The robot was made from Ecoflex 00-10 with NdFeB particles with an average diameter of $5\mu m$. This was rolled around a glass rod before being magnetised. It should be possible to make the robot bio-compatible, but the authors haven't tested it.

The robot can form multiple shapes including, flat, curves and "s" shaped. Sequences of these shapes can be combined to provide locomotion modes. A wave motion is used to swim on the surface of water, while jelly fish swimming (with a Reynolds number of Re=$74 - 190$) is used below the surface. A rolling motion inspired by beetle larvae is used to separate it from the surface of the water. It can walk like a caterpillar or roll. It can't roll across gaps greater than its diameter, but less than its length. Magnetic force can be used to increase jump height; it can be used for other motions, however it requires more energy than magnetic torque and is inherently unstable from a control point of view [51]. This work was expanded in [52] to consider locomotion strategies for confined, liquid filled, spaces.

Sudo et al. presented a magnetically controlled robot for swimming in viscous liquids. It consists of a magnetic head with a flexible tail, perpendicular to the axis of magnetisation. When actuated by an oscillating magnetic field the magnetic head rocks, causing a wave to travel down the tail driving the swimming motion. The swimming motion was successfully demonstrated in glycerine [53].

Kim et al. present a method for printing ferromagnetic material with selectively orientated magnetism. Neodynium-iron-boride (NdFeB) particles are included in the ink, as the ink passes through the nozzle a magnetic field orientates the particles. Magnetic fields can be used to control the structures. This gives the structure several modes of movement, including rolling, leaping, and crawling. By changing shape it is also able to reconfigure flexible electronics within its body to create different circuits to illuminate different patterns of LEDs [54].

Shape-programmable matter is a class of active material with a controllable geometry. Lum et al. consider an elastomer beam with a mixture of active and passive elements and a universal technique for programming the shape. Ecoflex 00-10 mixed with aluminium powder was moulded into the beam shape. Once cured a variable width strip was laser cut out and ecoflex 00-10 mixed with NdFeB powder was poured in to form the active portion. The varying width of the active portion dictates the response to the magnetic field, giving the desired shape [55].

Fusco et al. used a shape switching hydrogel tube for targeted drug delivery. They coupled a thermo-responsive hydrogel with either graphene oxide for near infra-red responsiveness, or silica-coated superparamagnetic iron oxide nano particles to provide magnetic actuation. The thermo-responsive hydrogel allowed reversible folding from a planer to a rectangular structure [56].

Soft magnetic robots have capabilities that their rigid counterparts don't. The flexible nature allows for multiple modes of actuation, making them more versatile in varied and unpredictable environments. This is particularly beneficial for applications in the gastro-intestinal tract where robots may need to both swim through fluid and walk on a solid surface.

2.4.3 Localisation of Magnets

A reliable method of localising magnets is necessary for closed loop control of a system, so that trajectory error can be calculated and corrected for. This is necessary to accurately navigate a magnet to a given location, as with a dead reckoning approach there will be a drift between the target location and the actual location of the robot, due to slipping and errors in the magnetic field generated.

Magnetic tracking can be either active or passive; in [57] the passive tracking of a permanent magnet to locate the tip of a growing robot is considered. The existing systems for localisation of growing robots are ultrasound, fibre Bragg grating, and magnetic tracking. This only allows for the tracking of one object. The system uses an array of 4 magnito-inductive sensors to locate the magnet in space. Three identification systems were used: an analytical model, long-short term memory (LSTM) model, and a hybrid model. Training data was used with the LSTM and hybrid model. The hybrid model was found to have

the lowest error. Increasing the velocity increased the localisation error, this was hypothesised to be due to hysteresis in the sensors. This approach also has potential for tracking the location of magnetic micro-robotics, which is something some of the other reproaches mentioned for growing robots, such as fibre Bragg grating, would not be suitable for.

An alternative method for tracking magnetic micro-robots was used in [58] using a triangular pattern of Hall-effect sensors to localise a magnet. By applying a magnetic field to the workspace, using an electromagnetic coil, it was demonstrated that non-magnetised ferromagnetic material, such as button batteries, can also be detected. This is because when in a magnetic field, ferromagnetic materials become temporarily magnetised. The magnetic field from these temporarily magnetised materials can be detected using the Hell-effect sensors.

Tiryaki et al. used a magnetic resonance imaging method to localise a magnetic micro-robots down to $300\,\mu$m in diameter within ex vivo porcine tissue [59]. This allowed for closed loop control, where the MRI was also used for actuation.

2.4.4 Control of multiple agents

Due to the nature of magnetic control, all magnetically actuated robots (often referred to as agents) operating within a given workspace receive the same, global, control input. This created difficulties when attempting to individually control multiple agents within the same space. Several methods for controlling multiple agents within a workspace have been developed.

Pawashe et al. developed a method of addressably controlling individual micro-robots using selective anchoring for use in reconfigurable robots. Reconfigurable robots offer the versatility to perform multiple tasks by taking on a different form. One issue with micron-scale configurable robots is the ability to disassemble for reconfiguration. Pawashe et al. propose sub-millimetre magnetic micro-robots actuated by an external magnetic field to create re-configurable 2D micro-assemblies. The magnetic micro-bot consist of a magnetic core (NdFeB particles in a polyurethane matrix), surrounded by a polyurethane shell to prevent the magnets coming into close contact. To separate two magnetically connected micro-bots the magnetic force needs to be overcome. This is done using an electrostatic grid to selectively anchor

the one of modules, the adjacent module is then rotated using the magnetic field until the attractive force is minimises so it can them move away. They performed experiments under silicone oil on four anchoring pads using an anchoring voltage of $400\,\mathrm{V}$ [60].

Diller et al. proposed a new method of controlling multiple agents in the same work space to allow for a non-specialised surface, with no anchoring forces, to be used. The approach uses geometrically dissimilar robots to give different resonance responses to actuation frequencies to selectively move individual robots. The robots move along the surface using a stick-slip motion in response to a saw tooth input from vertical magnetic coils; at the sharp change at the top of the saw tooth the robot momentarily slips in response to the high angular acceleration.

Each robot will travel at a different speed in response to a given actuation frequency. By sequentially pulsing different frequencies in different directions multiple robots can be navigated to independent goal locations . As the length of each pulse becomes shorter the robot paths approximate a straight line [61] [62].

Diller et al. show that a unique force can be applied, using a magnetic field gradient, to each agent if its orientation is unique and known. A rotating magnetic field is used to orientate the robots. As a result of different magnetic and fluid drag properties they have unique phase lags, the time taken to reach the target angle after an input is made with the magnetic field. This phase lag is determined from the fluid drag torque and the applied magnetic torque. The robots are $400 - 4,000\,\mu$m, the authors expect the approach to work down to tens of micrometers and at low Reynolds numbers, but not at the nano meter scale.

A vision based feedback system was used with top and side view cameras. The robots were manufactured using soft photo lithography and moulding. NdFeB or soft iron particles were used with polyurethane to give both magnetically hard and soft robots. An air pocket was used to make the robots neutrally buoyant [63].

Salehizadeh et al. investigated the interaction between a pair of magnets and proposed a method of independently positioning them in both two and three dimensional space, using an external magnetic field. It was found that when

two magnets are parallel and at a relative position of 90° to each other they repel, when the angle between the magnetic moments is 0° (coaxial) they attract, and when at an angle of 54.74° there is no attraction or repulsion force between the magnets, but there is a tangential force causing them to process around each other. The authors first considered the under actuated case, where only the in-plane orientation of the magnets was controlled, then the fully actuated case where the out of plane angle was also controlled. In both simulation and experiment the authors were able to position the magnets using the proposed control methods, with the fully actuated approach reaching the set-point faster. They proposed that two input control could be used to control two magnets in three dimensional space as an under-actuated system, but were unable to perform physical experiments to verify this [64].

2.5 Conclusion

Magnetically wirelessly actuated robots can have a wide variety of uses, including in medical robotics where they show great potential for navigating capsule robots. This is possible because of the ability of magnetic fields to safely pass through human tissue. Despite this magnetic actuation is limited to locomotion and performing basic manipulation tasks for a single robot. The ability to drive more complex mechanisms is limited by the limited number of degrees of freedom and any magnetic forces or torques applied to the robot act on the robot as a whole, rather than driving mechanisms on the robot. The number of robots that can be actuated in the same work space is limited by the fact the magnetic field acts in the same way on all of them, with no means to addressably control individual robots.

This thesis focuses on developing solutions to these problems. It does it by developing two different designs of magnetic motor, capable of being actuated without applying any net torque or force to the robot, allowing mechanisms to be driven while it is stable without the need to anchor it to its surroundings.

Chapter 3

Magnetic Force Driven Wireless Motor

3.1 Chapter preface

Material from: 'Cameron Duffield and Shuhei Miyashita, 'Magnetic Force Driven Wireless Motor, In: Annual Conference Towards Autonomous Robotic Systems (TAROS2020) Lecture Notes in Computer Science, vol. 12228., published [2020], pp. 409-412, [Springer]' [1]

A wirelessly actuated motor has wide potential application in in-vivo mechatronic devices, due to the absence of power and control cables from outside the device. This chapter presents a magnetically actuated wireless motor with no net force acting on the device. The developed motor has a double crank; each connecting rod includes a 5 mm neodymium magnet at the end, actuated using a magnetic field produced by an electromagnetic coil system located nearby. The magnetic gradient field aligned parallel to the direction of the magnet produces a magnetic force. The magnets are oppositely oriented, so experience attraction and repulsion forces, the crank converts this into a rotational motion. By altering the direction of the magnetic field, these forces are switched, and by using a ratchet a rotational motion in a single direction is produced.

3.2 Introduction

Recent advances have been made with implantable medical robots. These implants often have tethers to provide electrical connections to the outside of the body [65], or in the case of soft robots pneumatic or hydraulic connections are used [66]. Magnetic induction based wireless power transmission is a promising approach, however, it necessitates the presence of electronics and a receiver coil within the device [35]. Magnetic direct drive mechanisms, where magnetic force or torque are transmitted in a non-contact manner, offer an alternative to on-board energy source or tethers. Small magnetic microrobots are one of the examples, where a magnetic field provided by an electromagnetic coil system directly actuates the robot [31]. Locomotion of magnetically controlled robots involves the entire body moving. Hu et al. developed a soft robot that exploits multiple modes of actuation including, rolling, walking, and swimming [51]. The method removes the energy source from the robot, allowing them to be smaller and lighter. However, this approach does not allow for the driving of mechanisms within the robot as a

net torque is applied to the robot body, causing it to rotate [4].

This chapter presents a novel magnetic drive mechanism using a double crank. A magnet in each connecting rod is directly actuated by a magnetic field, producing a rotational motion. Thanks to the opposed directions of magnetic forces, the motor experiences zero net force, thus minimising the impact on the local environment where it is situated.

3.3 Concept and Development

The objective of a motor is to create a rotational motion from a simple input. It is necessary to convert the uniaxial magnetic field from a single coil, or pair of coils, to a rotational motion. A single coil produces a magnetic field gradient, which applies a force to a magnetic dipole within the field. This force can be used to create a linear motion in a part, which can, in turn, be converted to rotational motion using a crank (Fig, 3.1). For a crank mechanism the linear motion needs to be reciprocating, with the frequency of the reciprocation and the crank diameter dictating the angular velocity of the output. This reciprocating motion can be produced by periodically reversing the input magnetic field gradient by reversing the current in the coil.

Due to the nature of a crank there is a point where the cranks are at either top-dead-centre or bottom-dead-centre and no torque is produced from any input force; this is because there is no distance between the pivot and the line the force is acting along. To get past his singularity the inertia of a fly wheel can be used, storing kinetic energy from the main part of the cycle and releasing it when there is no input torque being produced.

It is necessary to match the frequency of the input magnetic field to the rotational speed of the crank. If the direction of the magnetic field is reversed before top-dead-centre is reached the rotation of the motor will reverse and it will stall. If the magnetic field is reversed too late the motor will stop at top-dead-centre, loosing the momentum of the flywheel, so when the field is reversed it is unable to pass the singularity. Exactly matching the actuation frequency with the speed of the motor, under varying load conditions, would require position feedback to the control system. One possible method of achieving this would be using visual feedback, however, this would severely

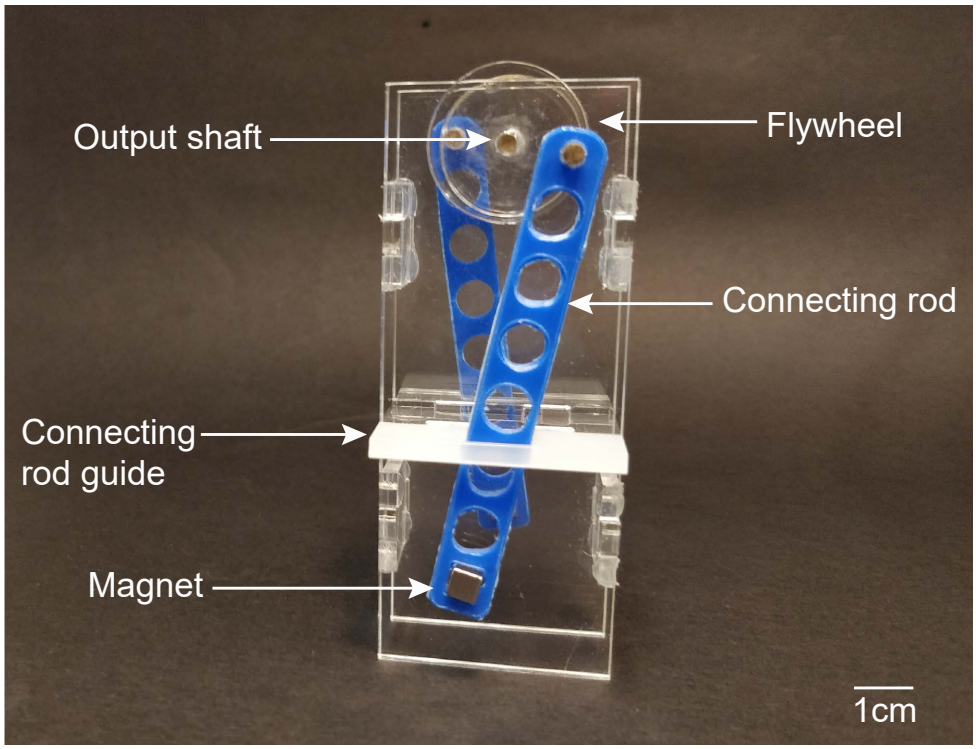

Figure 3.1.: A motor consisting of a crank mechanism driven by a pair of magnets and using a flywheel to overcome the singularity at top-dead-centre.

restrict the potential applications of the motor to ones where a line of sight can be maintained. Having a brief period with no magnetic field applied around when the cranks are at top dead centre makes the exact timing of the field reversal less critical, making the open loop control of the motor easier. This does mean, however, there is no input torque for this part of the cycle, making the motor liable to stalling from an applied load; this is likely to happen even without the break in the applied magnetic field due to the reduced torque near top-dead-centre.

To over come the challenges around top-dead-centre, this point can be completely removed from the cycle. Fig. 3.2 shows how the torque is at a maximum when the cranks are horizontal, showing that it is beneficial to restrict the motion of the cranks to near this angle in order to maximise the output torque. Simple restricting the travel of the crank would produce an oscillating rotation of the output shaft, requiring a mechanism to convert this into a continuously rotating output.

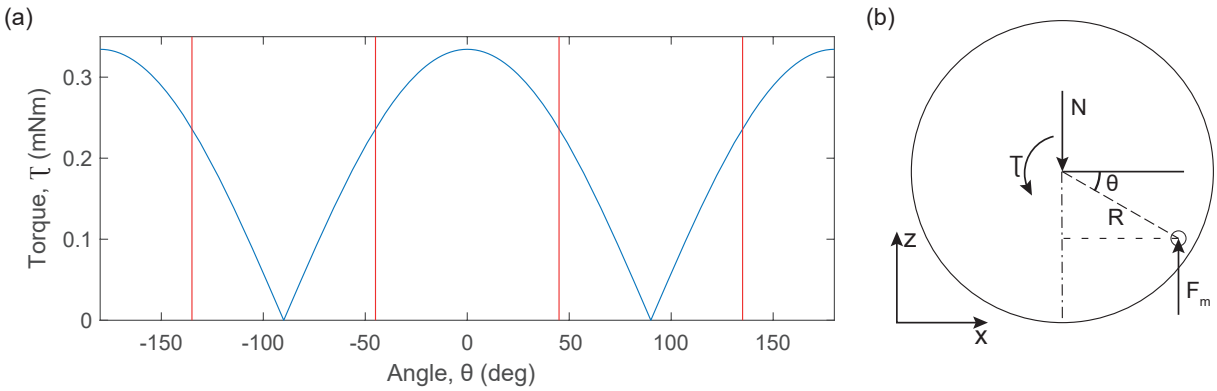

Figure 3.2.: (a) A graph of showing the output torque from the crank based motor through the cycle. The benefit of restricting the angle of travel to maximise torque can be seen from the vertical lines highlighting where the motion is restricted to and how the torque is greatest within that range. (b) A freebody diagram showing the forces acting on the crank

3.4 Method

The developed motor consists of two counterweighting cranks, with $180°$ phase difference, on each of which is a $5\,\text{mm}$ cubic neodymium iron boron (NdFeB) magnet at the end (Fig. 3.3).

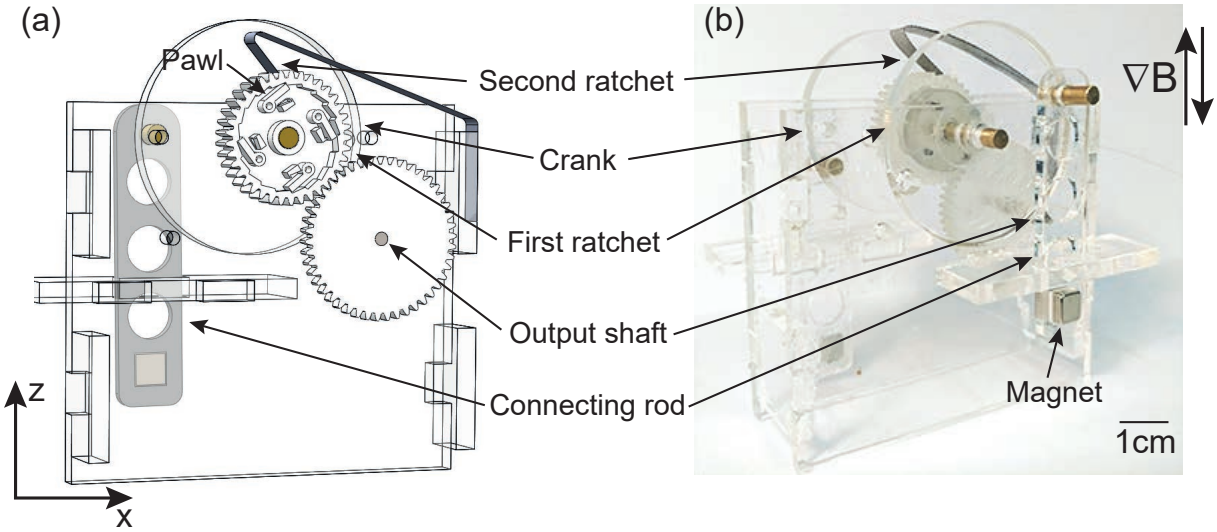

Figure 3.3.: The developed magnetic force driven wireless motor. (a) CAD section view showing the internal details of the first ratchet, and (b) photograph.

The magnets are vertical, with opposite orientation, this ensures there is no net magnetic force acting on the motor from the external magnetic field. The magnetic field gradient ($0.14\,\text{Tm}^{-1}$) is applied vertically from a $200\,\text{mm}$

diameter electromagnetic coil embedded $40\,\text{mm}$ below the workspace, and can periodically switch the orientation. A crank converts the linear motion of the connecting rod to rotary motion. To remove the singularity at top dead centre the crank is designed to oscillate 45° either side of horizontal. A double ratchet mechanism is used to convert this oscillating rotation to rotation in a single direction and prevent the load back-driving the motor. The first ratchet consists of four pawls within a saw-tooth ring gear. The second ratchet uses a combined pawl and pawl spring against the involute tooth driving gear.

For the driving stroke the magnetic field gradient is applied in the negative z direction, moving the crank clockwise. The geometry of the design prevents the crank from rotating past $\theta = 45^\circ$. The field gradient is then reversed, the first ratchet disengages and the crank moves counter-clockwise for the recoil stroke. The maximum torque is given when the crank is horizontal ($\theta = 0^\circ$) and the minimum is at the two extremes of motion ($\theta = -45^\circ$, $\theta = 45^\circ$). The control of the magnetic field is open loop. The angular position of the output shaft can be calculated for open-loop position control from the number of driving strokes performed.

3.5 Model

The magnetic force, $\vec{F}_m$, on a magnet with moment $\vec{m}$, in a magnetic field $\vec{B}$ is given by

$$\begin{aligned} \vec{F}_m &= (\vec{m} \cdot \nabla)\, \vec{B} \\ &= \left(\frac{\partial \vec{B}}{\partial x} \frac{\partial \vec{B}}{\partial y} \frac{\partial \vec{B}}{\partial z} \right)^T \vec{m}. \end{aligned} \tag{3.1}$$

Referring to Fig.3.2 (b) which shows the relation of a free body diagram of the system, with Eq. (3.1), The producible torque about the output shaft, τ, is

$$\tau = 2\, n\, \frac{\partial \vec{B}}{\partial z}\, \vec{m}\, R\, \cos\theta - Fr, \tag{3.2}$$

where the coefficient 2 represents the use of two magnets, n is the used gear ratio, R is the crank radius, and Fr is torque loss to friction in the mechanism. For the motor presented n is $1.243:1$, the prime gear ratio ensures even wear on the gear teeth, reducing hunting.

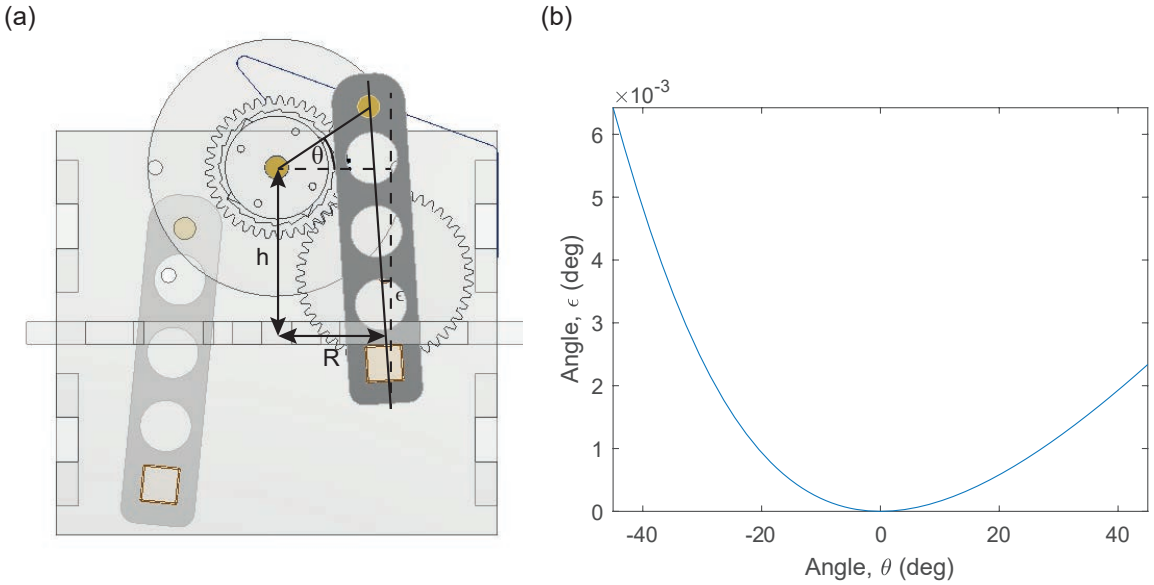

Figure 3.4.: (a) The geometry of the crank and connecting rod used for the advanced model, (b) the relationship between ϵ and θ.

This model does not account for the reduction in force on the magnet caused by the misalignment of the magnet with the field. This misalignment occurs due to the connecting rod being at an angle to the vertical due to the rotation of the crank and the geometry of the guide Fig. 3.4 (a). The angle of the connecting rod (ϵ) is given by:

$$\epsilon = \arctan\left(\frac{R(1-\cos\theta)}{R\sin\theta + h}\right), \tag{3.3}$$

where h is the height between the axis of the crank and the connecting rod guide. The relationship between ϵ and θ is shown in Fig. 3.4 (b). This can be used to find the vertical component of the magnetic moment (m_z):

$$m_z = |\vec{m}|\cos\left(arctan\left(\frac{r(1-\cos\theta)}{r\sin\theta + h}\right)\right). \tag{3.4}$$

The angle of the two connecting rods are different as one is at a positive value of θ and the other is at a negative value, so the vertical magnetic moment needs to be calculated separately for each of the two magnets. This can then be substituted into Eq. (3.2) to give the motor torque:

$$\tau = n\frac{\partial\vec{B}}{\partial z}\left(m_{z1} + m_{z2}\right) R\,\cos\theta - Fr, \tag{3.5}$$

where m_{z1} is the vertical component of the magnetic moment for the first magnet and m_{z2} is the vertical component of the magnetic moment for the second magnet. These two values are different due to one being in the up position while the other is in the down position.

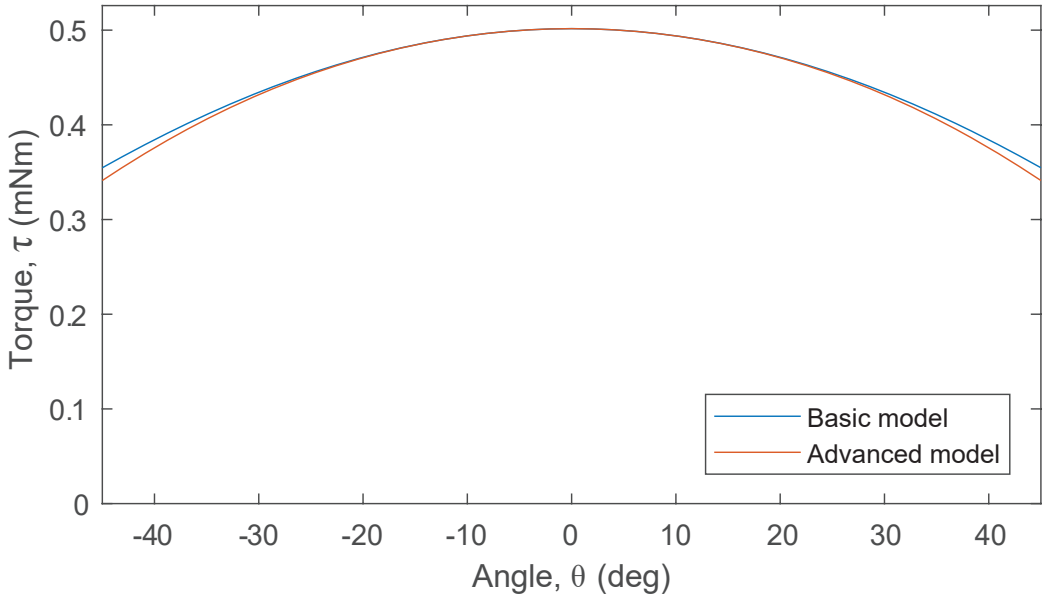

Figure 3.5.: A comparison of the basic and advanced models, showing how there is no difference when the crank is horizontal and 3.8 % difference at the extremes of the travel.

Fig. 3.5 Shows both the basic (Eq. (3.2)) and advanced (Eq. (3.5)) models of motor torque, assuming no friction. When the crank is horizontal there is no difference between the two models, as the connecting rod is vertical. The greatest difference between the two models is when the crank is at the limits of its travel ($\theta = \pm 45°$), where the discrepancy between the models is just 3.8%. For the geometry of the motor presented the difference between the models is negligible, and so the basic one can be used for simplicity. If, however, the connecting rods were shorter relative to the crank radius, the difference would be much more significant, requiring the advanced model for accurate results.

3.6 Fabrication

The housing parts are laser cut from 3 mm, and the connecting rods from 2 mm, sheet acrylic using a CO_2 laser cutter. The gears and ratchet parts are manufactured from Formlabs clear resin using a Form 2 SLA printer. The 3mm diameter shafts were cut from brass (CZ121/CW614N) rod and 2mm diameter stainless steel rod. Small pieces of Ecoflex 00-10 were used for the pawl springs in the ratchet mechanism. The second ratchet was cut from a 0.1 mm thick steel sheet (full hard, cold rolled, low carbon 1008-1010) and bent to shape.

The mechanism was assembled using acrylic adhesive (RS) and cyano acrylate (Loctyte).

3.7 Results

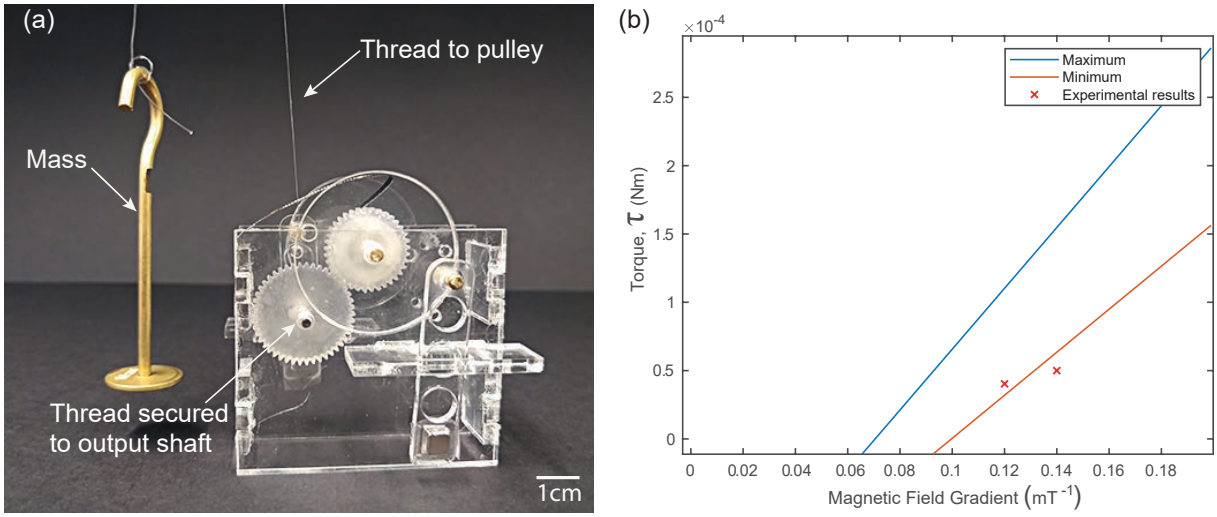

Figure 3.6.: Measurement of torque. (a) The experimental setup, (b) Theoretical and provisional experimental plot of torque τ. Two data points are insufficient to draw firm conclusions on the accuracy of the model, but do give an initial indication of its potential. Fig. 4.6 results for the torque of an improved design of motor using the same principle and shows a stronger correlation with more data points.

The output torque of the motor was measured using a simple hoist mechanism (Fig. 3.6 (a)). A length of mono-filament nylon thread was secured to the shaft, passed up over a pulley, and down to a known mass to provide the load. The friction in the mechanism was measured by removing the connecting rods, winding the thread around the output shaft and adding mass until the mechanism rotates. This gave $Fr = 0.15 \times 10^{-3} \pm 0.01 \times 10^{-3}$ Nm. Fig. 3.6 (b) shows the measured and calculated motor torque for a given magnetic field gradient. The maximum line represents the point when the crank is horizontal and torque is greatest, while the minimum line shows where the crank is at its lowest or highest point (45° from horizontal) and the torque is at its minimum. The experimentally measured values are the greatest load at which the motor could complete the full cycle, so correspond to the minimum torque line. For each test the motor was allowed to run continuously for a length of time to demonstrate that it was capable of continuous operation at this load. As only two data points were collected only limited conclusions can be drawn from the data; it is impossible to tell if the relationship is linear or a polynomial. The

provisional experimental results in Fig. 3.6 (b) do show that for the values tested the model is a reasonable fit for the data. Only two data points were able to be collected due to the equipment being inaccessible for half a year because of the COVID-19 pandemic; on returning to the lab some oil (3-IN-ONE) which had been added to the first ratchet had dried out making the motor unusable. Further results for an improved motor design based on the same principle are shown in Fig. 4.6, these results confirm the linear relationship between magnetic field gradient and output torque.

3.8 Scalability

This section investigates the effect of scaling the design on the output torque of the motor. Eq. (4.2) shows the output torque is proportional to the crank radius (R). Eq. (4.2) also shows how the torque is proportional to the magnetic moment (m); this is given by:

$$m = \frac{1}{\mu_0} B_r V, \tag{3.6}$$

where μ_0 is vacuum permeability ($4\pi \times 10^{-7}$ Hm^{-1}), B_r is the residual flux density (1.2 T), and V is the volume of the magnet. The volume, and hence the magnetic moment, is proportional to the cube of the edge length. The combination of the two gives that the torque is proportional to the fourth power of the overall size of the motor, assuming all components are scaled proportionally. Fig. 3.7 shows how the output torque increases as the motor size is increased; this does not account for friction in the system, which would become proportionally more significant as the size reduced.

3.9 Discussion and Conclusion

A magnetically actuated wireless motor driven by a magnetic field gradient, capable of producing 0.05 mNm of torque, has been presented. The motor allows for a continuously rotating output from an alternating magnetic field input by using the novel double ratchet mechanism to eliminate the singularity at the top-dead-centre of a crank. This gives the advantage, over existing approaches, of having a very simple input from a single electromagnetic coil. The established approach for creating a torque in magnetic robots is to use multiple coils to create a rotating magnetic field. The design of the mechanism

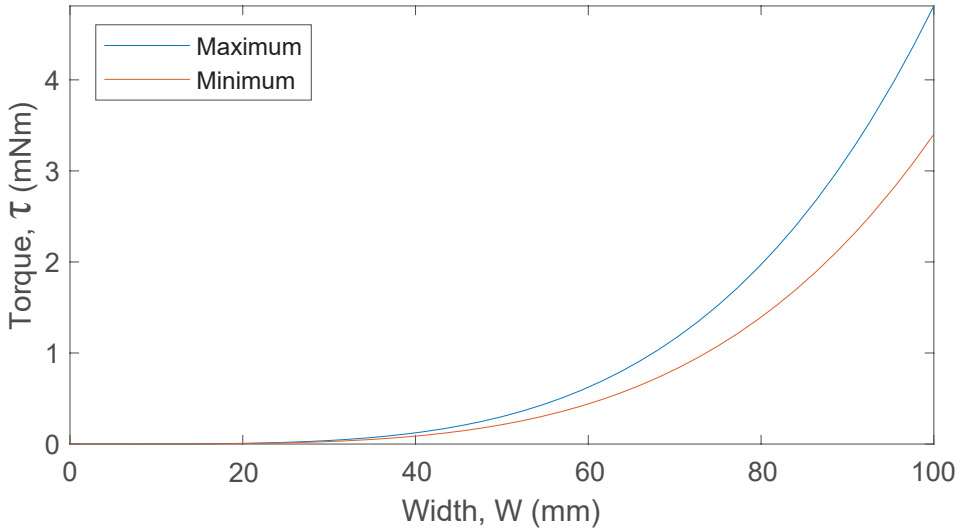

Figure 3.7.: How the torque output of the motor varies as the overall width (W) is increased for a $14\,\mathrm{Tm}^{-1}$ magnetic field gradient.

means that the force acting on the magnets and the weight of the cranks are balanced. This means the device experiences net zero force from the applied magnetic field gradient and so is stable in operation.

Two different models have been presented, one simplified model and one more advanced model that accounts for the misalignment of the connecting rod. For the geometry of the motor presented the difference between the models is $3.8\,\%$, so is negligible. If the crank diameter was greater, or the connecting rod shorter, then the difference would be much more significant. The effect of scaling the motor on the output torque has been modelled. The design shows promise to be scaled down; if all elements of the design are scaled down proportionally the output torque reduces with the fourth power. There is also scope to redesign the motor to reduce the size with little reduction in the output torque.

The use of an alternating magnetic field, instead of a rotating magnetic field, allows for the motor to rotate on any axis on the same plane and even multiple motors with different orientations to operate simultaneously within the same workspace. The output torque was measured and compared to experimental values for validation. It was found that there are significant torque losses in the design, with $75\,\%$ of the output torque being lost to friction. These losses mainly occur in the four bearings on the shaft and between the two gears, some torque is also lost in friction between the connecting rods and the crank.

Future work includes improvement of the design to reduce the torque lost to friction and to reduce the size of the motor.

Chapter 4

Wirelessly Magnetically Actuated Motor for Tissue Regeneration Robotic Implant

4.1 Chapter preface

Material from: ©2022 IEEE. Reprinted, with permission, from [Cameron Duffield, Abigail F Smith, Daniela Rus, Dana Damian and Shuhei Miyashita. 'Wirelessly Magnetically Actuated motor for Tissue Regeneration Robotic Implant(accepted)'. In: IEEE International Conference on Intelligent Robots and Systems (IROS). IEEE. 2022, pp. 465–471] [2] Abigail F. Smith assisted with the experiments using biological tissue.

In biomedical engineering, robotic implants provide new methods to restore and improve bodily function, and regenerate tissue. A significant challenge with the design of these devices is to safely actuate them for weeks or months, while they are residing in a patient's body. Magnetic, and other force-at-distance actuation methods, allow mechanisms to be controlled remotely and without contact or line of sight to the device. In this chapter, a novel magnetic field driven wireless motor is presented. The motor drives a robotic implant for the treatment of long gap oesophageal atresia and short bowel syndrome. The motor is equipped with two oppositely oriented permanent magnets which experience forces in opposite directions when a magnetic field is applied tangential to the magnets' directions. The implant can produce a force of 2 N. It is demonstrated with an ex-vivo porcine oesophagus.

4.2 Introduction

Wirelessly controlled robots show great potential to be used for biomedical applications [67]. Telesurgery robots are widely clinically approved and are used to improve the outcomes of surgical interventions [68, 69]. Tethered crawlers have been shown to improve the effectiveness of certain medical procedures, such as colonoscopies [70, 71]. Untethered robots [72, 73] provide a new solution to gastrointestinal (GI) diseases, incorporating drug release and wireless actuation techniques. Medical robots in vivo have also shown promise in foreign matter retrieval [58, 74], targeted drug delivery [75] and ophthalmologic procedures [76]. Another area of interest is the implementation of robotic implants for long-term therapies. Such devices are able to reside in the body and achieve effective functions and therapies. Examples include supporting heart function [77], performing as an artificial

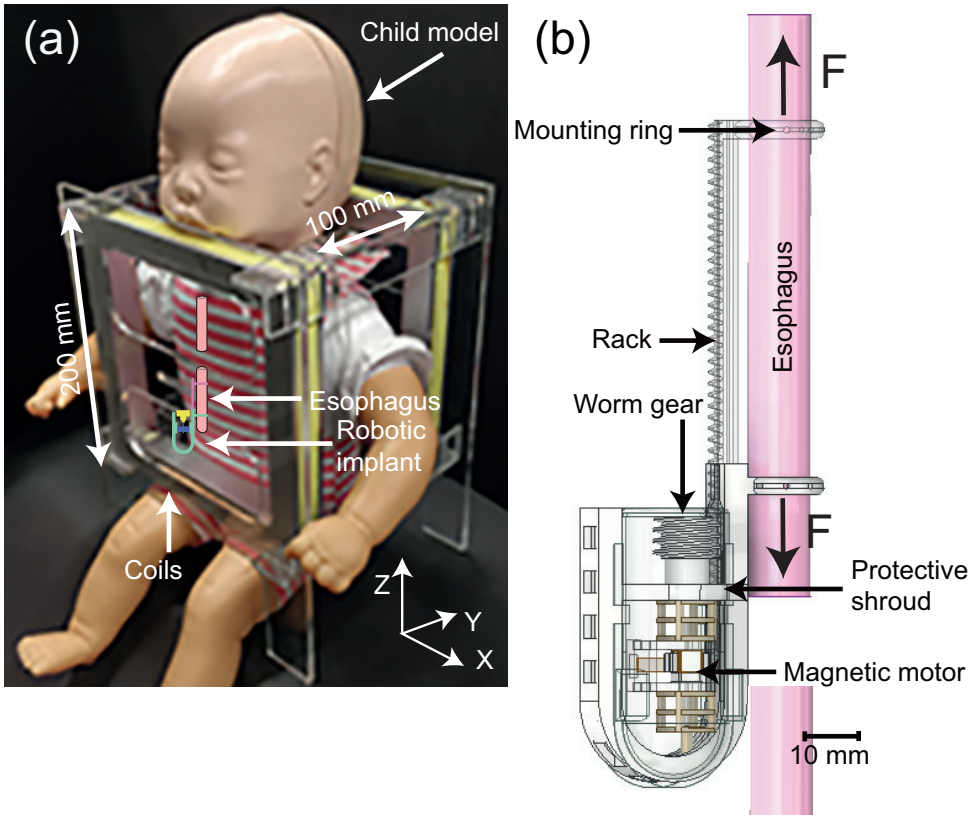

Figure 4.1.: The developed wirelessly powered robotic implant. (a) Shows the control coils and where the device would be positioned in a patient. (b) Shows details of parts of the robotic implant

pancreas [78] and tissue regeneration [79].

One of the significant challenges with designing robotic implants is power delivery and control [80]. Conventional motors require a source of electricity to run which could be provided by wires passing into the body or batteries. Alternatively, magnetic control can be used as a form of force-at-distance actuation. Magnetic fields are used to apply forces and torques to a magnetized robot [31, 51, 55, 81, 82]. Using magnetic fields to control devices wirelessly has been shown to be a plausible solution [83]. Magnetic fields are able to pass through common materials, including biological tissue, making magnetic actuation a suitable method for robots purposed for biomedical applications as magnetic fields of up to 7T are approved for use in MRI machines with no adverse effects on a patient.

Existing robots using magnetic control move the entire robot as a solid body by changing the orientation of the magnetic field [84] [85]. One of the recognized approaches is to apply a continuously rotating magnetic field,

requiring a complex arrangement of coils that are capable of creating a magnetic field of any orientation [86].

This chapter continues on the work from Chapter 3 and [1] to present a magnetic wireless motor that produces zero net torque and net force powered by electromagnetic field from a pair of coils. As extension of the previous work, this chapter introduces a motor with improved torque, more than a 60% reduction in body size and integrated in a robotic implant capable of stimulating tissue growth through mechanical therapy. The single pair of coils used to drive the motor greatly simplifies the equipment required and control of the robot compared to the existing magnetic control approaches.

This motor is incorporated into a device to lengthen tubular organs by applying a uniaxial force, advancing previous work [87]. The device could be used to improve the treatment of oesophageal atresia or short bowel syndrome. The treatment of oesophageal atresia traditionally requires multi-week sedation and ventilation. Sutures attached to the oesophagus are manually pulled from outside.

4.3 Methods

This section first details function of the robotic implant for stimulating growth in tubular organs, then the details of the motor used to drive it. The working principle of the motor is explored, before a model to describe the output torque and the maximum speed of the motor is developed. The methods used to fabricate and actuate the motor are presented. Finally, the effects of scaling the motor on the output torque is considered.

4.3.1 Robotic implant

The implant (Fig. 4.1) consists of two rings sutured to the oesophagus. The first ring is connected to the main housing, while the second is connected to a rack. The rack is driven by the magnetic motor with a worm gear with a 2 mm pitch. All moving parts are contained within a shroud to prevent damage to surrounding tissue. The rack has a travel of 45 mm with the force being unaffected by the extension. A force of 2 N has been shown to stimulate growth in porcine oesophagus in vivo. The 20 mm length of tissue grew an average of 2.5 mm per day [79]. Magnetic control makes the implant design

inherently safe. Magnetic control is forced based, by setting the magnetic field gradient the operator determines the maximum force the system is able to apply. This is in contrast to position based control where the displacement is set and the robot applies the force necessary to achieve this, which could in some instances could lead to tissue damage as a result of excessive force being applied. The elongation of the implant can be detected using an array of hall effect sensors outside the body, as demonstrated in Liu et al. [58], to allow the position to be detected without any electronics being in the implant, or wires passing through the body.

4.3.2 Wireless motor

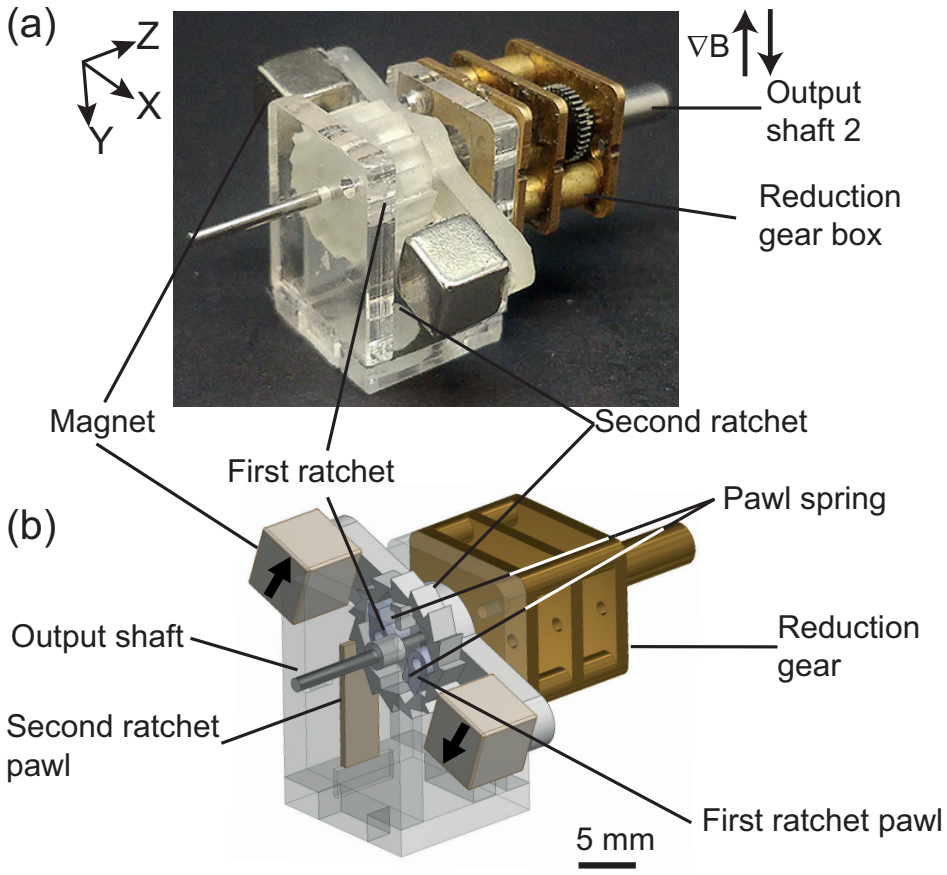

Figure 4.2.: The developed magnetic force driven wireless motor showing the double ratchet mechanism. (a) Photograph and (b) CAD section view.

For a magnetic motor to convert a magnetic field into rotary motions about a different axis, a magnetic field gradient that periodically reverses direction was chosen as the control power input. This allows for a reduction of net torque of the device or operation of multiple motors. This applies a force to any magnet in the field. A crank mechanism is used to convert this force to a torque. The

developed motor uses two counter-weighting cranks, with $180°$ phase difference. At the end of each cranks is a magnet, the two magnets face in opposite directions (Fig. 4.2). This ensures that the system is balanced, and gravity does not affect the operation. This means when one has an upwards force from the magnetic field, the second has a downwards force, ensuring there is no net force acting on the motor.

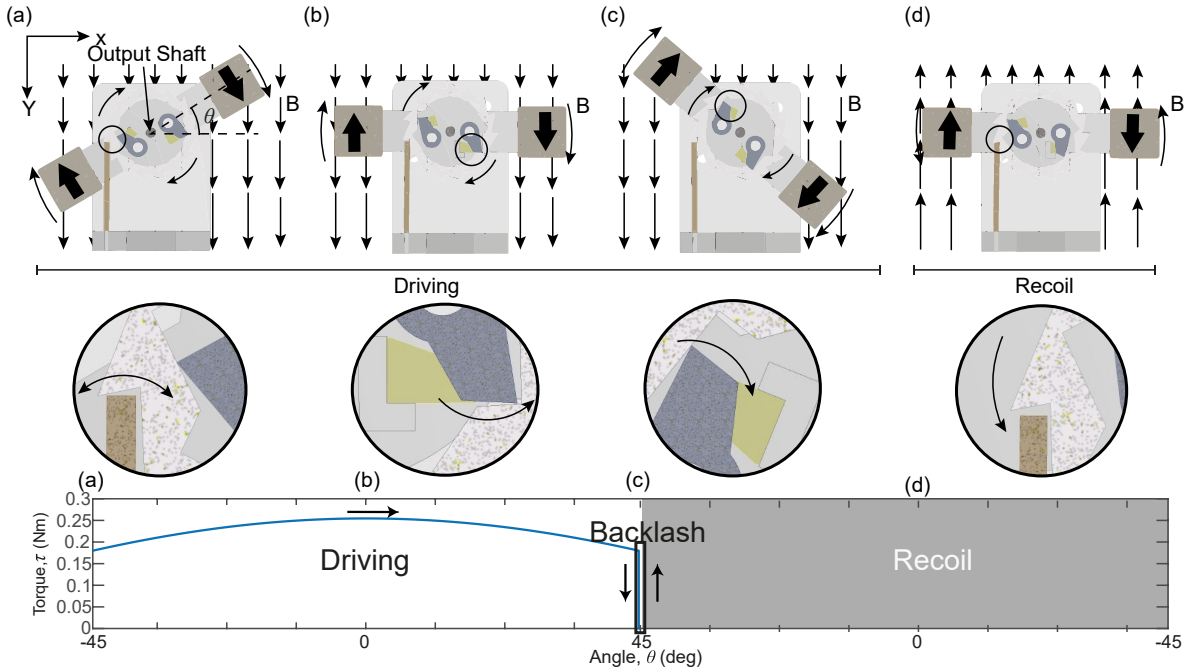

Figure 4.3.: The motion of the motor. (a) The driving stroke with the cranks at the highest point, and minimum torque, inset showing the disengaged second ratchet; (b) horizontal cranks giving the greatest torque, inset showing the engaged first ratchet pawl and decompressed Ecoflex™ pawl-spring; (c) the cranks at the end of the driving stroke, minimum torque, insert showing the second pawl with compressed pawl-spring; (d) the field gradient is reversed for the cranks to move back for the recoil stroke, inset showing the engaged second ratchet.

A crank converts the force acting on the magnet to rotary motion. When the cranks are vertical (top dead centre), the magnets are perpendicular to the magnetic field. This means there is no magnetic force, leading to a singularity. To remove this singularity the cranks' oscillation is limited to $45°$ either side of horizontal, this also keeps the motor near the maximum torque region where the cranks are horizontal. A double ratchet mechanism converts this oscillating rotation to rotation in a single direction and prevents the load back-driving the motor. The output torque is increased by a $1{:}290$ reduction gear box.

The first ratchet consists of two pawls within a saw-tooth ring gear, Fig. 4.2 (b).

The pawl carrier is free to rotate on the shaft, while the output gear is fixed to the shaft to transfer the torque. The two pawls are offset by half a tooth, meaning only one engages at any one time. This doubles the number of engagement point to 20, reducing the backlash. The second ratchet uses a combined pawl and pawl spring against the external saw tooth gear required to prevent back-driving, this has 15 engagement points. This means the motor only rotates in a single direction and can hold an unlimited load even without any magnetic field.

Fig. 4.3 shows the main stages of the motion of the motor. The cycle begins with the cranks inclined by $45°$ ($\theta = 45°$) (Fig. 4.3 (a)). A downwards magnetic field is applied, applying opposing forces to the two magnets, rotating the cranks clockwise. This engages the first ratchet, rotating the shaft and disengaging the second ratchet. When the cranks is horizontal (Fig. 4.3 (b)) the magnets are aligned with the magnetic field, giving the motor the maximum torque. When the cranks are declined by $45°$ ($\theta = 45°$) the magnet hits the end-stop, ending the driving stroke. When a magnetic field is then applied upwards this applies an opposite force to the magnets, causing the cranks to rotate anticlockwise (Fig. 4.3 (c)). The first ratchet disengages, disconnecting the cranks from the output shaft, while the second ratchet engages to prevent the load from back-driving the motor. This recoil stroke returns the cranks to the starting position, completing the cycle.

4.3.3 Model

To understand the properties of the motor, a model is presented for the output torque and speed of the motor. The motor is driven by the force of a magnetic field on the magnet at each end of the crank. The magnetic force on a magnet, $\vec{F}_m$, with magnetic moment $\vec{m}$, in a magnetic field $\vec{B}$ is given by

$$\begin{aligned} \vec{F}_m &= (\vec{m} \cdot \nabla)\, \vec{B} \\ &= \left(\frac{\partial \vec{B}}{\partial x} \frac{\partial \vec{B}}{\partial y} \frac{\partial \vec{B}}{\partial z} \right)^T \vec{m}. \end{aligned} \tag{4.1}$$

When the magnet is out of alignment with the magnetic field gradient, the force is reduced. To calculate this reduced force the vector component of the magnetic field gradient parallel to the magnetic moment is taken. Using the free body diagram of the system, shown in Fig. 4.4 with Eq. (4.1), the torque

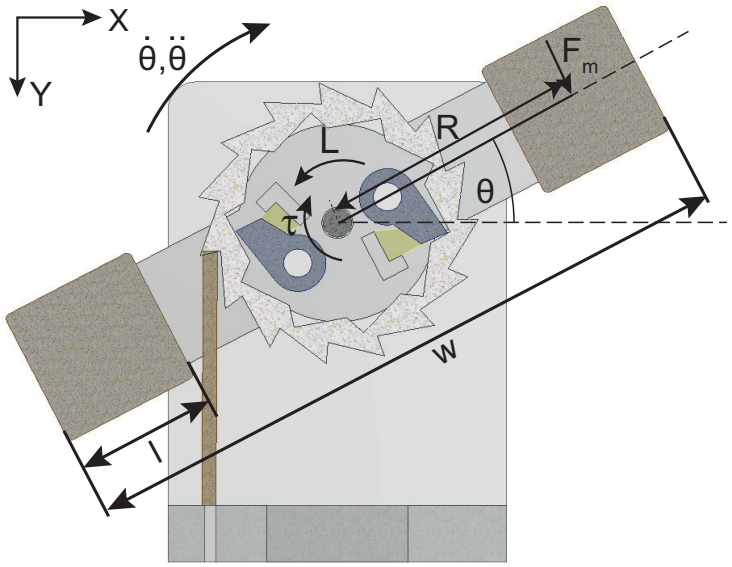

Figure 4.4.: A simplified free body diagram of the crank, showing the principle dimensions, forces and torques about the output shaft while the magnetic field is applied.

produced about the output shaft, τ, is

$$\tau = 2\,n \left\| \frac{\partial \vec{B}}{\partial y} \right\| \|\vec{m}\|\, R\, \cos\theta - F_r, \tag{4.2}$$

where the coefficient 2 represents the use of two magnets; it is assumed that the magnetic field gradient is constant across the work space and so both magnets experience a force of equal magnitude. n is the ratio of the gear box, R is the crank radius, and F_r is an empirical friction term. As there are two magnets of equal mass, the system is balanced and so weight does not affect torque.

The force from the robotic implant is given by:

$$F = \eta\, \frac{2\,\tau\,\pi}{P}, \tag{4.3}$$

where P is the worm screw pitch, and η is an empirical efficiency term.

The implant extension velocity, v, is given by

$$v = \frac{\gamma}{2\pi n} p f, \tag{4.4}$$

where v is the rack speed, p is the pitch of the rack, n is the ratio of the gearbox, f is the magnetic field frequency, and γ is the angle the crank passes through each driving stroke. For the motor presented $\gamma = \frac{\pi}{2}$ radians.

This is based on the assumption that the motor completes a full cycle is with each cycle of the magnetic field. If the actuation frequency, or load, is high then the motor will "step out" in a similar manner to a stepper motor.

When the motor is not subject to any load, the frequency is limited by the angular velocity. The time taken to reach angle θ from the initial position is given by:

$$T = \sqrt{\frac{2I(\theta - c)}{K\, I\, \cos(\theta) - 2L}}, \tag{4.5}$$

where c is the initial angle of the crank, L is the load on the motor, $K = \frac{2\,\frac{\partial \vec{B}}{\partial z}\,||\vec{m}||\,R}{I}$ and I is the moment of inertia of the rotating parts,

$$I = 2\rho V R^2, \tag{4.6}$$

where ρ is the density of the magnet ($\rho = 7516$ kg m^{-3}) V is the volume of the magnets (125 mm^3), and R is the radius of the crank (10 mm). This assumes the mass of the crank arm is low compared to the mass of the magnets.

By making θ equal to $\alpha/2$, to give the time for the crank to travel a full stroke, the step out frequency can be found using,

$$f_{so} = \frac{1}{2T}, \tag{4.7}$$

for the motor demonstrated, the model gives a no-load step-out frequency of 13.15 Hz.

Above the step-out frequency, the motor speed decreases with increasing actuation frequency. For both rolling [88] and swimming [89] robots, the velocity of the rack for the implant is given by:

$$v = \frac{\gamma}{2\pi n} p \left(f_a - \sqrt{f_a^2 - f_{so}^2} \right), \tag{4.8}$$

where f_a is the actuation frequency, and f_{so} is the step-out frequency. The net torque acting on the system is given by:

$$\Sigma\tau = \Sigma\, \vec{F_m}\, \vec{P}, \tag{4.9}$$

where $\vec{F_m}$ is the force from a magnet, and $\vec{P}$ is the position vector for where the force is acting, perpendicular to the force. All forces are parallel to the magnetic

field, meaning all position vectors are in the xy plane. This shows that for a single motor, a net torque will act on the system, if two motors are used, with opposite orientation, there will be no net torque acting on the system.

4.3.4 Motor fabrication and electromagnetic coil system

The robot body was cut from 2 mm cast acrylic sheet. Ratchet parts were manufactured using Form 2 SLA printer using clear resin (Formlabs), clear resin was chosen as it exhibits similar material properties to other resins produced by Formlabs which are certified for medical use. Small pieces of Ecoflex™ 00-10 (Smooth-On) were used for the pawl springs in the ratchet mechanism. The second ratchet was cut from a 0.5 mm thick low density polythene and bent to shape. The magnets used were 5 mm cubic neodymium iron boron (NdFeB) (Supermagnete). The reduction gear box is a commercially available unit with 1:290 reduction (Pololu). The mechanism was assembled using an acrylic adhesive (RS) and cyanoacrylate adhesive (Loctite). The worm gear was FDM printed (Mojo) using ABS, using a different material to the rack reduces friction compared with manufacturing both parts from the same material. All components are contained within a protective shroud made from photo-curable resin (Formlabs) meaning the device can be made bio-compatible.

Three electromagnetic coil systems were used. Magnetic field gradients of up to $0.37\,\mathrm{Tm}^{-1}$ were applied horizontally from two square coils of 200 mm side length and 100 mm separation. For tests requiring a vertical magnetic field gradient a Helmholtz coil of 180 mm diameter was used to provide a magnetic field gradient of up to $0.37\,\mathrm{Tm}^{-1}$ and a field strength of up to 15 mT. When a flat surface above the coil system was needed a single horizontal coil of 200 mm diameter 40 mm below the work surface was used to apply magnetic field gradients of up to $0.14\,\mathrm{Tm}^{-1}$ was used. The magnetic field strengths of each coils system were found experimentally using a Gauss-meter. The magnetic field strengths used are well below the static magnetic field strength of $0.046 - 8\,\mathrm{T}$ used in MRI machines [90]; demonstrating that it is safe to use in a medical setting.

4.3.5 Scalability

In this section, we investigate the impact of scaling down the motor on the output torque. Eq. 4.2 shows how the torque is proportional to the magnetic

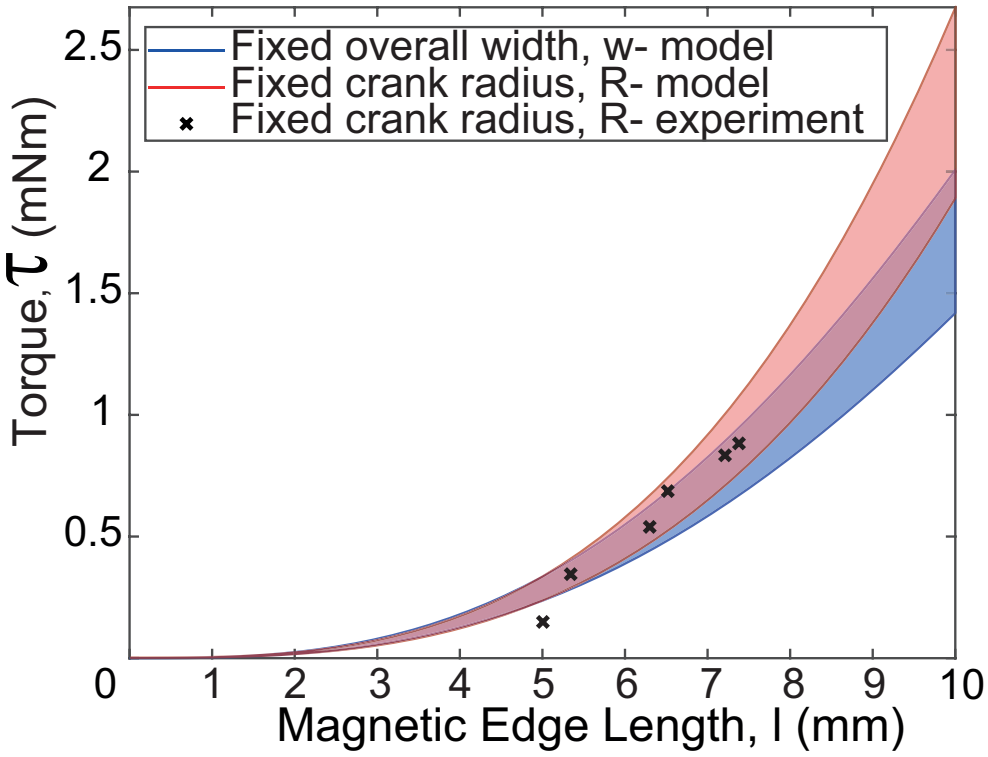

Figure 4.5.: The effect of increasing the size of the magnets used where first the overall width (w) is fixed, then the crank radius is fixed (R). The shaded region is the range between the peak and minimum torque without the reduction gearbox. Each data point is from the motor run continuously for a length of time to demonstrate that it was capable of continuous operation at this load.

moment (m); this is given by $m = \frac{1}{\mu_0} B_r V$ where μ_0 is vacuum permeability ($4\pi \times 10^{-7}$ Hm^{-1}), B_r is the residual flux density (1.2 T), and V is the volume of the magnet. For a cubic magnet this means the magnetic moment, and motor torque, are proportional to the edge length cubed, as shown in Fig. 4.5.

Scaling down the device is also limited by the practical minimum feature resolution which can be made by a given manufacturing technique. The smallest components are the pawl springs in the first ratchet, and the finest details are the gear teeth. These components could be made half the current size without significantly changing manufacturing techniques. The maximum size of the motor may be limited for in vivo applications. The equivalent magnetic dipole for a cubic magnet passes through its centre, meaning as the magnet size is increased the dipole moves closer to the centre of the crank, reducing its effective radius. This leads to a compromise between maximizing the volume of the magnet and the crank radius. Eq. (4.5) gives the torque of

the motor of width W and a cubic magnet of edge length l

$$\tau = \frac{\partial \vec{B}}{\partial z} \frac{1}{\mu_0} B_r \, l^3 \, (W - l) \, \cos\theta. \tag{4.10}$$

Fig. 4.5 shows the affect of increasing the magnet size for both a fixed overall width of the motor, and for a fixed crank length. The plot shows that the magnet size greatly influences the output torque of the motor, meaning that the largest magnets possible should be used. For experiments in this chapter the width was fixed at $25\,\text{mm}$ and $5\,\text{mm}$ cubic magnets were used as these are the greatest stock size of magnet that clears the ratchet mechanism.

4.4 Experimental Results

Experiments were conducted to characterize the performance of the magnetic motor. The output torque for a given magnetic field gradient was investigated, as was the angular velocity for a given actuation frequency. The Characteristics of the robotic implant were then investigated, with the output force being measured and an ex-vivo experiment being carried out.

4.4.1 Torque model and evaluation

A hoist mechanism was used for the experimental torque measurement. A length of mono-filament nylon thread was attached to the shaft, passed up over a pulley, and down to a load. A known mass (± 0.001 g) was used for the load, and the magnetic field gradient gradually increased until the motor was able to lift the mass.

Fig. 4.6 shows the measured and calculated motor torque for a given magnetic field gradient. The experimentally measured values shown in the graph are the greatest load at which the motor could complete the full cycle, meaning they represent the minimum torque at any point in the cycle, which occurs where the crank is at $\pm 45°$. The graph shows the model and experimental results diverging at greater loads; this is thought to be caused by the increased normal force in the bearings from the load. The load applied by suspending a mass from a thread wound around the output shaft of the motor, this applies a radial force in the bearing. As this normal force increases, so

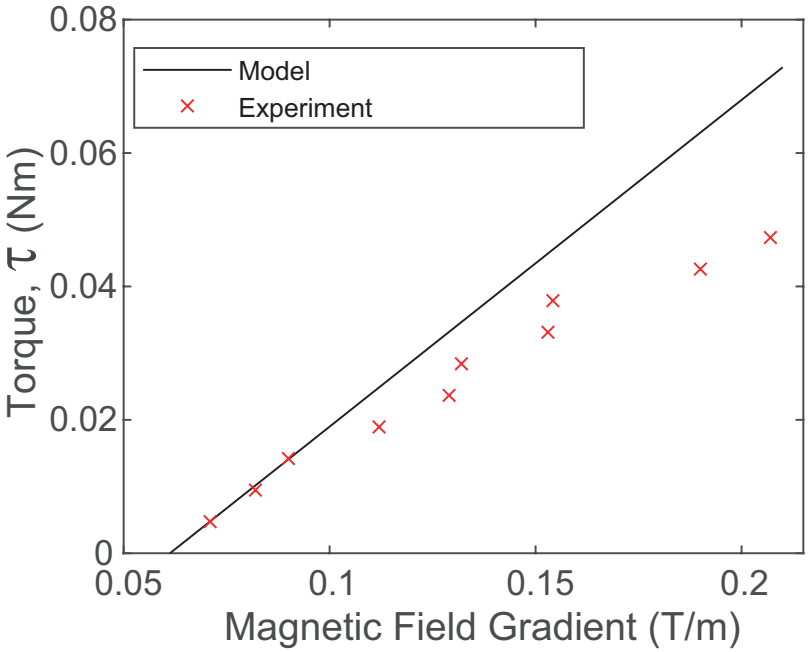

Figure 4.6.: Plot showing the output torque of the motor, both experimentally and modelled. It can be seen that the model is initially a good fit for the data, before diverging for greater magnetic field gradients. This divergence is believed to be caused by greater friction in the system at greater loads due to increased normal forces in the bearings. Each data point is from the motor run continuously for a length of time to demonstrate that it was capable of continuous operation at this load.

does the frictional load; this is not captured in the model as only the no-load friction was considered, leading to divergence from the experimental results. Each data point is from the motor run continuously for a length of time to demonstrate that it was capable of continuous operation at this load. The model for the motor torque is proportional to the magnetic field gradient (Eq. 4.2) with a peak torque where the cranks are horizontal, and a minimum torque where they are inclined at $45°$. From these results it was determined that the friction term for the motor is $F_r = 0.03$ Nm. This was done by considering the magnetic field gradient required for the motor to operate at low loads and fitting the model to the results.

Fig. 4.7 Shows how the angular velocity of the motor increases proportionally to the input magnetic field frequency, up until the step-out frequency, at 13 Hz, where the angular velocity rapidly decays, as is predicted by the model. This is due to the inertia of the crank making it unable to move at the angular velocity required to keep instep with the actuating magnetic field. It can be seen that at 6 Hz the angular velocity briefly decays before again becoming proportional

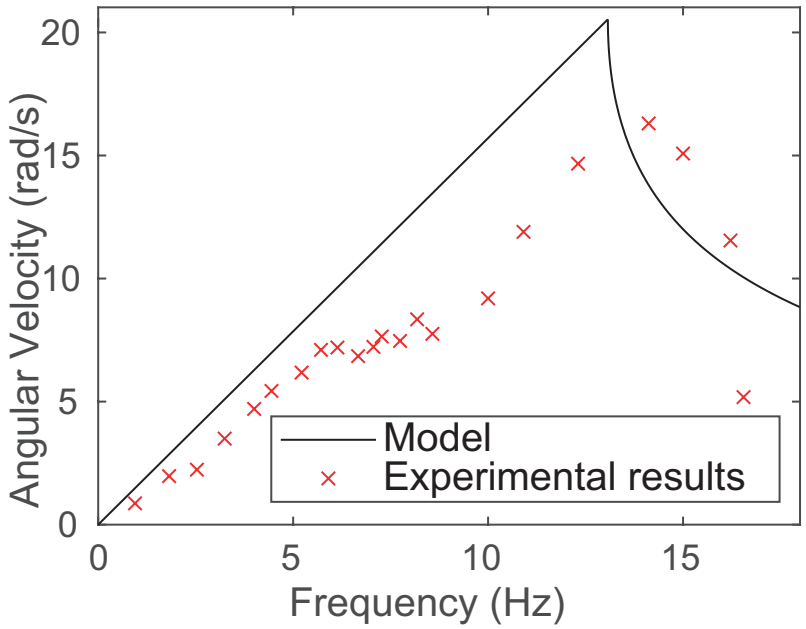

Figure 4.7.: The angular velocity of the motor without the reduction gearbox against the input frequency. It can be seen that at frequencies over the step-out frequency of 14 Hz the speed reduces, this is close to the modeled step-out frequency of 13.2 Hz.

to the input frequency. This is thought to be due to the discrete nature of the ratchet; at the higher frequencies the crank isn't able to move quite far enough to move by the same number of points of engagement on the outer ratchet, and so there is now a fixed offset between the model and the experimental data. Each data point in Fig. 4.7 was calculated as an average angular velocity for multiple rotations of the motor shaft.

4.4.2 Robotic implant characterization

The force from the implant was characterized using a similar method to torque, by hanging calibrated weights from the mounting ring and reducing the magnetic field until it was unable to lift the mass. The modelled and predicted values for the force are shown in Fig. 4.8. Each data point is from the motor run continuously for a length of time to demonstrate that it was capable of continuous operation at this load. The efficiency term was determined to be $\eta = 0.2$. When implanted it is possible the robotic implant won't be perfectly positioned within the coil system. It is necessary that this does not pose any risk to the patient. The implant continues to operate when rotated 30° horizontally and 43° vertically from the ideal position. If the implant is moved from the centre position, the force from the implant is reduced, making it a fail safe

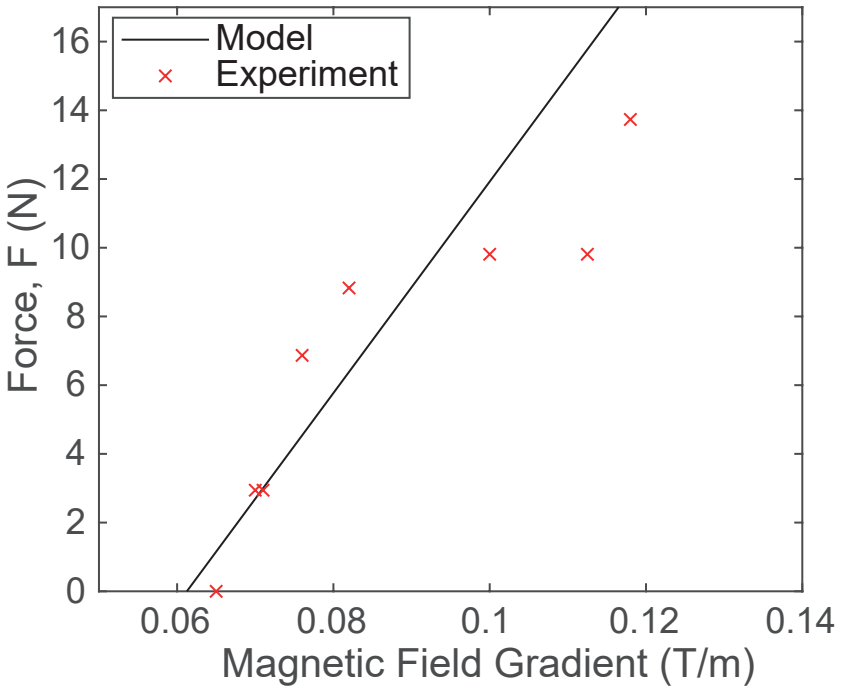

Figure 4.8.: Plot showing the implant force against magnetic field gradient. Each data point is from the motor run continuously for a length of time to demonstrate that it was capable of continuous operation at this load.

system.

The force from the implant on a phantom oesophagus (made from Ecoflex™ $00-30$, Smooth-On) was measured using a compression force sensor (Fig 4.9). The coils were activated until the target force was reached after 40 minutes, before being turned off. The implant can continue to hold the desired force for extended periods of time without requiring any energy input, as the mechanism is non-backdrivable. For the clinical application the magnetic field would only need to be applied for short periods at regular intervals with no need for the patient to remain in the coil system between these. To prevent to coils overheating, the data was collected across multiple runs.

The implant was demonstrated using an ex-vivo porcine oesophagus. The oesophagus was sourced from an abattoir and is a by-product form the meat industry. The oesophagus was sutured, with simple interrupted sutures, to the attachment rings of the implant (Fig. 4.10). The oesophagus measured 11 mm in diameter when relaxed. The distance between the two attachment rings was 75 mm before stretching. The implant was able to stretch the tissue 5 mm in

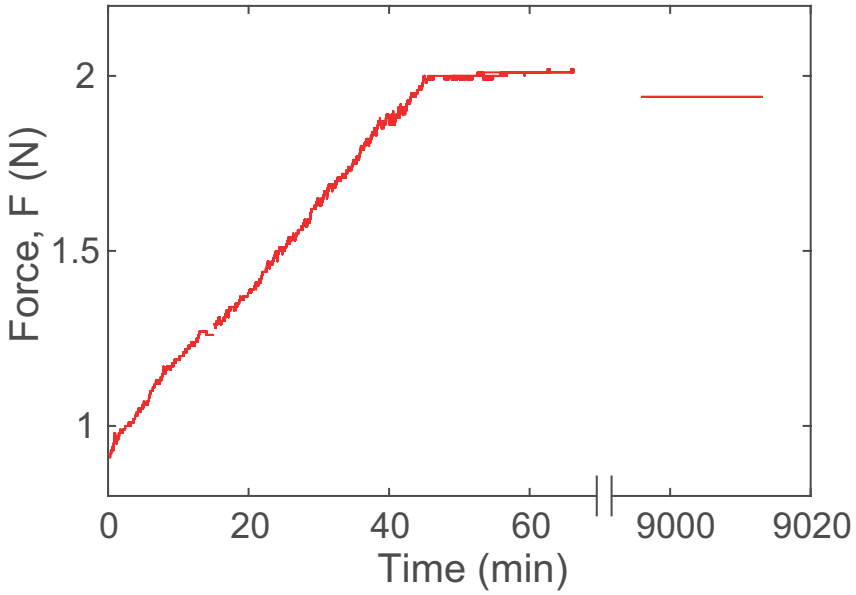

Figure 4.9.: The force from the implant on a phantom oesophagus against time, showing how once the input power is stopped the implant maintains a near-constant force, for multiple days if required, due to the mechanism being non-backdriveable. The coils were turned off after 40 minutes, once the implant reached the target force demonstrating the force holding capability of the implant. 2N of force has previously been shown to stimulate tissue growth.

10 minutes 42 seconds (6% extension) with a force of 2 N. These results show that the robotic implant is able to successfully apply the forces required to stimulate tissue regeneration to ex-vivo oesophageal tissue.

4.5 Discussion and Conclusions

This chapter presents a wirelessly actuated robotic implant for tissue regeneration. The implant has been demonstrated to produce 2N of force and hold the force without continued energy input. This has been demonstrated with both phantom and ex-vivo porcine oesophagi. 2 N of force have previously been shown to stimulate tissue growth, during animal trials.

The implant shown is driven by a novel magnetically actuated motor. The magnetic motor is driven by an externally applied uni-axial magnetic field gradient, and has been characterized for torque and speed. The motor experiences net zero force due to the magnetic force and weight countering mechanism, which was difficult to achieve with conventional approaches with

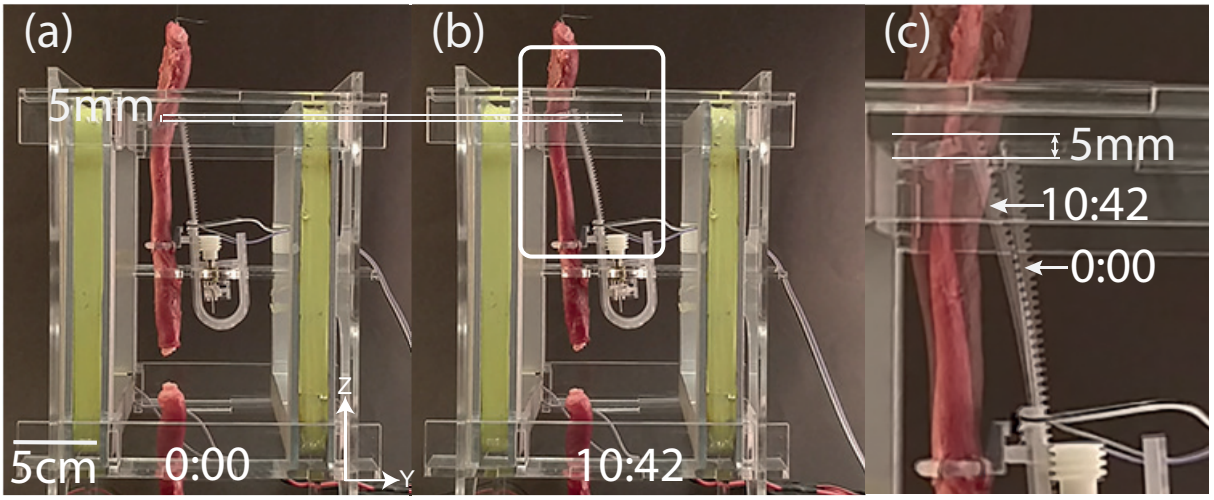

Figure 4.10.: Implant stretching an ex vivo porcine oesophagus by 5 mm over 10 minutes and 42 seconds. (a) The initial position at 0 seconds, showing the oesophagus in its relaxed position. (b) The oesophagus after 10 minutes and 42 seconds, the oesophagus has elongated by 5 mm. (c) Enlarged view showing the elongation of the oesophagus. See video 1 for more detail.

magnetic field. The uni-axial magnetic field application means the direction of torque producible from the motor depends on its orientation, hence versatile combinations of multiple motors in a single body are possible or multiple robots acting within the same work space, as shown in this chapter. The presented mechanics showed a promising scalability in the motor size down by 15% keeping the output torque above 1 mNm, and was fully functional when submerged in water, as there are no electronic parts.

Future work includes implementing position detection using hall effect sensors and scaling down the device by half using photolithography techniques.

Chapter 5

Remotely Actuated Magnetic Motor for Unconstrained Capsule Robots

5.1 Chapter preface

The content of this chapter is under review by a journal. [Cameron Duffield, Jialun Liu, Yuqi Zhang, George Ashton, Daniela Rus, Dana D. Damian, and Shuhei Miyashita. 'Remotely Actuated Magnetic Motor for Unconstrained Robotic Capsule'].The working mechanism of the motion was developed by Shuhei Miyashita, Daniela Rus, and Etienne Perroux. The work on button battery detection in this chapter was carried out by Yuqi Zhang as part of his MRes project. The experiments to find the constant for the soft magnets were carried out by George Ashton as part of his MEng project.

The realisation of ingestible robots for use inside the body, has long been hampered by the limitations of mechatronic components, including battery life, motor power and computational power. With the advent of capsule endoscopes guided by an external magnetic field, it is expected that an ingested mechanical capsule, will be able to perform clinical treatments utilising magnetically actuated motors. However, the conventional method of transferring magnetic torque to a remotely located magnetic body, by applying a rotating magnetic field, merely results in rotating the entire body, not the desired mechanism. In this study, this problem was solved by applying a magnetic field to a newly developed magnetic motor with a special magnet arrangement, allowing the body of the motor to remain stationary, while the output shaft rotates. The magnetic motor is lightweight (3.7 g) and has two magnets. When an external magnetic field is applied, the magnets rotate and align with it, before continuing to rotate, and aligning, due to their interaction with each other, to achieve a half rotation. A further half rotation is achieved by the magnetic field being applied in the opposite direction and the magnets' interaction, resulting in continuous drive of the motor. We investigated the characteristics of this motor and integrated it in a capsule that retrieves an accidentally ingested button battery from the stomach. The entire robotic capsule does not rotate due to this motor's characteristic of zero net torque. Instead, it's able to extend its arm, and sweeps it around itself, successfully retrieving a button battery under certain conditions. This study demonstrates how a capsule without electronics could achieve a series of mechanical functions within the body, opening up new possibilities for small-sized battery-less robots, together with the possibility of their further miniaturisation and the use of biodegradable materials.

5.2 Introduction

Despite the recent advancements towards the realisation of a small autonomous robots that can move inside the human body for non-invasive medical treatments, various technical obstacles must still be overcome to ensure their clinical viability. One of the most notable issues is the limited battery capacity due to the small size of the robot, which rules out the use of conventional electric motors. The alternative to using such motors is the use of external magnetic fields to directly apply torque to a ferromagnetic material in the robot. Such a driving magnetic field is either produced by electromagnetic coils [91–93] or permanent magnets [50] positioned outside the body. This method provides a means of wirelessly supplying power to the robot while inside the body and removes the necessity for electronics within the robot [6, 67, 82, 84, 85, 94, 95]. The targeted applications include capsule endoscopes navigating using either rolling [4], swimming [96], or self propelling using vibro-impact [10, 97], and used for biopsy [7, 98] and drug delivery [99, 100], medical implants [101], encapsulation and transportation [102], cutting with scissors [103], accessing constrained environments [104], and tissue penetration [105].

While a free-floating rigid object has six degrees of freedom (DOF), three translational and three rotational; five navigational DOF of a magnet have been achieved with eight electromagnetic coils to enable any magnetic field or field gradient to be produced in the workspace, allowing for translation in three axes and rotation in two [106], and a sixth DOF have been achieved by having a non-uniform magnetisation to act as a moment arm on the micro-robot [48]. If further DOF are required on a free-floating (or an unconstrained) body beyond the navigational function, a method of applying a further mode of magnetic field and an additional mechanism that can be driven by this field must be devised. For example, in [7, 107], a technique is used in which a permanent magnet in the capsule is moved using the gradient of the magnetic field. In [12], the extra DOF is achieved passively by the chemically-induced deployability of an origami structure in the presence of surrounding fluids. The previously developed magnetically actuated motors such as the device in [50], however, experience a net torque on the whole motor from the external magnetic field, resulting in the motor's pose being unstable without the robot being secured by reaction forces from its surroundings [1, 2]. It is therefore required that a robot using this motor is either

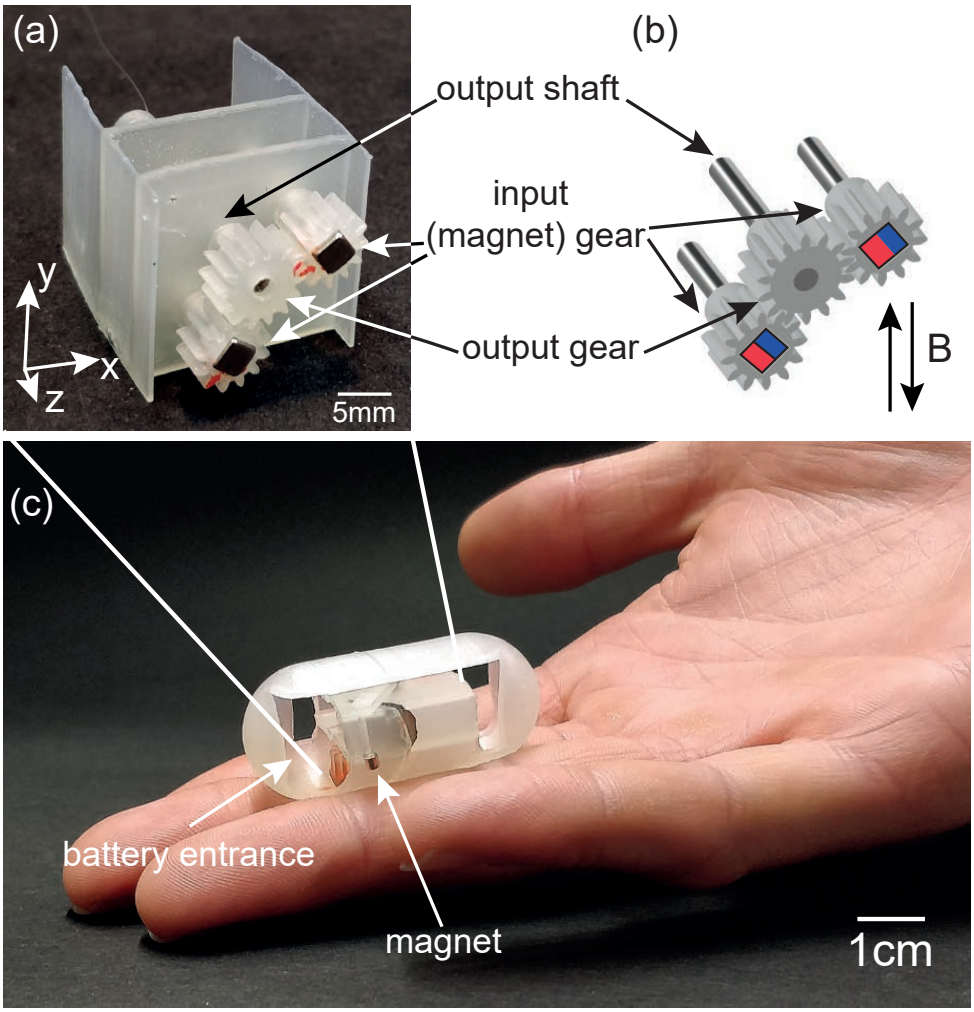

Figure 5.1.: Arrangement of magnetic motor, (a) photograph, and (b) CAD model. (c) Capsule incorporating the motor.

fixed in its environment or has a wide enough base to provide stability; in the case of [2] it is possible to use two counter-rotating motors to balance the torque and provide stability.

Taking these challenges into consideration, in this chapter, I present a centimetre-scale magnetically-actuated motor to enable extra degrees of freedom in an unconstrained capsule. The motor, shown in Fig. 5.1 (a) in a photo and (b) in a CAD model, utilises a periodically reversing external magnetic field to apply torque to a pair of permanent magnets. The motor consists of three meshing gears, the outer two of which have identical shapes and incorporate cubic permanent magnets (3 mm NdFeB) in specific orientations, called input gears. The output (central) gear is connected to the output shaft, delivering the total output torque to the desired load. The motor

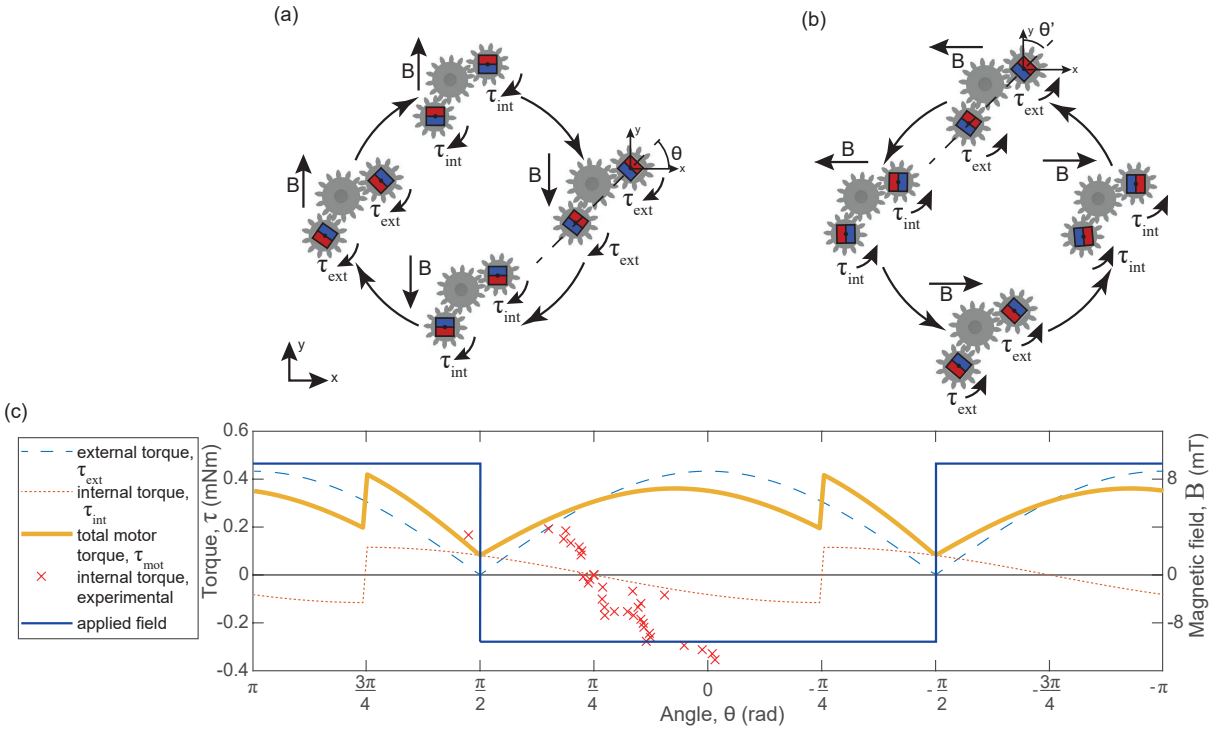

Figure 5.2.: Operation of the motor. (a) The operating cycle of the motor, showing how the magnets first align with the magnetic field next, as the magnetic field is reversed, the internal torque causes the magnets to align with each other. Then the magnets align with the magnetic field in the positive Y direction. Finally, as the field is again reversed, and the magnets align with each other and the cycle repeats (b) The motion of the motor running in reverse; but applying the magnetic field from the side the motor can be made to run in reverse. (c) A graph of the motor torque through the operating cycle, showing internal, external, and total torque, both modelled and experimental values.

primarily rotates due to the torque applied by the external magnetic field, with the interaction between the two magnets. In our system, the endoscopic capsule shown in Fig. 5.1 (c) is equipped with a ferro magnetic steel sheet that is magnetised by the applied magnetic field. As a rotating magnetic field is not being used to induce rotational motion, a ferromagnetic body can be integrated to align to the external magnetic field and stabilise the pose. When at an angle to the external magnetic field a torque acts on it, acting to align it with the magnetic field. This cancels the external torque acting on the motor, thereby achieving zero net torque applied to the capsule. This results in the capsule remaining stationary while the motor shaft is rotating.

As a proof of concept, this motor was used to actuate an arm coming out of the endoscopic capsule to "grab" and retrieve an accidentally ingested

button battery inside the body. Accidental ingestion of button batteries can be highly harmful, as short circuits through the tissue can lead to chemical burns in the gastro-intestinal tract from hydroxides formed [108]. This can lead to severe injury including erosion of tissue and paresis of vocal chords [109, 110], or if not treated early enough can lead to death as a result of fistulization and haemorrhage leading to blood loss into the stomach [111, 112]. Over $3,000$ people in the US alone accidentally ingest button batteries every year, requiring medical imaging techniques such as x-rays to identify the location [113] and potentially requiring endoscopy to remove the battery [114]. Lee et al. investigated the medical records of 76 children with ingested foreign objects, of these 12 involved batteries and 5 were in the stomach. Of the cases where the battery was in the stomach 1 patient had major complications, and 3 had moderate complications [114].

Alternatively systems for coating batteries with waterproof quantum tunnelling composite coatings to prevent them from conducting when ingested have been developed [115], however, this has seen little uptake. Previous work has been done to develop magnetically actuated robots for the removal of ingested button batteries; however, these do not encapsulate the battery, leaving the terminals exposed to potentially cause further damage during removal [11], or focus on dressing the wounds caused by the battery [116]. The proposed capsule, alongside a method of remotely localising a button battery and identifying its type using an array of Hall-effect sensors, building on the work presented in [117], acts as a first-of-a-kind concept that would be able to augment the arsenal of treatments available for this scenario.

5.3 Methods

This section first details the mechanics of the motor, followed by the mechanics of the capsule that houses the motor and retrieves a battery. Since there is a limit to the size of the button batteries that can be retrieved due to the limited size of the capsule, a wireless identification method for the type of button battery is subsequently presented.

5.3.1 Motor Design and Operation

The motor consists of two input (magnet) gears each containing a $3\,$mm cube magnet, these magnets sit on a line at $\frac{\pi}{4}$ rad to the axis of the magnetic field (Fig. 5.1). The magnet gears have 12 teeth of $0.5\,$mm modulus. These gears mesh with a central gear connected to the output shaft, allowing the torque from both magnets to be transmitted to the load. The centre gear has 14 teeth, giving a gear ratio of $1:1.6667$, the non-integer ratio helps to reduce hunting by ensuring even wear on the gear teeth. By changing the gear ratio of the input gears and the output gear, it is possible to change the output torque (or angular velocity) of the output shaft. All results are shown as for a $1:1$ gear ratio.

Fig. 5.2 (a) shows the operating cycle of the motor in the forward (clockwise) direction. Initially the magnets are aligned with each other due to the interaction of their magnetic fields. Applying the magnetic field exerts a torque on the two magnets, resulting in a rotation of $\frac{3\pi}{4}\,rad$ to align with the external magnetic field, $\theta = \frac{\pi}{2}\,rad$). This is denoted as the "external torque" (τ_{ext}). The interaction of the magnetic fields from the two magnets apply a further "internal torque" (τ_{int}) as the magnets move to align with each other, resulting in an additional rotation of $\frac{\pi}{4}\,rad$ ($\theta = \frac{\pi}{4}\,rad$). Applying the magnetic field in reverse then results in the magnets rotating a further $\frac{3\pi}{4}\,rad$ in the same direction ($\theta = -\frac{\pi}{2}\,rad$). The magnets align with each other, completing the last $\frac{\pi}{4}\,rad$, achieving a full revolution ($\theta = -\frac{3\pi}{4}\,rad$), ready for the cycle to restart. Repeating this alternating external magnetic field results in a continuous rotation of the output shaft.

Fig. 5.2 (b) shows how the motor can be reversed by applying the alternating magnetic field from the side. θ is transposed to become θ' which is clockwise from the positive y axis to keep the angles consistent with the forwards rotation. The magnets are initially aligned with each other due to the internal torque ($\theta = \frac{\pi}{4}\,rad$). The magnets then align with the external magnetic field due to the external torque ($\theta = -\frac{\pi}{2}\,rad$). The internal torque again makes the magnets align with each other ($\theta = -\frac{3\pi}{4}\,rad$). The magnets align with the external magnetic field ($\theta = \frac{\pi}{2}\,rad$), ready to restart the cycle. Fig. 5.2 (c) shows the torques of the motor through the cycle. The internal torque is the torque of the magnets acting on each other, while the external torque is the torque from the external magnetic field acting on the magnets. The two of these sum to give the total output torque of the motor. It can be seen how the internal torque

reverses as the magnets pass through parallel at $\frac{3\pi}{4}$ rad and $-\frac{\pi}{4}$ rad, and how the negative internal torque, from $\frac{\pi}{4}$ rad to -$\frac{\pi}{4}$ rad and from -$\frac{3\pi}{4}$ rad to -π rad and π rad to $\frac{3\pi}{4}$ rad, reduces the total motor torque compared with the external torque.

5.3.2 Capsule Design

We present a two-step approach consisting of battery type identification and battery retrieval and encapsulation using the capsule. An array of Hall-effect sensors are used to determine the type and location of an ingested battery, and thus confirm if it is a size that the capsule is able to encapsulate. The capsule, powered by the novel magnetic motor, is then used to encapsulate the button battery for safe removal from the body. Fig. 5.3 shows the capsule for the retrieval of ingested button batteries from the stomach with Fig. 5.3 (a) an overview of the design and Fig. 5.3 (b) a top view showing the area swept by the arm. The capsule is 45 mm long and 20 mm in diameter, and the arm is 15 mm from the centre-line of the capsule. The capsule has a motor in the base to keep the weight low and help the capsule naturally sit in an upright position. The output shaft of the motor is connected to an arm, initially within the capsule, with a 2 mm cylindrical magnet on the end. When the motor is actuated the arm rotates, sweeping a circular area. When the magnet is close to a button battery it attracts the battery, connecting it to the arm. The arm continues on its circular trajectory, pulling the button battery in through the capsule entrance. The button battery is captive in the capsule, as it is too large to fit out through the arm exit from the capsule, while the arm is able to pass through the exit if it is not connected to a battery.

The capsule also incorporates the magnetic pose control system for the capsule to rotate to the correct orientation. This is achieved by two low carbon steel sheets, each measuring $10 \times 5 \times 0.127$ mm. Being a ferromagnetic material, when in a magnetic field the sheet becomes temporarily magnetised, causing a torque to act on the steel sheet, thus making the entire capsule align with the magnetic field. This generates a torque that cancels the external torque, thereby achieving zero net torque applied to the capsule. This results in the unconstrained ("free-floating") capsule remaining stationary while the motor shaft is rotating. When the magnetic field reverses the magnetisation of the steel also reverses. This ensures the capsule remains in the same orientation as the magnetic field alternates. Due to the symmetry of the

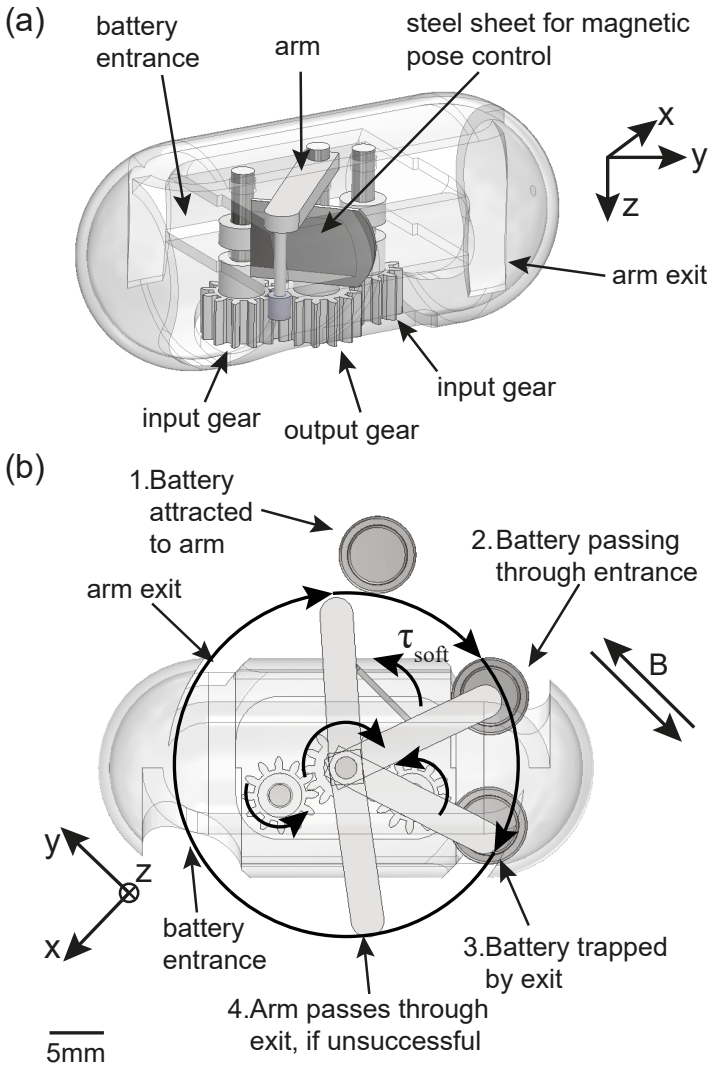

Figure 5.3.: Details of the parts of the capsule (a) CAD model. (b) Diagram showing the region swept by the arm, illustrating an LR261 battery passing through the entrance and being trapped by the narrow exit from the capsule

capsule there are two possible orientations. The steel is positioned $\frac{\pi}{4}$ rad to the axis of the capsule to correctly orientate the motor relative to the magnetic field, while also maximising the space within the capsule by allowing the motor to be along the centre-line of the capsule. In Fig. 5.4 it can be seen that within 2 s of the alternating magnetic field being applied the capsule is correctly orientated relative to the magnetic field. This is shown in Supplementary Video 1. When the pose of the capsule is disturbed, it again returns to the correct orientation and remains there until the magnetic field is switched off. There is a small steady state error in the angle of the capsule, well within what is acceptable for the operation of the motor. This is caused by the torque of the

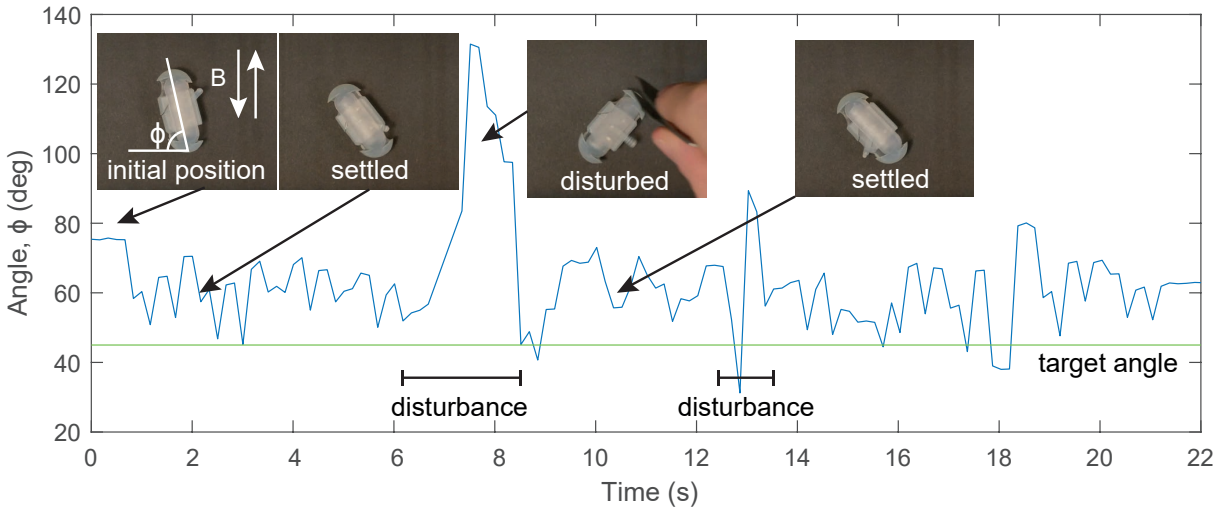

Figure 5.4.: Demonstration of the magnetic pose control, with a plot showing angle of the capsule to the horizontal, and disturbances at 7 s and 13 s and the capsule returning to the correct orientation. The capsule is initially at the wrong angle to the magnetic field to operate correctly. After 6 s the capsule experiences a disturbance, forcing it away from the correct angle. The capsule then returns to the correct orientation close to $\frac{\pi}{4}$ rad to the magnetic field, allowing the motor to operate well. The capsule then remains in the desired position as the motor continues to run. There is some steady state error in the angle of the capsule, this is small enough it doesn't impact the operation.

motor being applied to the capsule, the steel sheet needs to be at an angle to the magnetic field to experience a torque to balance this.

5.3.3 Model

A mathematical model was made to describe the torque produced by the motor at a given angle and external magnetic field. The external torque (τ_{ext}) is the torque from the external magnetic field acting on the magnets in the motor, the internal torque (τ_{int}) is the torque from the two magnets acting on each other, and the motor torque (τ_{mot}) is the sum of the two to give the total output from the motor. The magnetic torque ($\vec{\tau}$) on a magnetic dipole in a magnetic field is given by:

$$\vec{\tau} = \vec{m} \times \vec{B} \tag{5.1}$$

where $\vec{m}$ is the magnetic moment, and $\vec{B}$ is the magnetic flux density. Eq. (5.1) is used to find the torque applied to the motor by the external magnetic field (τ_{ext}), given by:

$$\tau_{ext} = 2\|\vec{m}\|\|\vec{B}\| \cos\theta, \tag{5.2}$$

where θ is the angle of the magnet counter-clockwise from the positive x-axis as defined in Fig 5.2. The 2 term comes from the two magnets, with equal magnetic moments, being subject to the same magnetic field.

The motor also has an internal torque from the interaction between the two magnets. The magnetic flux density ($\vec{B}$) from a dipole using the Ampère model [118] is given by:

$$\vec{B}(\vec{m},\vec{p}) = \frac{\mu_0}{4\pi\|\vec{p}\|^3}\left(3(\vec{m}\cdot\hat{p})\hat{p} - \vec{m}\right) + \frac{2\mu_0}{3}\vec{m}\delta^3(\vec{p}), \tag{5.3}$$

where $\vec{m}$ is the magnetic moment ($0.0258\,\mathrm{Am}^2$ for the magnets used), μ_0 is the permeability of free space ($1.256 \times 10^{-6}\,\mathrm{NA}^{-2}$), p is the distance from the magnetic dipole, $\vec{p}$ is the position vector, and $\delta^3(\vec{p})$ is the three dimensional dirac delta function. The Ampère model assumes a perfect magnetic dipole, and can be used to approximate the field of a permanent magnet at distances sufficient that the size and shape of the magnet are not significant. This can be simplified to give the magnetic field parallel (B_z) and perpendicular (B_x) to the axis of the magnetic dipole:

$$B_x(\vec{p}) = \frac{\mu_0}{4\pi}\|\vec{m}\|\left(\frac{3\cos\beta\sin\beta}{\|\vec{p}\|^3}\right), \tag{5.4}$$

$$B_z(\vec{p}) = \frac{\mu_0}{4\pi}\|\vec{m}\|\left(\frac{3\cos^2\beta - 1}{\|\vec{p}\|^3}\right), \tag{5.5}$$

where β is the angle from the axis of magnetic dipole. Using Eq. (5.1) and the geometry of the system we can get the torque between the two magnets (τ_{int}) for a given angle of rotation:

$$\tau_{int} = \begin{cases} 2\dfrac{3\mu_0\|\vec{m}\|^2}{8\pi r^3}\cos\left(\theta - \dfrac{3\pi}{4}\right), & \sin\left(\theta + \dfrac{\pi}{4}\right) > 0 \\ 2\dfrac{3\mu_0\|\vec{m}\|^2}{8\pi r^3}\cos\left(\theta + \dfrac{\pi}{4}\right), & \sin\left(\theta + \dfrac{\pi}{4}\right) < 0, \end{cases} \tag{5.6}$$

where r is the distance between the centers of the magnets. When $\sin(\theta + \frac{\pi}{4}) = 0$, τ_{int} is undefined due to the discontinuity as the magnets are parallel to each other.

To get the total torque output from the motor (τ_{mot}) Eq. (5.2) is added to Eq. (5.6) giving:

$$
\begin{aligned}
\tau_{mot} &= \tau_{int} + \tau_{ext} \\
&= \begin{cases} 2\frac{3\mu_0\|\vec{m}\|^2}{8\pi r^3}\cos\left(\theta - \frac{3\pi}{4}\right) + 2\|\vec{m}\|\|\vec{B}\|\cos\theta, \\ \qquad\qquad \sin\left(\theta + \frac{\pi}{4}\right) > 0 \\ 2\frac{3\mu_0\|\vec{m}\|^2}{8\pi r^3}\cos\left(\theta + \frac{\pi}{4}\right) + 2\|\vec{m}\|\|\vec{B}\|\cos\theta, \\ \qquad\qquad \sin\left(\theta + \frac{\pi}{4}\right) < 0\,. \end{cases}
\end{aligned} \tag{5.7}
$$

The torque output from the motor is shown in Fig. 5.2 (e) alongside the corresponding positions of the gears. This shows the repeating pattern of the internal and external torques and the internal torque reversal at the point where the magnets are parallel ($\theta = \frac{3\pi}{4}$ rad and $\theta = -\frac{\pi}{4}$ rad).

This model can be used to optimise the design parameters of the motor for the intended application. The main parameter to change is the distance between the two magnets; this is a compromise between having close magnets to maximise internal torque, but not so close that the internal torque is too great for the external torque to overcome. Fig. 5.5 shows the effect of changing the magnet spacing. Fig. 5.5 (a) shows how the torque profile of the motor changes with the magnet spacing, for a magnetic field of 7 mT. It can be seen that, if the magnets are too close together, the torque can go negative, meaning the internal torque is opposing motion and is too great to be overcome by the external torque. Conversely, if the magnets are too far apart, the total torque becomes very low at angles were there is little external torque being applied. Fig. 5.5 (b) shows the effect of changing the magnet spacing on the minimum torque produced by the motor at any point in the cycle, for a range of applied magnetic fields. This shows how, by increasing the magnetic field, the magnets can be placed closer together to increase the output torque. Fig. 5.5 (c) shows the optimum magnet spacing to maximise output torque for an applied magnetic field. This is found by taking the magnet spacing at peak of each curve in Fig. 5.5 (b) and plotting this against the magnetic field strength.

To operate the motor effectively, it is essential that the motor is correctly orientated relative to the magnetic field. To achieve this, a system of magnetic pose control has been developed using a sheet steel in the capsule which acts as a soft magnet, aligning with the magnetic field. When in a magnetic field the steel is magnetised with the magnetic moment (m) proportional to the

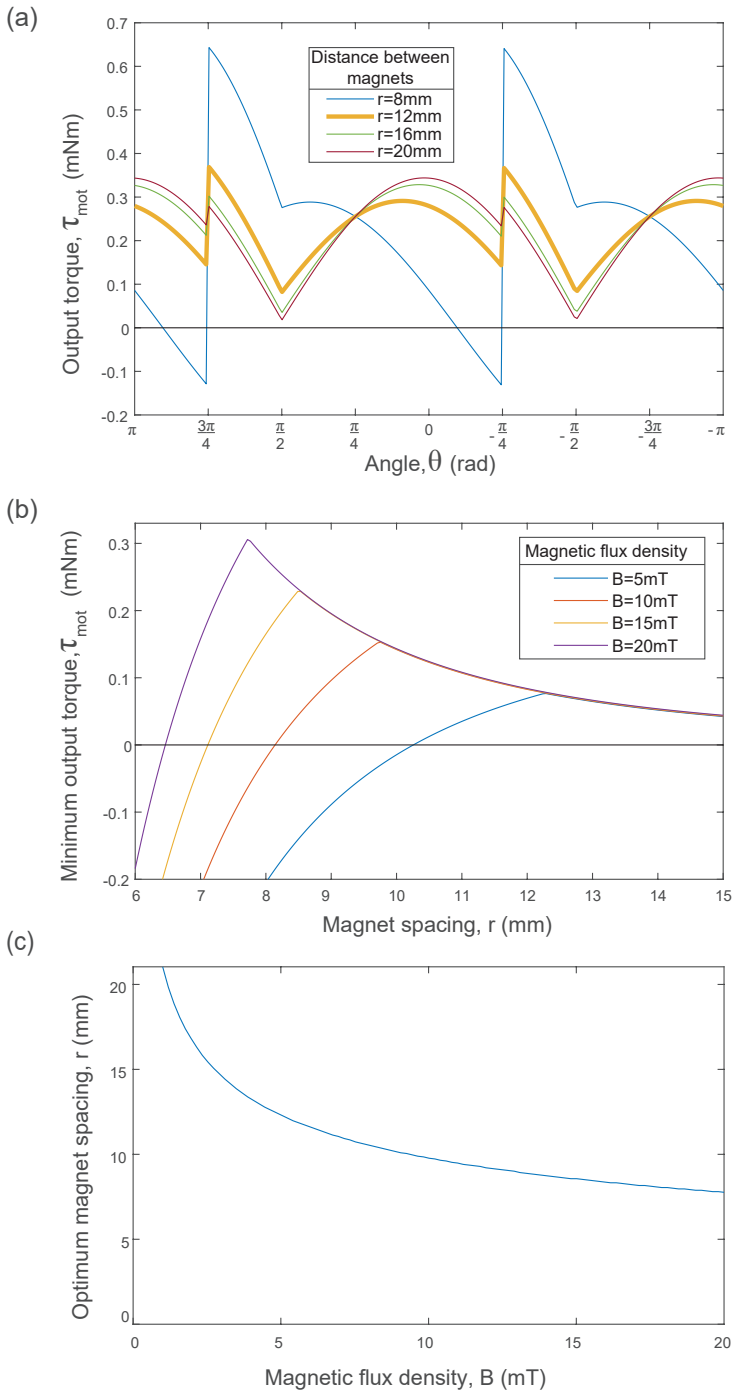

Figure 5.5.: The effect of magnet spacing on the torque output of a motor using 3 mm cubic magnets. (a) The effect of magnet spacing on the torque profile of the motor for a 7 mT magnetic field, the spacing of 12 mm used in this chapter is shown in yellow (b) The output torque of the motor against the spacing between the magnets for a range of magnetic fields. This is the minimum output torque from any point in the cycle. (c) the optimum magnet spacing to maximise output torque for a given magnetic field strength

applied magnetic field (B). Using Eq. (5.1) the torque acting on a soft magnet (τ_{soft}) in a magnetic field can be given by:

$$\tau_{soft} = k\|\vec{B}\|^3 \sin\alpha, \tag{5.8}$$

where k is an empirical constant specific to the shape and material used, and α is the angle between the major axis of the soft magnet and the magnetic field. For the sheet used in this study k was found to be 380×10^3 Nm T^{-3} by placing it on a torsional spring in a known magnetic field and comparing the deflection with that of a known magnet. Supplementary Material 5.3.5 shows the details of the experimental setup.

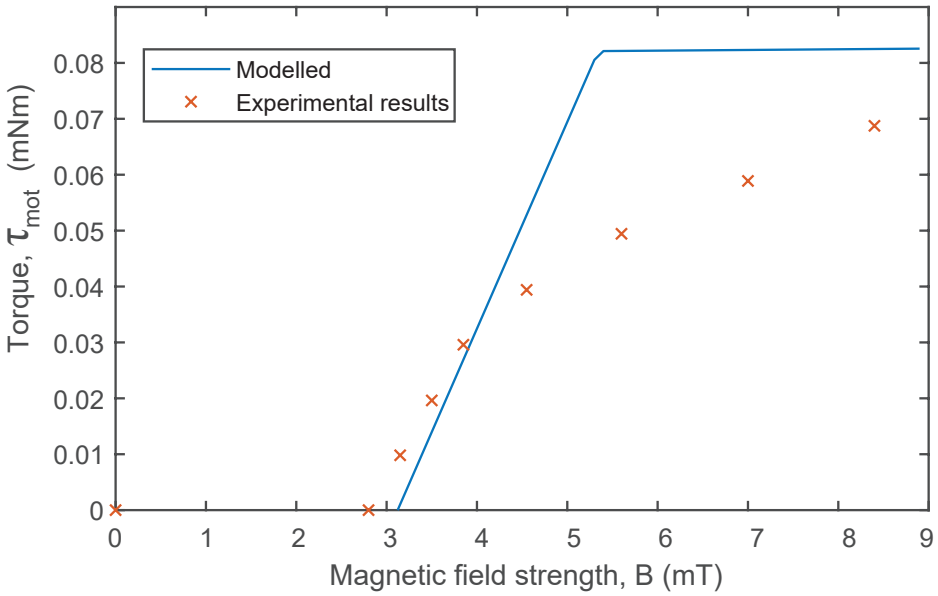

Figure 5.6.: Torque of the motor against magnetic field strength, experimental and modelled. There is no torque below the field strength required to overcome the internal torque. It then increases with field strength up until the point where internal torque is the limiting factor, then is constant with increasing field strength. Each data point is from the motor run continuously for a length of time to demonstrate that it was capable of continuous operation at this load.

Fig. 5.6 shows the output torque (τ_{mot}) against magnetic field strength. Each data point is from the motor run continuously for a length of time to demonstrate that it was capable of continuous operation at this load. The output torque is considered to be the least torque produced at any point in the cycle, Section 5.3.5 shows the experimental setup. There is no torque below the field strength required to overcome the internal torque of the motor. It then increases with the field strength up until the point where the internal torque becomes the limiting factor. From then on, the output torque remains constant. The model is a good

fit for the experimental data where the magnetic flux density is low. There is, however, some discrepancy between the model and the experimental data around the region where the motor transitions from being limited by the external torque (τ_{ext}) to the internal torque (τ_{int}) being the limiting factor.

The angular velocity of the motor (ω) is proportional to the actuation frequency (f_a), up to the step-out frequency (f_{so}):

$$\omega = 2\pi f_a. \tag{5.9}$$

When the actuation frequency exceeds the step-out frequency the motor speed decreases as the actuation frequency, further increases. This has been shown for both swimming [89] and rolling robots [88] and is given by:

$$\omega = 2\pi(f_a - \sqrt{f_a^2 - f_{so}^2}). \tag{5.10}$$

Fig. 5.7 shows the angular velocity increasing proportionally to the actuation frequency, the model shows a good fit to the data. It can be seen that there is no stepping out within the frequency range of the coil system used. Each data point is the average angular velocity over multiple revolutions.

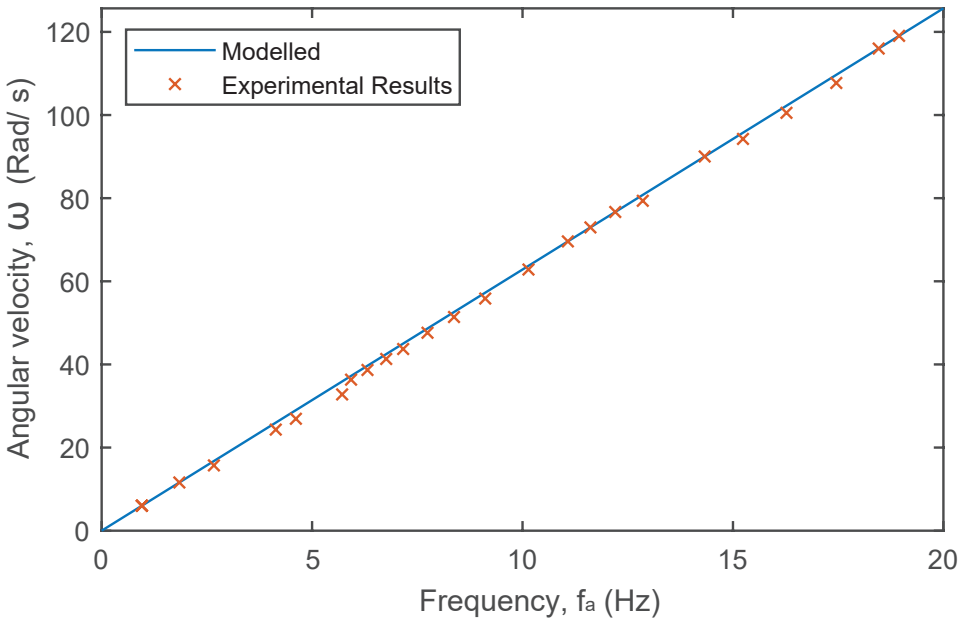

Figure 5.7.: Angular velocity of the motor against actuation frequency, experimental and modelled. The figure shows the speed increasing proportionally to the actuation frequency. The motor does not step out within the frequency range of the coil system. Each data point is the average angular velocity over multiple revolutions.

5.3.4 Fabrication

The main components of the capsule were manufactured with Form 3 SLA printer using durable resin (Formlabs), durable resin was chosen as it exhibits similar material properties to other resins produced by Formlabs which are certified for medical use, but is more transparent, making the capsule mechanism easier to see. The magnets used were 3 mm cubic neodymium iron boron (NdFeB) (Supermagnete). For the steel sheet to control the capsule orientation, two low carbon steel sheets (RS, full hard, cold rolled) were used. The ferromagnetic steel has no permanent magnetism, however, it becomes magnetised when placed within a magnetic field. The capsule developed weighs just 5.13 g and measures 45 mm in length and 20 mm in diameter, and the motor on its own weighs 3.7 g, measuring 20 mm by 20 mm by 20 mm.

5.3.5 Experimental Setup

The experimental setups used in this chapter to characterise the properties of the motor and test the capsule are outlined in this section.

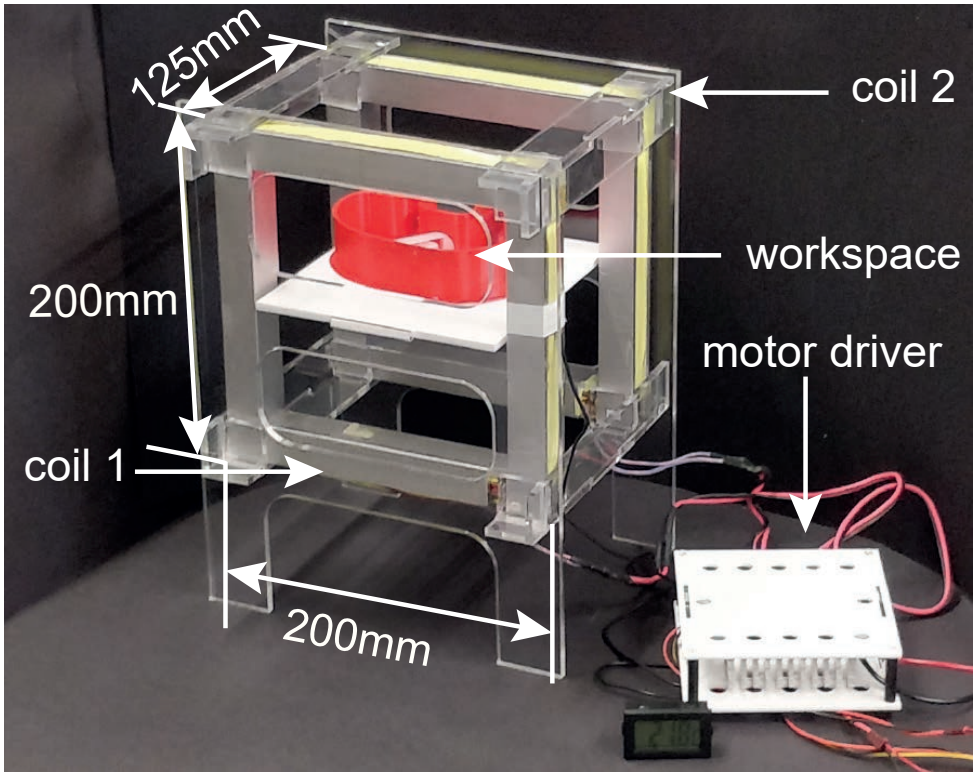

Figure 5.8.: The coil system used for capsule demonstrations, with stomach model shown on the workspace. Coils 1 and 2 are identical and parallel allowing a near uniform magnetic field to be produced across the entire workspace.

Capsule actuation by the electromagnetic coil system.

For the capsule demonstration, a horizontal magnetic field is required, to extend the workspace, a pair of coils were used (Fig. 5.8). Magnetic fields of up to $14\,\text{mT}$ were applied horizontally from two square coils of $200\,\text{mm}$ side length and $125\,\text{mm}$ apart with a horizontal workspace along the center axis of the coils. The coil system is designed to fit an infant with the stomach within the workspace. The magnetic fields used are well below the static magnetic field strength of 0.046 - $8\,\text{T}$ of MRI machines [90], this shows that these magnetic field can safely be used in a medical setting. All coils were controlled using Sabertooth 2x32 motor drivers (Dimension Engineering).

Magnetic moment of a soft magnet

To find the constant of magnetism, k, in Eq. (5.8) torque acting on a representative sample of steel sheet of the same dimensions as that used in the capsule was experimentally measured.

The torque acting on the material for a given magnetic field and angle were found by measuring the angular deflection of an elastomeric (Ecoflex 00-10, Smooth-on) torsional spring. The properties of the spring were found by applying a known torque using a known magnet in a known magnetic field. The experimental setup is shown in Fig. 5.9.

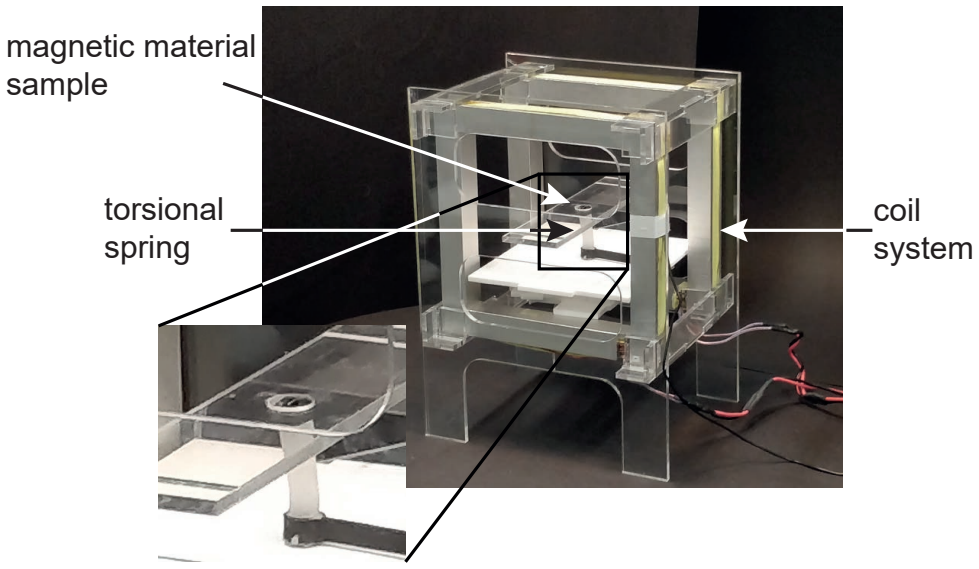

Figure 5.9.: Figure of the experimental set up used to measure the torque acting on a piece of magnetic material, showing details of the elastomeric torsional spring used to measure torque.

Torque measurements

The output torque of the motor was measured by winding a mono-filament thread around the output shaft, passing it over a pulley, and down to a known mass (Fig. 5.10). This applies a known torque as a load to the motor. The mass was increased until the motor was unable to turn to get the stall torque for an applied magnetic field. The magnetic field was created using a single, horizontal, magnetic coil 200 mm in diameter and 40 mm below the work surface. The internal torque was measured using the same set up, but without applying an external magnetic field and measuring the angle of the magnets.

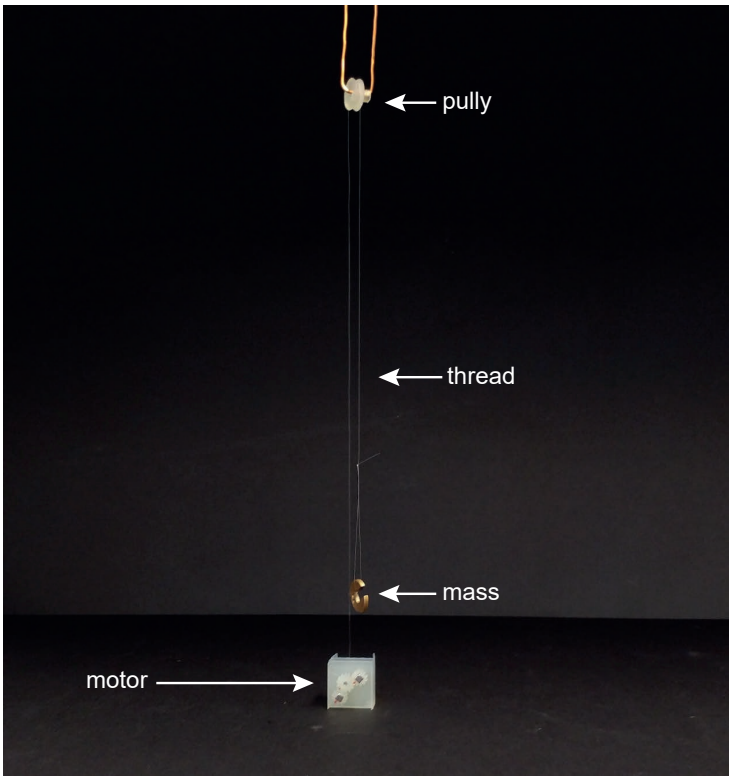

Figure 5.10.: Figure of the set up for measuring the torque of the motor showing the known mass used to apply a load via a mono-filament thread. The coil is below the work-surface

5.3.6 Battery type detection

The localisation and detection of the type of button battery are based on the trilateration method, a common method for localisation [117]. An array of Hall-effect sensors and a magnetic coil are placed below the workspace where a button battery is placed. For button battery detection tests, a single 200 mm diameter electromagnetic coil embedded 40 mm below the workspace, capable of magnetic fields of up to 9 mT, was additionally used, as

used in [117]. The magnetic coil produces vertical magnetic field to magnetise the button battery. The hall-effect sensors read the magnetic flux density of the magnetised button battery and then classify the type of the button battery using the sensor readings. The Hall-effect sensors used in this setup are A1389 analogue linear Hall-effect sensors (Allegro Inc.). These sensors are arranged in an array on a printed circuit board (PCB) which is positioned on a 2D plane. The total sensing area provided by the PCB is $32.15\,\text{cm}^2$, allowing for accurate detection and measurement of magnetic fields in the surrounding environment. Three neighbouring sensors are arranged in an equilateral triangle with a side length of $15\,\text{mm}$. The magnetic field strengths read by the three sensors are converted to distances to run the classification algorithm for determining the button battery type.

Among the commonly used button batteries, three representative sizes of batteries, LR621 ($\varnothing 7 \times 2.2\,\text{mm}$), LR44 ($\varnothing 11.4 \times 5\,\text{mm}$), and CR2032 ($\varnothing 19 \times 3\,\text{mm}$) (Fig. 5.11 (b)) were selected. When a button battery is placed in the working area above the Hall-effect sensor array, the magnetic coil produces vertical magnetic fields to magnetise the button battery, and then the magnetic flux density of the magnetised button battery is read by the three nearest Hall-effect sensors. The nearest Hall-effect sensors receive higher magnetic flux densities than the rest of the sensors, therefore by finding the largest three sensor readings, the nearest three sensors can be determined. By using the data reading from the nearest three sensors, the location of the button battery can be calculated [117], and the button battery type can be detected. 90 sets of the data from the nearest three sensors were taken by placing three different types of batteries above the sensor array and reading the sensor data. The obtained dataset is the training set for the support vector machine (SVM) classification algorithm which is used to classify the button battery type. The dataset and the two classification surfaces are shown in Fig. 5.11 (a). It can be seen that the accuracy of classification using the classification surfaces is 81% for LR621, 58% for LR44, and 72% for CR2032.

5.4 Results

The results of the experiments carried out are outlined in this section. They are split into the results of the battery type detection and the success rate of the capsule at encapsulating a button battery in different scenarios.

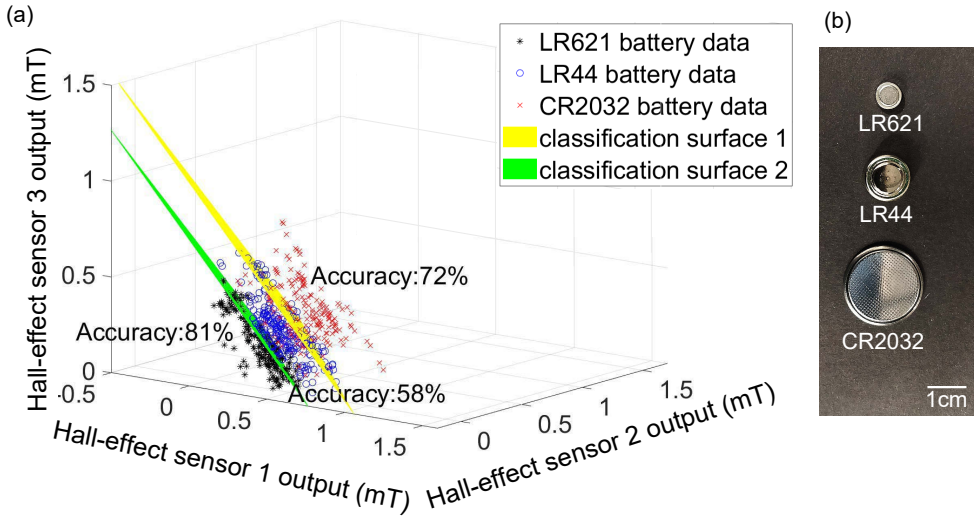

Figure 5.11.: (a) The dataset for SVM classification algorithm and the classification surfaces. (b) The batteries used for the tests.

5.4.1 Battery detection

For battery classification, three different types of batteries, LR621, LR44, and CR2032 were placed in turn on the workspace and ran the SVM classification algorithm to detect the button battery type. In our setup, there is a 6 mm gap between the workspace and the Hall-effect sensor array. It is possible to increase this distance by generating stronger magnetic fields to magnetise the button battery. However, the strength of the magnetic field that can be produced is limited by the magnetic coil available in our system. In order to improve the accuracy of the classification, the classification algorithm was run five times for each button battery sample. The button battery type which is the most frequent was chosen as the final detection result. The detection results are shown in Fig. 5.12. The figure depicts the proportion of tests in which the battery was accurately recognised, and in cases where the button battery type was misidentified, the type that was identified instead. The LR621 was correctly identified 93% of the time and it can only be misidentified as LR44; the LR44 was correctly identified 72% with one third of the incorrect identifications being CR2032 and the remainder being LR621; and the CR2032 was correctly identified 89% of the time with 90% of misidentifications being as LR44. This indicates that the average accuracy rate of the proposed classification method is 85% across all battery types. In cases where mistakes occur, the batteries are identified incorrectly as one of similar dimensions.

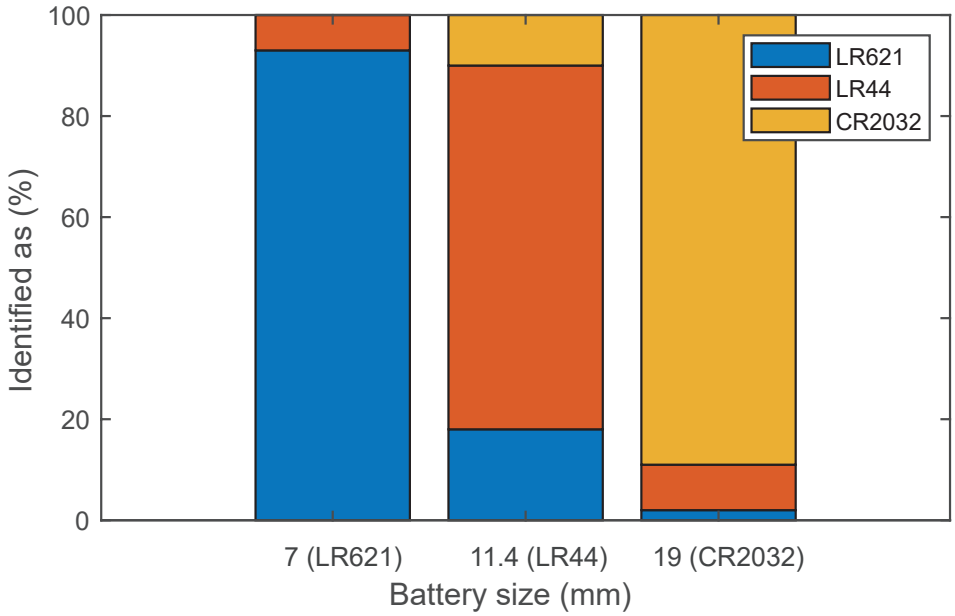

Figure 5.12.: The accuracy of identifying the button battery type among five trials.

5.4.2 Capsule encapsulation test

The proposed capsule was tested using an LR621 battery, (Fig. 5.13) in a model of a child's stomach (PLA). The capsule starts near the battery (Fig. 5.13 (a)). When the alternating magnetic field is applied the arm begins to rotate (Fig. 5.13 (b)) while the orientation of the capsule remains stable. It can be seen that when the arm swings over the button battery (Fig. 5.13 (c)) the button battery is attracted to the magnet and is picked up by the arm. The arm then continues on its path into the body of the capsule, through the battery entrance, with the button battery (Fig. 5.13 (d)), preventing it from coming into contact with the tissue. The button battery is then trapped by the narrower arm exit, preventing the arm from continuing out of the capsule. In the figure the battery is horizontal, this is the position where the battery sits naturally. If the battery were to be balanced on its edge, the battery would be closer to the magnet as the arm passes over to it, making it easier for the capsule to pick up. Fig. 5.14 shows a failed attempt at retrieving the button battery, Fig. 5.13 (a) the capsule is in position ready to encapsulate the battery, Fig. 5.14 (b) the capsule arm rotates to pick up the battery, Fig. 5.14 (c) the battery is attracted to the motor magnets, Fig. 5.14 (d) the motor is jammed by the battery connected to the motor magnets, preventing further operation of the motor and the battery from being correctly encapsulated.

These tests were preformed on a hard plastic surface, which differs from the soft

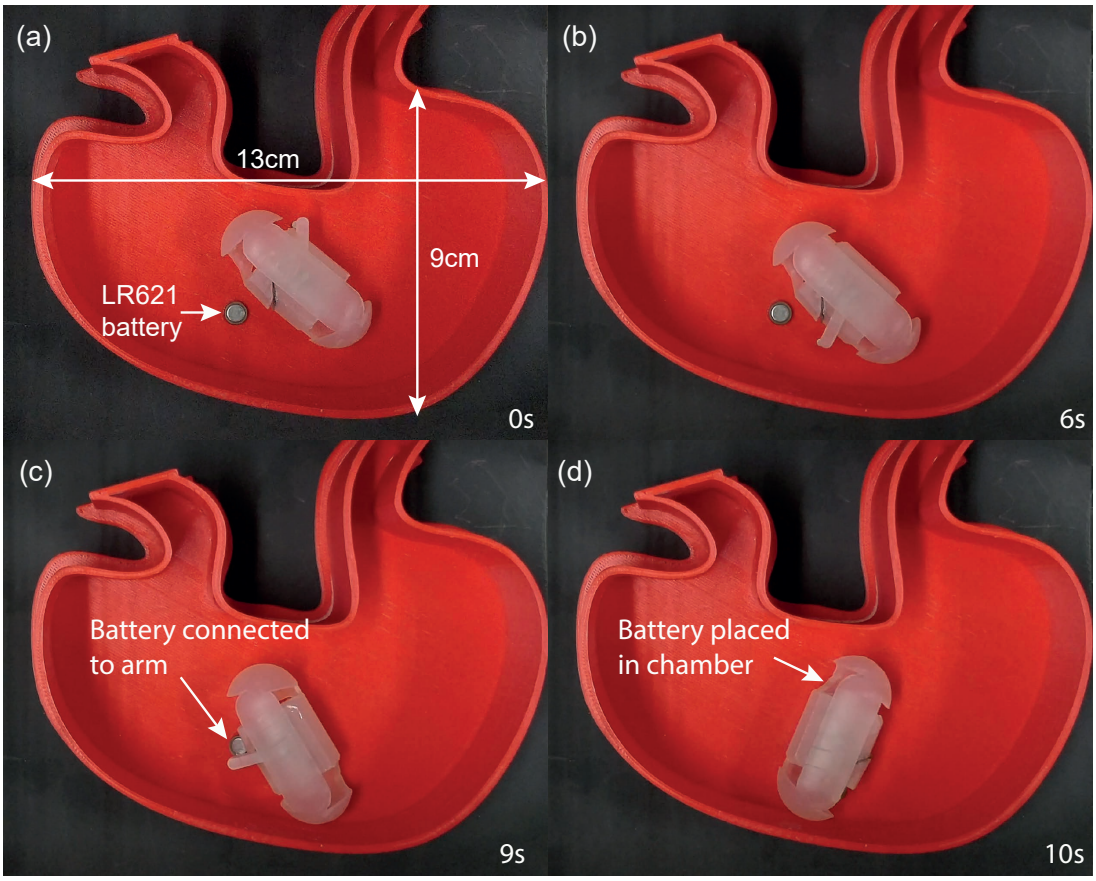

Figure 5.13.: A demonstration of the capsule encapsulating a button battery in a child-sized stomach model. (a) In position ready to capture the battery. (b) Arm rotating to sweep over the battery. (c) Battery connecting to the magnet on the end of the arm. (d) Placing the battery in the storage area ready for transport out of the body.

and uneven surface of the inside of the stomach. The capsule as also been tested on a rough surface (1000 grit silicon carbide paper, RS), it was found that the increased friction made the angle of the capsule more stable, but it took longer to rotate to the correct orientation. It is also possible that the capsule would become stuck in a ridge in the surface of the stomach, and be unable to correctly align with the magnetic field. The capsule would need to be sightly modified by covering the exposed gears, to prevent pinching of the tissue.

The success rate of the capsule at encasing the button battery is summarised in Fig. 5.15. Of the trials (15 trials) where the button battery was within 5 mm of the capsule 47% of times the button battery was successfully placed within the capsule and 73% of times it was successfully picked up by the arm. Of the times the battery was outside of the workspace (more than 5 mm from the capsule) (15 trials) the battery was successfully placed within the chamber 13% of times

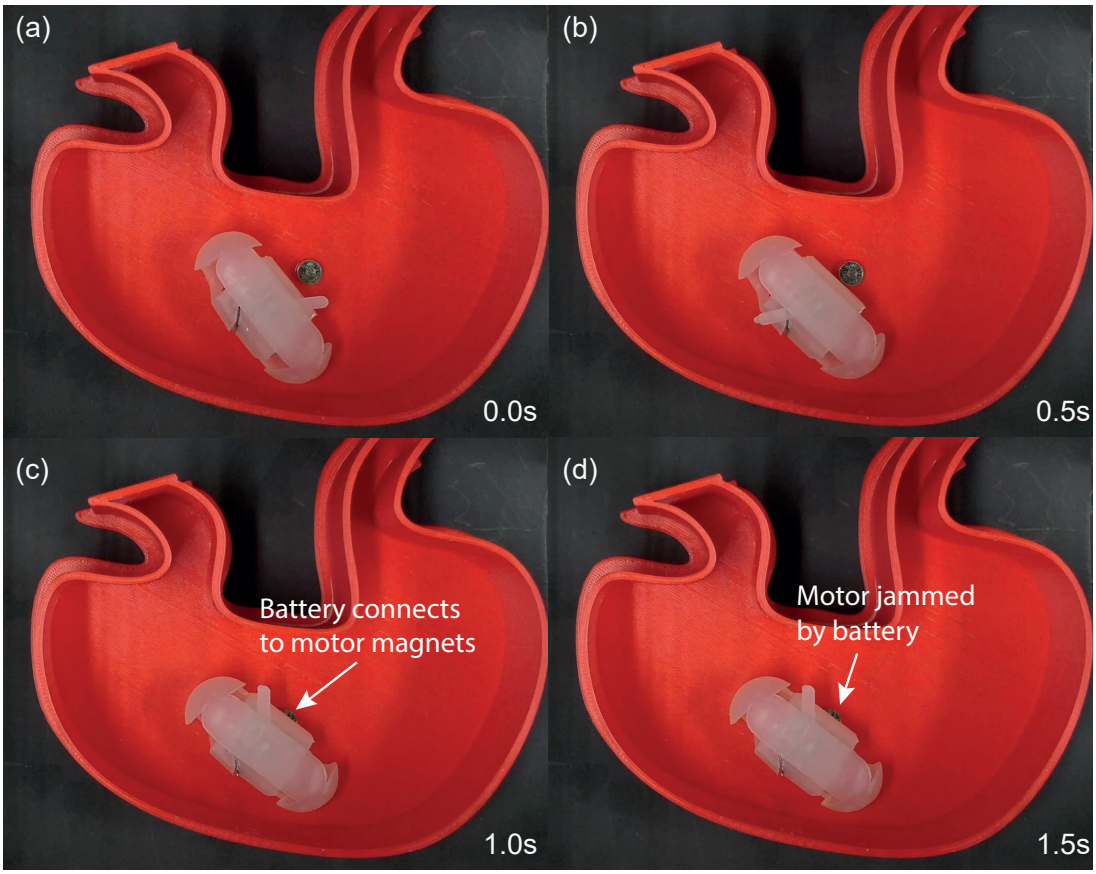

Figure 5.14.: The failure of the capsule to encapsulate the battery: (e) The capsule in position ready to encapsulate the battery. (f) The capsule arm rotating to pick up the battery, the battery moving towards the motor magnets. (g) The capsule with the battery connected to the motor magnets. (h) The motor jammed by the battery, preventing further motion of the arm.

and 27% of times it was picked up by the arm. This shows how the capsule can be highly successful when it is close to the battery, however, the success rate reduces significantly once the battery is outside of the area swept by the arm.

5.5 Discussion and Conclusion

In this study, a magnet motor rotated by an external alternating magnetic field was developed, and its effectiveness was demonstrated by the ability of an ingestable capsule to extend its arm and retrieve a button battery. The capsule developed weighs only 5.13 g, as it contains no electronic components. It can turn the motor inside it without being turned by the external magnetic field, due to the motor's characteristic of zero net torque.

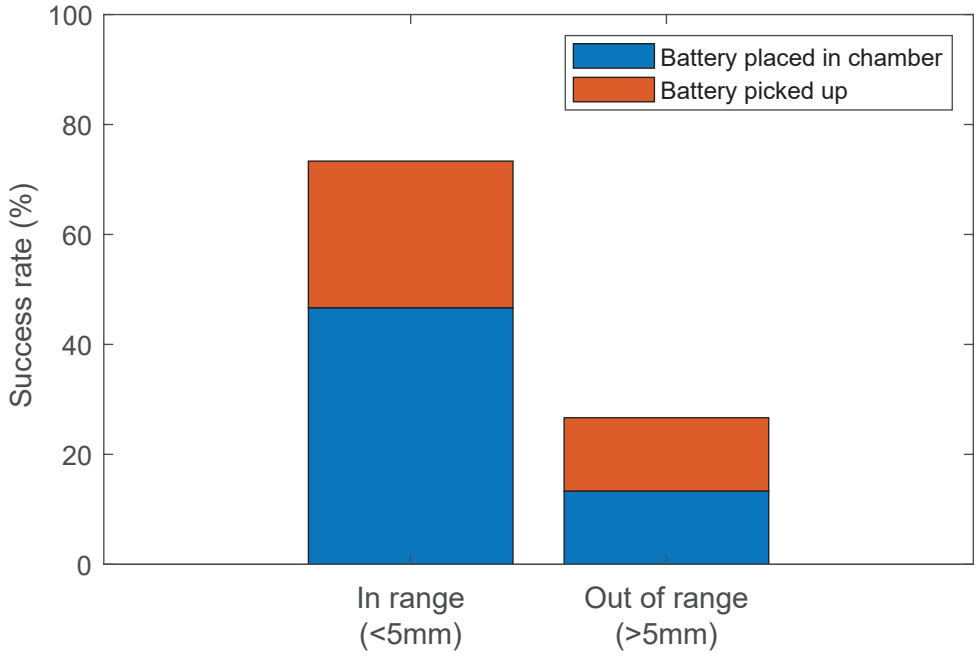

Figure 5.15.: A summary of the success rate of the capsule at picking up a 5mm diameter button battery.

The motor can also rotate in the opposite direction by applying the magnetic field from a perpendicular direction. As this approach does not rely on transmission gears to minimise the net torque applied, it can be achieved without reducing the speed of the motor, and a transmission gear can be implemented if further torque increase is desired.

The current capsule design needs reducing in size by 50% to fit inside a #000 capsule. #000 is the largest capsule approved by the Food and Drug Administration (FDA) for human consumption, so this is necessary for the capsule to enter clinical trials. The challenge associated with this is that the torque of the motor (τ_{mot}) decreases as the scale of the motor is reduced, necessitating the friction in the mechanism to also be reduced to allow the arm to still rotate freely; the space within the capsule available to store batteries would also be reduced.

The pose control system is capable of holding the capsule at an acceptable angle to the magnetic field while the motor is operated, however, there is some steady state error caused by the torque applied to the motor. If desired this could be reduced by increasing the size of the steel sheet, or eliminated by adjusting the angle of the steel sheet to the axis of the capsule.

Larger sizes of battery cannot currently be encapsulated by the capsule, due to the limited space within the capsule. It can, however, connect to the battery with the magnet arm. This problem is likely to be limited, as if a child is unable to swallow a large capsule, they would be unable to swallow the larger sizes of battery. The battery detection and identification makes it possible to determine whether the capsule is appropriate to use for a given patient, or if endoscopic removal is required.

The capsule needs to be near to the battery to retrieve it. This problem could be overcome by using external magnetic fields to navigate the capsule by making it "walk" with a stick-slip motion [32] or roll [7, 107] to a position where the battery can be reached by the arm. This can be achieved by adding additional coils to the control system, to allow magnetic fields to be produced in any direction. Future work includes the development of mechanisms to navigate the capsule to a target location and further miniaturisation of the capsule.

Chapter 6

Discussion

6.1 Control of multiple motors

One key advantage of using magnetic motors, driven by an alternating magnetic field, over using a magnetic in a rotating magnetic field, is that multiple motors can be operated in the same workspace. The alternating field input means that the different motors can be in any orientation, so long as they are on the correct plane, and all rotate in response to the same input. If a rotating magnetic field is used then all the axes of rotation need to be parallel and the direction of rotation the same, limiting the potential applications.

6.1.1 Implementation to mobile robots

A version of the magnetic motor presented in Chapter 4 was incorporated as a mobile robot. The reduction gearbox was removed to increase speed of the output and enabling two wheels to be connected directly to the output shaft as shown in Fig. 6.1. The combined pawl and pawl spring for the second ratchet (shown in Fig. 4.2) was made from low carbon steel (RS, full hard, cold rolled).

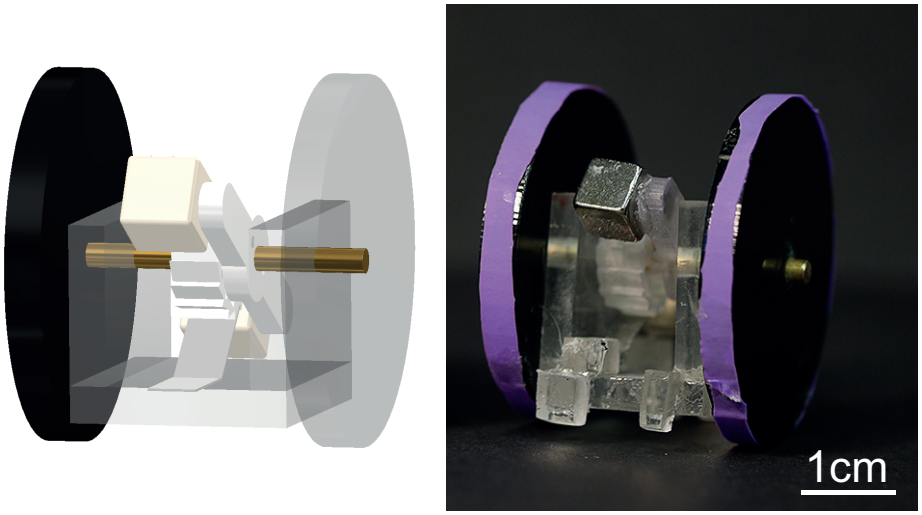

Figure 6.1.: The developed mobile robot equipped with the wireless motor: CAD and physical realisation.

The robot is actuated using an alternating $0.11\,\mathrm{Tm}^{-1}$ magnetic field gradient with a frequency of 2 Hz allowing it to move (Fig. 6.2 (a)). The robot moves forwards during the driving stroke of the motor, then stops for the recoil stroke. Fig. 6.2 (c) shows how the robot speed increases with the frequency of the magnetic field, derived both from an analytical model and experimentally. Once the step out frequency of the motor is exceeded, the robot speed decreases exponentially with increasing actuation frequency. When below the step-out frequency the

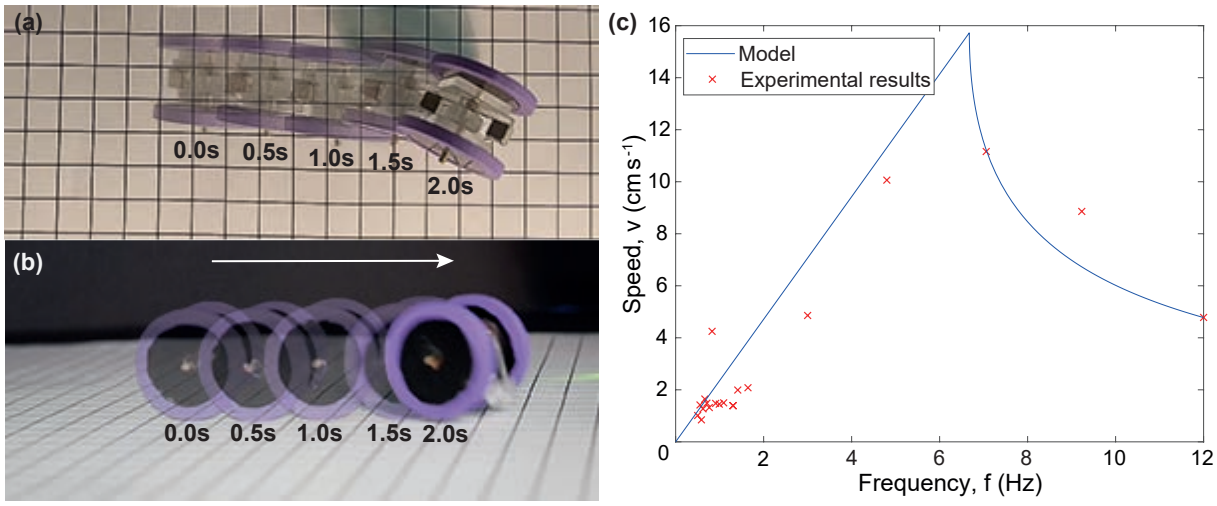

Figure 6.2.: (a) The motor demonstrated in mobile robot actuation with a 2 Hz magnetic field (grid size 1cm). (b) Side view of the mobile robot. (c) The robot speed against actuation frequency, showing how the speed increases proportionally to the actuation frequency up until the step out frequency, before exponentially decaying.

speed given by:

$$v = \gamma f_a \pi d, \tag{6.1}$$

where v is the robot velocity, γ is the angle the crank passes through each driving stroke, f is the magnetic field frequency, and d is the diameter of the wheels.

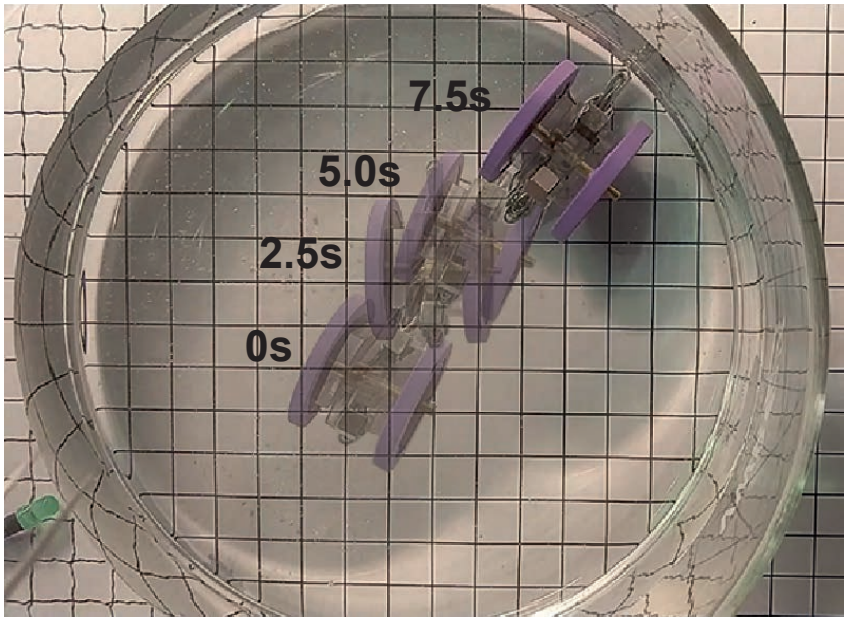

Figure 6.3.: The robot operating under water (grid size 1 cm).

The absence of electronic components in the motor's body offers an advantage that the motor can be used in an aqueous environment or inside

the body. We demonstrated this feature by running the robot entirely immersed in water in Fig. 6.3. The robot is actuated with a magnetic field of $0.14\ \mathrm{Tm}^{-1}$ at 2.5 Hz, and $2\,\mathrm{g}$ extra mass was added to the robot in the form of lead solder to improve the grip on the wet glass surface. It is presented that the motor successfully wheels the body at a speed of $0.9\,\mathrm{cm/s}$ under water.

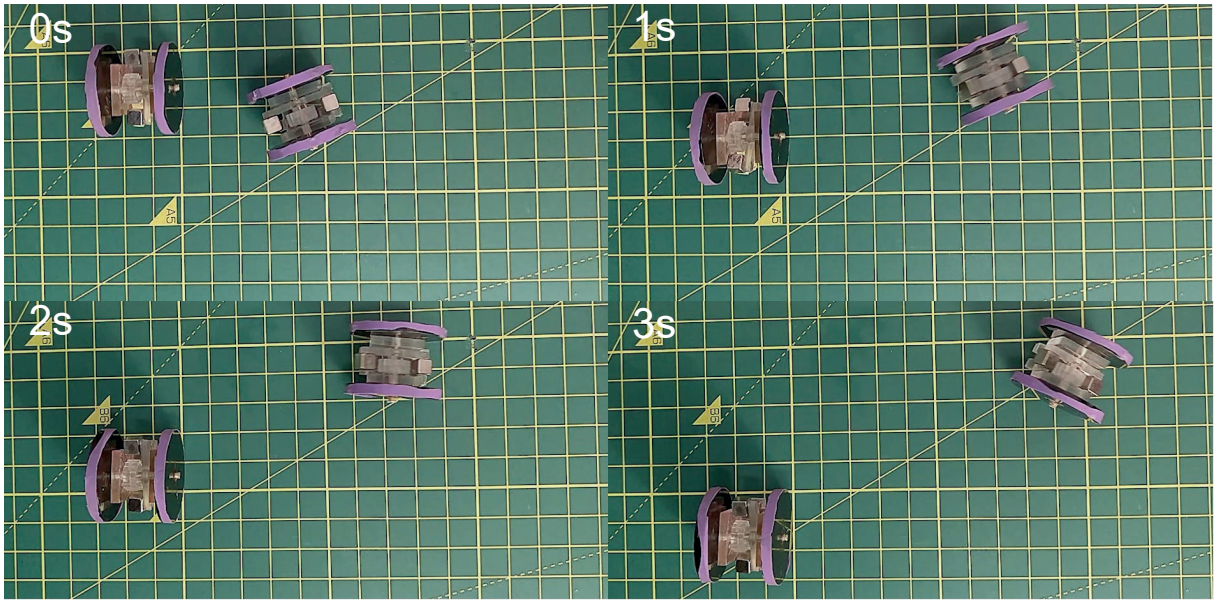

Figure 6.4.: Demonstration of multiple mobile robots operating in the same work space with a $1.6\,\mathrm{Hz}$ magnetic field. Images are at $1\,\mathrm{s}$ intervals on a $1\,\mathrm{cm}$ grid.

Due to the simple magnetic field input it is possible to have multiple robots operating within the same workspace, as demonstrated in Fig. 6.4, even if they are travelling in different directions. If two mobile robots get within $10\,\mathrm{mm}$ of each other the attractive force between their magnets is too great to overcome and they become magnetically attached to each other. This limits the number of robots which are able to operate in a given area. It is also possible to include multiple motors on the same robot rotating in opposite directions. This means the input torques act in opposite directions, creating no overall net torque. To be most effective it would be necessary to have the motors set up so that the driving strokes occur simultaneously. The steering of the robots was not considered, however, one possible method to achieve this would be to implement a system of pose control similar to that demonstrated in Section 5.3.2.

6.1.2 Addressable Control

Being able to operate multiple motors simultaneously increases the potential applications of magnetic actuation. It is, however, still limited by the fact that all the motors are actuated simultaneously. To solve this, and further increase the potential applications, it is necessary to have a method of individually addressing the motor to be actuated.

One method of addressing motors is to design the magnetic actuation system to be spatially selective, providing different inputs to different areas of the workspace [101], or selectively anchoring individual agents [119]. This has the limitation that the locations of the robots needs to be precisely known and a specialist system for generating magnetic fields is required. Instead of this certain characteristics of the motors can be exploited to allow the desired motors to be operated while the others remain stationary. This allows the control to be more versatile and work for motors which are near to each other, or moving around more within the workspace. Table 6.1 summarises the features which can be used to address a motor and which motors possess these features, including two as yet undeveloped hypothetical motors which would allows, by using different combinations of features, for four motors to be addressed.

Table 6.1.: The features of a motor which can be exploited for addressability, showing two of the motors presented and two hypothetical motors.

Motor	**Low frequency (0 Hz - 10 Hz)**	**High frequency (15 Hz - 20 Hz)**	**Field gradient (0.05 T m^{-1} - 0.4T m^{-1})**	**Uniform field (3 mT - 14 mT)**
Magnetic Force Motor (Chapter 4)	✓		✓	
Magnetic Torque Motor (Chapter 5)	✓	✓		✓
Hypothetical Motor 1	✓	✓	✓	
Hypothetical Motor 2	✓			✓

One example of a feature which has been exploited previously is resonance frequency [61]. This approach can be adapted for motors with different step-out frequencies. By having two motors with different step-out frequencies, both motors can be actuated at a low frequency, while at a higher frequency only the motor with the greatest step-out frequency will operate. This is summarised in Fig. 6.5 where the relationship between actuation frequency and angular velocity is shown for two motors as described by Eq. 4.8 for the magnetic force motor, and Eq. 5.9 for the magnetic torque motor. The Magnetic Torque Motor (Chapter 5) is shown with a 4:1 reduction so that at low frequencies it matches the angular velocity of the Magnetic Force Motor (Chapter 4). The figure shows how above the step-out frequency of the force motor the angular velocities rapidly diverge, allowing the torque motor to be driven with little response from the force motor. This approach can be applied to any pair of motors with significantly different step-out frequencies.

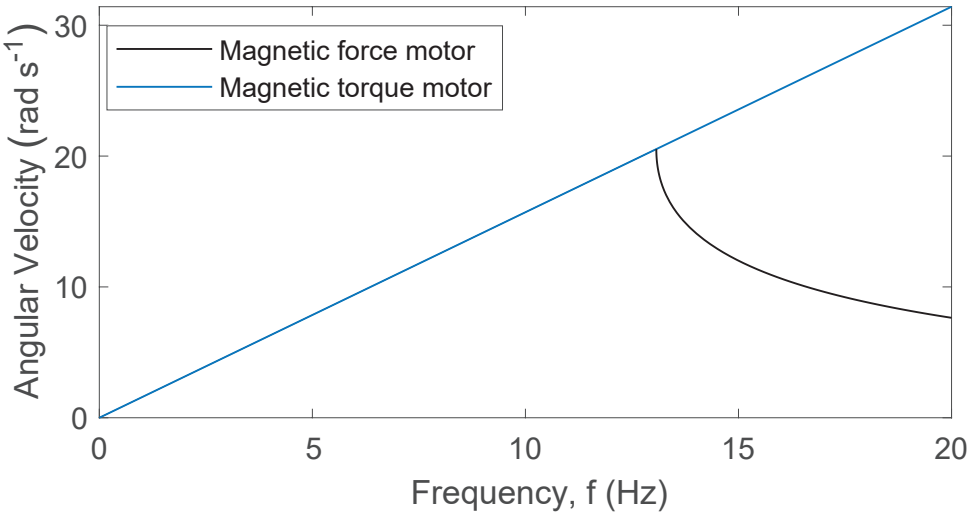

Figure 6.5.: The frequency response of both the magnetic force motor, and magnetic torque motor with a 4:1 reduction to match the angular velocities, showing how at high actuation frequencies the response of the force motor is significantly reduced, while the torque motor's response remains high. This comes from Eq. 4.8 and Eq. 5.9.

Another feature which can be used to address motors is whether they rely on magnetic field gradients to generate a force, or magnetic fields to generate a torque. A magnetic dipole experiences a torque when placed at an angle to a magnetic field. When placed in a magnetic field gradient a magnet experienced a force acting on it. Having developed one motor which relied on torque from a magnetic field and a second which relies on force from a

magnetic field gradient it is possible to selectively control them by producing either a magnetic field or a magnetic field gradient.

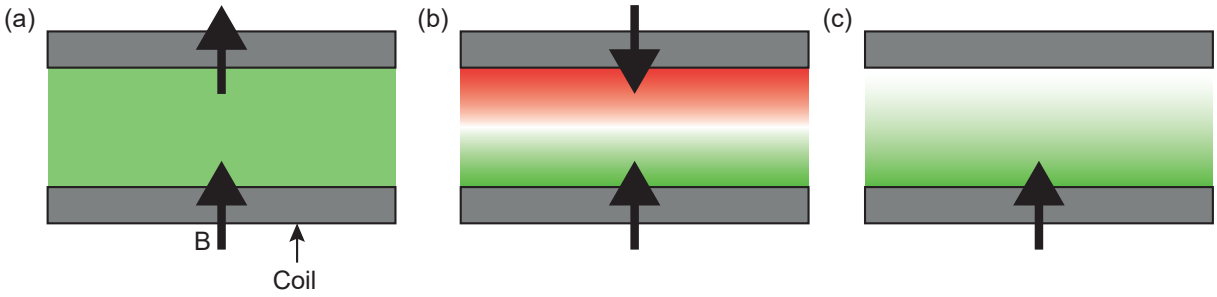

Figure 6.6.: A Helmholtz coil configuration with (a) a uniform magnetic field with no gradient for the operation of magnetic torque based motors, (b) a uniform magnetic field gradient with no magnetic field at the working platform for the operation of magnetic force based motors, and (c) both a magnetic field and a magnetic field gradient at the working platform for the operation of both kinds of magnetic motor.

A Helmholtz coil is a system of two identical coils positioned coaxially one coil radius apart; they can be used to produce either a uniform magnetic field, or a uniform magnetic field gradient. When both coils are producing a magnetic field of equal strength in the same direction the area between the coils has a uniform magnetic field, and hence no magnetic field gradient (Fig. 6.6 (a)). This can be used to actuate a magnetic torque based motor while a magnetic force based motor will be unaffected. By reversing the current in one of the coils such that they produce magnetic fields in opposite directions a constant magnetic field gradient is produced across the area between the coils (Fig. 6.6 (b)). At the centre point between the coils the absolute magnetic field is zero; at this point a magnetic torque based motor will be unaffected while a magnetic force based motor will operate. The exact point of zero magnetic field can be moved by adjusting the relative magnetic field strengths of the two coils; similarly, a magnetic field and a magnetic field gradient of any ratio can be produced allowing both kinds of motor to be operated simultaneously (Fig. 6.6 (c)).

The combination of both the use of field gradient and frequency allow for four motors to be addressed. When the motors are being driven with a low actuation frequency, the high frequency motor of the relevant kind (magnetic torque or force) will also operate, which may be a limitation in certain circumstances.

6.2 Comparison of Motors

Fig. 6.7 shows the motors presented in this thesis, including a reduced size magnetic torque motor measuring 1 cm by 1 cm by 1 cm and using 1.5 mm cubic magnets (6.7 (f)). Tab. 6.2 summarises their properties alongside the published data for the motor presented by Hong et al. in [50] and a 6 V DC motor (RS 752-2005). The key characteristics for each motor are shown, including their torque, speed and power as well as the kind of input they need to operate.

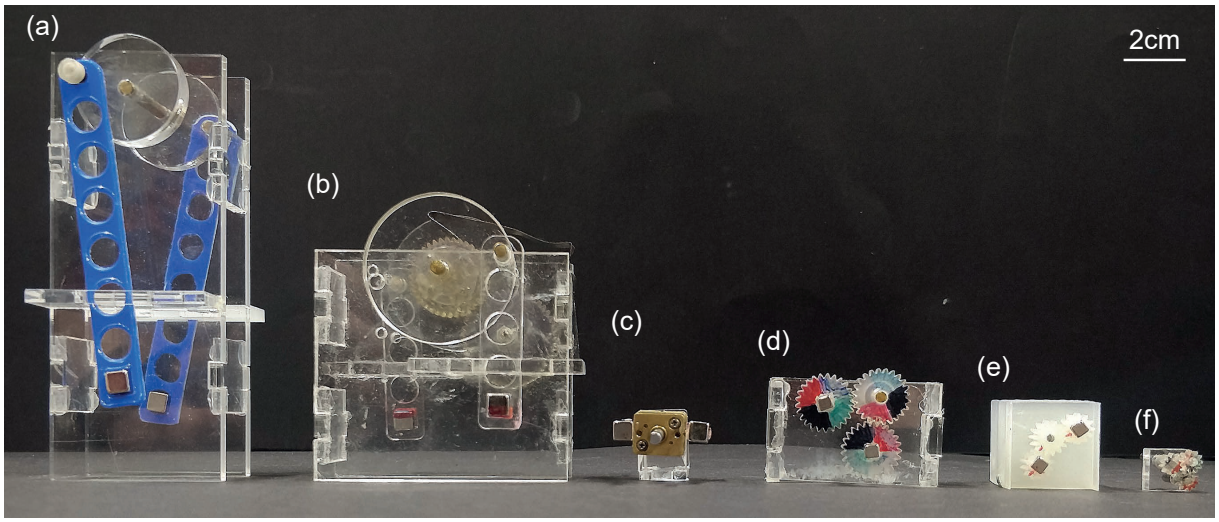

Figure 6.7.: A comparison of the motors presented in this thesis. (a) original concept for the crank motor, (b) Magnetic Force Motor (Chapter 3), (c) Magnetic Force Motor (Chapter 4) with reduction gear box, (d) original torque based motor, (e) Torque Motor (Chapter 5), and (f) reduced size torque based motor using 1.5 mm cubic magnets.

Table 6.2.: Comparison of magnetic motors alongside the published data for a magnetically actuated gearbox and a DC motor.

	Physical properties		Outputs			Inputs			Capabilities	
Motor	**Mass (g)**	**Size (mm)**	**Stall Torque (mNm), ($Nm\,kg^{-1}$)**	**Step-out Frequency (Hz)**	**Power (mW), ($W\,kg^{-1}$)**	**Input Power (W)**	**Field Strength**	**Magnetic field**	**Pose Control possible**	**Reversible**
Magnetic Force Motor (Chapter 3)	47.3	61 ×44 ×67	0.05 (0.00106)			240	0.14 Tm^{-1}	Alternating field gradient	Sometimes	No
Magnetic Force Motor (Chapter 4)	3.5	24 ×17 ×12	45 (12.9)	14		240	0.2 Tm^{-1}	Alternating field gradient	Sometimes	No
Torque Motor (Chapter 5)	3.7	20 ×20 ×19	0.07 (0.0189)	20*	1.05 (0.284)	240	8.5 mT	Alternating field	Yes	Yes
Hong et al. Motor [50]	$\geq$ 0.0132	3	0.182* (13.8)	40*	0.134 (10.15)		6.8 mT	Rotating field	No	Yes
6V DC Motor (RS 752-2005)	10	12 ×10 ×25	39.8 (3.98)	225	580 (58)	1.02	N/A	N/A	No	Yes

*Tested up to this value

6.2.1 Actuation methods

Magnetically actuated motors have a number of advantages compared to conventional electrical motors. The greatest advantage is that magnetically actuated motors receive the energy to operate from the applied magnetic fields, while electrical motors need a supply of electricity. This electrical supply could come in the form of wires to an external power source; this gives an essentially unlimited supply of energy and the power is only limited by the cross-section of the wires, however, this restricts the potential for remote applications and in-vivo medical applications where a route for the wires to reach the motor would need to be made, increasing the invasiveness of any medical procedure. The alternative to wires is to have batteries onboard the robot to store the electrical energy. The use of batteries allows the robot to be untethered, making it highly suited for remote control and use in enclosed spaces, such as within the body.

Magnetic motors also offer a number of advantages over existing magnetic actuation techniques. One key advantage is the ability to have multiple motors operating simultaneously within the same workspace with different axes of rotation; this is made possible by removing the rotation magnetic field, required for conventional magnetic control of a rotating part, and replacing it with a simple oscillating magnetic field or field gradient. This simpler actuation means the coil systems used to actuate the robots can be simplified; to create a rotating magnetic field, for a conventional system, requires a minimum of three coils, often more are used in practice.

The approach of using magnetic motors presented requires only a single coils, or two in a Helmholtz configuration if addressable control is required. Having two different types of magnetic motor, one using magnetic field gradient and the other using magnetic fields, allows for addressable control of two motors, this is difficult to achieve using a conventional rotating magnetic field approach.

When a rotating magnetic field is used to apply torque to a robotic system a net torque inevitably acts on the whole system. By using a magnetic motor it is possible to counteract this either by using a magnetic pose control system to align the robot with the magnetic field, or by using two counterrotating motors. Tab. 6.2 shows how the magnetic torque based motor is always able to make use of a pose control system, however, it is only sometimes possible with a magnetic force based motor. This is because the pose control system

presented in Chapter 5 relies on a magnetic field to create the torque countering that applied to the motor, such a magnetic field is always present for a torque motor. If a magnetic force based motor is rotated using a magnetic field gradient with no magnetic field at the point of the motor the pose control won't be able to generate the required torque. In order to use a magnetic field to drive a mechanism on a robot which is free to move within its environment, such as a capsule endoscope, it is essential to have a system like this to prevent the entire robot moving. This makes a magnetic motor the only option for driving mechanisms in applications where electronics would be unsuitable.

The ability to run magnetic motors in reverse limits their potential for use in some applications. The force based motor cannot be operated in reverse, while the torque based motor can be reversed by changing the angle the magnetic field is applied by $90°$. The use of the magnetic pose control system, however, prevents the torque based motor from being reversed by making the motor align with the new magnetic field and continue to rotate in the same direction.

Magnetic motors open up possibilities not possible with either a conventional electric motor, or magnetic actuation using rotating fields. With magnetic motors it is possible to have wireless control of mechanisms which are free to move without applying an net torque to the robot body, addressably control multiple motors within the same workspace, while also having unlimited operating life due to not having to rely on onboard batteries.

6.2.2 Output torque

The main function of a motor to to apply torque to a gear or shaft, and so transmit power as rotational motion. The power of a motor is the torque multiplied by the angular velocity, the ratio of these can be adjusted while the power kept constant by using gears.

Magnetic motors also have a number of limitations when compared to the alternatives. The speed and torque are limited by the strength of the applied magnetic field or magnetic field gradient. In the case for the magnetic force motor this is 4.7 mNm (1.3 Nm kg^{-1}) at 0.2 Tm^{-1} without a gear box, and the magnetic torque based motor presented is limited to 0.07 mNm (0.019 Nm kg^{-1}) at 8.4 mT.

Magnetic Force Motor (Chapter 3) can be seen to have a much lower output torque compared with Magnetic Force Motor (Chapter 4), despite using the same working principle and the same size of magnets. This is due to refinements of the design to remove unnecessary moving parts that caused significant frictional losses, reducing the output torque. The Torque Motor (Chapter 5) has significantly lower torque compared with the Magnetic Force Motor (Chapter 3), this makes it less suited to applications where large torques are required, unless it is combined with a reduction gear box to increase the output torque. The conventional DC motor (RS 752-2005) offers greater torque than any of the magnetic alternatives, if large torques are required and the necessary wires or batteries are not prohibitive for the application.

6.2.3 Speed and power

The angular velocity of a motor is important as, when multiplied by the torque, it gives the overall power of the motor. The step-out frequency of a motor is the maximum actuation frequency which can be used to actuate it. Above this frequency the motor is unable to rotate fast enough to keep up, and so the angular velocity no longer increases with the actuation frequency. The step-out frequency of Torque Motor (Chapter 5) is greater than that of Magnetic Force Motor (Chapter 4) due to the lower moment of inertia of the motor parts, this was achieved by eliminating the crank from the design and having the magnets, the heaviest component, rotating about their centre line. The force based motor does not rotate a full revolution for each cycle of the magnetic field, further reducing the output angular velocity to $18\,\%$ that which the torque based motor was tested up to.

The Hong et al. Motor [50] is tested up to a higher input frequency compared with the Torque Motor (Chapter 5). This is because the input magnetic field was a permanent magnet connected to a motor to generate the rotating field. The Hong et al. Motor [50] produced $13\,\%$ of the power of the Torque Motor, however, when considered per unit mass it produced 36 times more power. The $6\,\mathrm{V}$ DC motor produced 552 times more power than the torque motor, but only 55 times more when considered per unit mass. This is greater than any of the magnetic motor alternatives, making the DC motor the best option for applications where electronics are possible.

6.2.4 Size and scalability

The size of the motor is important for many applications where space or weight are critical. For implants, reducing the size of an implant, such as that presented in Chapter 4, allows it to be used in younger children [87] or so the motor takes up less space within a capsule, allowing more room for payload or mechanisms. In order to free an electrical robot from its tether and make it wireless batteries can be added to provide an onboard energy source. Batteries add significantly to the bulk and mass of a robot, especially as the scale is reduced or long operating times are required. They also have a finite life, meaning a compromise has to be made between the size of the robot and the bulk they provide, this need to be carefully considered to avoid running out of stored energy before all the tasks are completed. Magnetic actuation gives the unlimited operating times and energy available to tethered robots, as well as the low mass and small body size removing the power supply form the robot makes possible, while having the untethered operating of a battery powered robot. The magnetic torque motor presented have a mass of 37 % of that of the DC motor shown in Tab. 6.2, before the mass of batteries is taken into consideration.

The simple construction of magnetic motors makes them low mass; the majority of components are low mass plastic parts with the majority of the weight coming from the magnets themselves. This simple construction also makes them low-cost to produce. No significant wear of components has been found during experiments, however, for applications with prolonged use at high loads harder materials may need to be specified.

To further reduce the size, the principle of the magnetic motor can be easily scaled, with the torque produced reducing proportionally to the volume of the magnets and for magnetic force based motors, the length of the cranks. Compared with using a single rotating magnet, magnetic motors have complex mechanisms. This makes them more challenging to manufacture at small scale and leads to friction and wear between components. This is, however, no worse than if a reduction gear box was used with the rotating magnet as in [50].

6.2.5 Motor efficiency

The efficiency of a motor is the ratio of the energy put in to the system, to the useful work produced. For a magnetic motor the input energy can be considered to be the electrical energy input to the magnetic coil system. Magnetic coil systems rely on a large amount of electrical power to operate; to run the motors at full power around 240 W of electrical power is used. For the 1.05 mW output of the torque motor this gives an efficiency of 0.44 %. This is compared with 57 % for the 6 V DC motor.This comparison is of a wireless motor to a wired one, so to be more comparable it is necessary to consider the extra inefficiency of a method of wireless power transmission to the DC motor. If this were to be done using inductive power transfer with a receiver coil connected to the motor an extra 25 % power loss would need to be included, reducing the overall efficiency to 43 % [120] [121]. This is assuming there is good alignment between the transmission and reviewer coils for the wireless power transfer; if there is poor alignment this efficiency can be significantly impacted. Magnetic motors are significantly less efficient than conventional DC motors, and so should only be used in applications where their other unique characteristics make them desirable, or in low power applications where the extra energy consumption is less significant.

6.2.6 Safety

The safety of any medical device is paramount to ensure the device does not cause any additional harm to the patient who is potentially already suffering as a result of a medical condition. Magnetic motors are safe for use in most applications, the magnetic fields used are well below the static magnetic field strength of 0.046 - 8 T of MRI machines [90], this shows that these magnetic field can safely be used in a medical setting. There are no electrical components to become hot or create sparks. The only components which are not biocompatible are the magnets, which can be coated in a biocompatible material, meaning toxicity isn't a problem. Magnetic motors are limited in the torque they can output by the input magnetic field, this prevents them from applying excessive force, leading to tissue damage when used for medical applications.

The mechanisms in the motors could potentially be trap tissue, injuring it, or become jammed with debris; this would be an issue with any mechanism, and

is not limited to the motors presented. Due to the torque of the motor being limited by the magnetic field the extent of any damage would be limited, the problem would also be completely resolved by surrounding moving parts with a housing. Despite this, before clinical use there will need to be standards written to regulate the safe use of this kind of device. Standards would need to encompass, among other things, the materials used, alongside existing regulations covering this, maximum allowable forces, and endure designs are such that they don't risk causing unwanted damage to tissue. This means that if the robot is designed appropriately a magnetic motor is safe to be used in medical applications.

6.2.7 Applications

Owing to their individual characteristics, different motor design are best suited to different applications. The 6 V DC motor provides the most torque, at the greatest speed to give the most power, while also being more efficient than driving a magnetic motor using a coil system. This makes it best suited to applications where speed and torque are required and it is possible to use electrical cables or position batteries near to the motor. This would include general mechatronics applications and conventional robotics.

Applications where wireless power transfer is required, or electronics are infeasible due to space or safety constraints, such as some ingestible or implantable robots, will be best served by a magnetically actuated motor. Where it is necessary to have a single motor driving a mechanism on a free to move robot the only option is a magnetic torque motor (Chapter 5) combined with a pose control system, as this is able to balance the torque applied to the motor. This would include applications such as capsule robots. If more torque is required, but the mechanism is capable of anchoring to its surroundings, this could be combined with a reduction gearbox, or a magnetic force motor motor uses instead. An example of this would be a robotic implant for applying forces to tissue, as demonstrated in Chapter 4.

Where size or weight are critical for the application then a rotating magnet approach as used in [50] may be best suited due to the simplicity of the design making size reduction less complex. This would be applicable to milli and micro-robots where addressable control is not necessary and the robot is stable enough to not spin with the applied magnetic field. Where multiple

motors with addressable control is needed then it is necessary to use both a magnetic force motor and a magnetic torque motor, or the two hypothetical motors proposed in Tab 6.1. This would be applicable to scenarios such as a single robot with multiple manipulators, or for multiple simple robots to allow them to collaborate on a task.

In conclusion, the best motor depends heavily on the task it is required to perform. It is necessary to consider how the motor will be powered, how much power is required from it, any space or weight limitations, as well as the number of motors which will be required for the task and how they will be addressed.

6.3 Conclusions

Magnetic motors open up a number of new capabilities which have not been achieved using existing approaches. Being wirelessly powered means that they can run indefinitely with no cables tethering them, unlike electric motors which are limited by either bulky batteries with finite lives or tethers connecting them to an external power source. Compared with existing magnetic control techniques magnetic motors have simplified control and offer additional degrees of freedom by allowing for multiple addressable motors to operate within the same workspace. When combined with a magnetic pose control system, magnetic motors allow for actuators on a robot to be actuated independently from the main robot body, which would be impossible with a conventional rotating magnetic field approach.

As with any actuator, the potential uses for magnetic motors are limited by the available torque and maximum angular velocity. However, by selecting a motor with properties most suited to the application the effect of these limitations on the final application can be minimised. These advantages mean magnetic motors can be used in situations where conventional motors would be unstable such as long term medical implants or capsule robots.

Chapter 7

Conclusions and future work

7.1 Chapter Contributions

This section outlines the contributions of each chapter in this thesis.

Chapter 3, Magnetic Force Driven Wireless Motor:

- A new concept for a magnetically actuated motor driven by an alternating magnetic field gradient is presented
- The output torque of the motor through its cycle was modelled
- The torque model was used to investigate the effect of scaling the design
- The motor was prototyped and provisional experiments carried out to indicate the validity of the torque model

Chapter 4, Wirelessly Magnetically Actuated Motor for Tissue Regeneration Robotic Implant:

- The motor concept from Chapter 3 is further developed to simplify the design, reducing the size, and increase the torque output
- The maximum speed of the motor is modelled
- The speed and output torque of the motor are experimentally investigated, validating the models
- The motor is presented in an implantable robot for tissue regeneration therapies for conditions such as long gap oesophageal atresia, or short bowel syndrome
- The performance of the implant is experimentally verified through ex-vivo trials

Chapter 5, Remotely Actuated Magnetic Motor for Unconstrained Robotic Capsule:

- A second novel concept and design of a magnetic motor, utilising magnetic torque instead of magnetic force, is demonstrated

- The torque output of the motor through its operating cycle is modelled and experimentally verified
- A novel system for controlling the pose of a robot using the motor independently from the actuation of the motor, allowing for more degrees of freedom, is presented
- The motor and pose control system are presented in a capsule robot for retrieving ingested button batteries from a patient's stomach
- The success rate of the capsule robot at retrieving button batteries from a phantom stomach is experimentally investigated

7.2 Conclusions

The available degrees of freedom in magnetically actuated robots is a critical challenge for expanding the applications they can be used for. Currently they are limited to five degrees of freedom: x, y, z translation, and rotation about two axes. The current systems of control are limited to manipulating robots as a single object and are unable to be used to drive mechanisms within a robot without moving the entire body. Hu et al. used a soft robot to add the potential to change the robot shape [51]; however, this is not capable of driving mechanisms.

Chapter 3 introduced a new concept of a magnetically actuated motor. The motor developed in this chapter used magnetic force to actuate a crank mechanism and relies on a pair of ratchets to convert this oscillating motion to a continuous rotation. Having two magnets with opposite orientation means the motor experiences no net force from the magnetic field. The motor has simplified actuation compared to existing magnetic control techniques; instead of relying on a rotating magnetic field it uses an alternating magnetic field gradient which can be produced using a single coil. This motor has two main disadvantages: firstly its size is excessively large, greatly limiting its potential applications; secondly the output torque is low due to large losses in the drive train.

The concept of the magnetic force based motor is expanded upon in Chapter 4, with an improved motor design solving the limitations of the first design. The

motor design is simplified by reducing the number of moving parts. This has two effects; firstly the size and mass of the motor are reduced, and, secondly, the losses in the motor are reduced because the reduction in moving parts reduces the sliding friction in the system. The output torque is also magnified for certain applications by the addition of a reduction gearbox. This motor is demonstrated in both a mobile robot and a robotic implant capable of elongating tubular organs for the treatment of long gap oesophageal atresia and short bowel syndrome.

A new motor design relying on magnetic torque is explored in Chapter 5. This motor design eliminates the reciprocating crank and the ratchets of the other motors. This increases the step-out frequency and means it does a full revolution for each cycle of the magnetic field, further increasing the angular velocity of the motor. A magnetic pose control system to control the orientation of the robot independently of the operation of the motor is developed; this has the effect of adding a degree of freedom to the operation of an unconstrained magnetic robot. The motor and magnetic pose control system are demonstrated in a capsule robot capable of picking up and encasing an ingested button battery.

These present new capabilities for magnetic actuation, introducing the possibility of actuating mechanisms within a magnetically actuated robot, while also independently controlling the pose. They also have potentially to be used for ingested or implanted medical robots where it is necessary to power them for long periods of time.

7.3 Future work

Future work for this research is necessary to improve its level of technological readiness and allow it to be applied to a wider range of applications. Work is being done to investigate methods of making the force based motor shown in Chapter 4 reversible. Potential methods being investigated include a gear box used to select between forwards and reverse gears. This would make the motor more versatile in the applications where it can be used.

Another area of future work is to reduce the size of the motors so they can be used in micro scale robots. Both motors show promise to be reduced in size; the

use of magnets for the power transfer allows the scaling down of the designs, and how this affects the torque output has been investigated. The components can be reduced in size using either photolithography and soft lithography techniques, or two photon lithography. It may be beneficial to reduce the part count of the force based motor to make it easier to assemble at the smaller scale, and adjust the part geometry to suit the different manufacturing techniques. This would allow the implant and capsule to be reduced to a size more acceptable by medical regulators.

As the magnetic torque based motor relies on magnetic fields, where as the magnetic force based motors rely on magnetic field gradients, this opens up the potential for addressable control of two motors within the same workspace. By using a Helmholtz coil system magnetic field can be produced with no gradient, or field gradients produced with a point without any magnetic field, meaning only one of the two motor styles is actuated at a time. This adds another degree of freedom to a magnetically actuated robot using this system. Addressable control needs further investigation into additional criteria which can be controlled to allow for more degrees of freedom. This would involve designing additional motors meeting the criteria of the two hypothetical motors proposed in Tab. 6.1. The motors should be combined in a application to effectively showcase the potential for addressable control.

References

[1] Cameron Duffield and Shuhei Miyashita. 'Magnetic Force Driven Wireless Motor'. In: *Annual Conference Towards Autonomous Robotic Systems*. Springer. 2020, pp. 409–412 (cit. on pp. 5, 30, 44, 61, 121).

[2] Cameron Duffield, Abigail F Smith, Daniela Rus, Dana Damian and Shuhei Miyashita. 'Wirelessly Magnetically Actuated motor for Tissue Regeneration Robotic Implant(accepted)'. In: *IEEE International Conference on Intelligent Robots and Systems* (*IROS*). IEEE. 2022, pp. 465–471 (cit. on pp. 6, 42, 61, 62, 127).

[3] Marco Pontin and Dana D Damian. 'Data-Driven and Compliance-Based Fault-Tolerance for a Flexible and Extendable Robotic Implant Coupled to a Growing Tissue'. In: *IEEE Robotics and Automation Letters* (2023) (cit. on p. 6).

[4] Gi-Shih Lien, Chih-Wen Liu, Joe-Air Jiang, Cheng-Long Chuang and Ming-Tsung Teng. 'Magnetic control system targeted for capsule endoscopic operations in the stomach—design, fabrication, and in vitro and ex vivo evaluations'. In: *IEEE Transactions on Biomedical Engineering* 59.7 (2012), pp. 2068–2079 (cit. on pp. 10, 31, 61).

[5] Cheong Lee, Hyunchul Choi, Gwangjun Go et al. 'Helical motion and 2D locomotion of magnetic capsule endoscope using precessional and gradient magnetic field'. In: *5th IEEE RAS/EMBS International Conference on Biomedical Robotics and Biomechatronics*. IEEE. 2014, pp. 1063–1067 (cit. on p. 11).

[6] Makoto Nokata, Satoshi Kitamura, Toshihiro Nakagi, Toshiro Inubushi and Shigeki Morikawa. 'Capsule type medical robot with magnetic drive in abdominal cavity'. In: *2008 2nd IEEE RAS & EMBS International Conference on Biomedical Robotics and Biomechatronics*. IEEE. 2008, pp. 348–353 (cit. on pp. 11, 61).

[7] Dongxu Ye, Junnan Xue, Sishen Yuan et al. `Design and control of a magnetically-actuated capsule robot with biopsy function'. In: *IEEE Transactions on Biomedical Engineering* 69.9 (2022), pp. 2905–2915 (cit. on pp. 11, 61, 83).

[8] Yang Liu, Marian Wiercigroch, Ekaterina Pavlovskaia and Hongnian Yu. `Modelling of a vibro-impact capsule system'. In: *International Journal of Mechanical Sciences* 66 (2013), pp. 2–11 (cit. on p. 11).

[9] Yao Yan, Baoquan Zhang, Joseph Páez Chávez and Yang Liu. `Optimising the locomotion of a vibro-impact capsule robot self-propelling in the small intestine'. In: *Communications in Nonlinear Science and Numerical Simulation* 114 (2022), p. 106696 (cit. on p. 11).

[10] Yao Yan, Bingyong Guo, Jiyuan Tian et al. `Evaluating the resistant force of an endoscopic capsule self-propelling in the small intestine'. In: *Archive of Applied Mechanics* 92.12 (2022), pp. 3861–3875 (cit. on pp. 11, 61).

[11] Shuhei Miyashita, Steven Guitron, Kazuhiro Yoshida et al. `Ingestible, controllable, and degradable origami robot for patching stomach wounds'. In: *2016 IEEE International Conference on Robotics and Automation* (*ICRA*). IEEE. 2016, pp. 909–916 (cit. on pp. 12, 64).

[12] Alexis du Plessis d'Argentré, Samuel Perry, Yoshitaka Iwata et al. `Programmable medicine: Autonomous, ingestible, deployable hydrogel patch and plug for stomach ulcer therapy'. In: *2018 IEEE International Conference on Robotics and Automation* (*ICRA*). IEEE. 2018, pp. 1511–1518 (cit. on pp. 12, 61).

[13] Haruna Iwasaki, Flavien Lefevre, Dana D Damian, Eiji Iwase and Shuhei Miyashita. `Autonomous and reversible adhesion using elastomeric suction cups for in-vivo medical treatments'. In: *IEEE Robotics and Automation Letters* 5.2 (2020), pp. 2015–2022 (cit. on p. 12).

[14] Manh Cuong Hoang, Viet Ha Le, Kim Tien Nguyen et al. `A Robotic Biopsy Endoscope with Magnetic 5-DOF Locomotion and a Retractable Biopsy Punch'. In: *Micromachines* 11.1 (2020), p. 98 (cit. on p. 13).

[15] Adam J Sperry, Trevor J Schwehr, Emma K Pinegar et al. `Screw-tip Soft Magnetically Steerable Needles'. In: *IEEE Transactions on Medical Robotics and Bionics* (2023) (cit. on p. 13).

[16] Kiyoshi Ioi. `A mobile micro-robot using centrifugal forces'. In: *1999 IEEE/ASME International Conference on Advanced Intelligent Mechatronics* (*Cat. No. 99TH8399*). IEEE. 1999, pp. 736–741 (cit. on p. 14).

[17] Aaron M Hoover, Erik Steltz and Ronald S Fearing. `RoACH: An autonomous 2.4 g crawling hexapod robot'. In: *2008 IEEE/RSJ International Conference on Intelligent Robots and Systems*. IEEE. 2008, pp. 26–33 (cit. on p. 14).

[18] Noah T Jafferis, E Farrell Helbling, Michael Karpelson and Robert J Wood. `Untethered flight of an insect-sized flapping-wing microscale aerial vehicle'. In: *Nature* 570.7762 (2019), pp. 491–495 (cit. on p. 14).

[19] Johannes James, Vikram Iyer, Yogesh Chukewad, Shyamnath Gollakota and Sawyer B Fuller. `Liftoff of a 190 mg laser-powered aerial vehicle: The lightest wireless robot to fly'. In: *2018 IEEE International Conference on Robotics and Automation* (*ICRA*). IEEE. 2018, pp. 1–8 (cit. on p. 14).

[20] Zhenlong Wang, Guanrong Hang, Jian Li, Yangwei Wang and Kai Xiao. `A micro-robot fish with embedded SMA wire actuated flexible biomimetic fin'. In: *Sensors and Actuators A: Physical* 144.2 (2008), pp. 354–360 (cit. on p. 14).

[21] Arne Burisch and Annika Raatz. `Investigation and strategies for precision of miniaturized robots with micro gears'. In: *Assembly Automation* 31.4 (2011), pp. 319–328 (cit. on p. 15).

[22] Baek-Chul Kim, Youngkwan Lee, Jae-Do Nam et al. `Smart material actuators for micro optical zoom lens driving systems'. In: *IEEE transactions on magnetics* 47.7 (2011), pp. 1999–2004 (cit. on p. 15).

[23] Jason Campbell and Padmanabhan Pillai. `Collective actuation'. In: *The International Journal of Robotics Research* 27.3-4 (2008), pp. 299–314 (cit. on p. 15).

[24] Yoshitaka Nakagawa, Hiroyuki Kageyama, Yuya Oaki and Hiroaki Imai. `Direction control of oriented self-assembly for 1D, 2D, and 3D microarrays of anisotropic rectangular nanoblocks'. In: *Journal of the American Chemical Society* 136.10 (2014), pp. 3716–3719 (cit. on p. 16).

[25] Ned Bowden, Scott RJ Oliver and George M Whitesides. `Mesoscale self-assembly: capillary bonds and negative menisci'. In: *The Journal of Physical Chemistry B* 104.12 (2000), pp. 2714–2724 (cit. on p. 16).

[26] Ned B Bowden, Marcus Weck, Insung S Choi and George M Whitesides. 'Molecule-mimetic chemistry and mesoscale self-assembly'. In: *Accounts of chemical research* 34.3 (2001), pp. 231–238 (cit. on p. 16).

[27] Takafumi Fukushima, Eiji Iwata, Kang-Wook Lee, Tetsu Tanaka and Mitsumasa Koyanagi. 'Self-assembly technology for reconfigured wafer-to-wafer 3D integration'. In: *2010 Proceedings 60th Electronic Components and Technology Conference* (*ECTC*). IEEE. 2010, pp. 1050–1055 (cit. on p. 16).

[28] Sehyuk Yim and Metin Sitti. 'SoftCubes: Stretchable and self-assembling three-dimensional soft modular matter'. In: *The International Journal of Robotics Research* 33.8 (2014), pp. 1083–1097 (cit. on pp. 16, 17).

[29] Kenneth C Cheung, Erik D Demaine, Jonathan R Bachrach and Saul Griffith. 'Programmable assembly with universally foldable strings (moteins)'. In: *IEEE Transactions on Robotics* 27.4 (2011), pp. 718–729 (cit. on p. 17).

[30] Daniela Rus and Cynthia Sung. 'Spotlight on origami robots'. In: *Science Robotics* 3.15 (2018), eaat0938 (cit. on p. 18).

[31] Shuhei Miyashita, Steven Guitron, Marvin Ludersdorfer, Cynthia R Sung and Daniela Rus. 'An untethered miniature origami robot that self-folds, walks, swims, and degrades'. In: *2015 IEEE International Conference on Robotics and Automation* (*ICRA*). IEEE. 2015, pp. 1490–1496 (cit. on pp. 18, 30, 43).

[32] Shuhei Miyashita, Steven Guitron, Shuguang Li and Daniela Rus. 'Robotic metamorphosis by origami exoskeletons'. In: *Science Robotics* 2.10 (2017), eaao4369 (cit. on pp. 18, 83).

[33] Ying Liu, Brandi Shaw, Michael D Dickey and Jan Genzer. 'Sequential self-folding of polymer sheets'. In: *Science Advances* 3.3 (2017), e1602417 (cit. on p. 18).

[34] Tomohiro Tachi. '3D origami design based on tucking molecule'. In: *The Fourth International Conference on Origami in Science, Mathematics, and Education, R. Lang, ed., Pasadena*. 2009, pp. 259–272 (cit. on p. 18).

[35] Mustafa Boyvat, Je-Sung Koh and Robert J Wood. 'Addressable wireless actuation for multijoint folding robots and devices'. In: *Science Robotics* 2.8 (2017), eaan1544 (cit. on pp. 19, 30).

[36] Anna B Baker, Duncan F Wass and Richard S Trask. `4D sequential actuation: combining ionoprinting and redox chemistry in hydrogels'. In: *Smart Materials and Structures* 25.10 (2016), 10LT02 (cit. on p. 19).

[37] Jun-Hee Na, Arthur A Evans, Jinhye Bae et al. `Programming reversibly self-folding origami with micropatterned photo-crosslinkable polymer trilayers'. In: *Advanced Materials* 27.1 (2015), pp. 79–85 (cit. on p. 19).

[38] Elliot Hawkes, Byoungkwon An, Nadia M Benbernou et al. `Programmable matter by folding'. In: *Proceedings of the National Academy of Sciences* 107.28 (2010), pp. 12441–12445 (cit. on p. 19).

[39] Yinan Sun, Yuqi Jiang, Hao Yang et al. `Salamanderbot: A soft-rigid composite continuum mobile robot to traverse complex environments'. In: *2020 IEEE International Conference on Robotics and Automation (ICRA)*. IEEE. 2020, pp. 2953–2959 (cit. on p. 20).

[40] Metin Sitti and Diederik S Wiersma. `Pros and cons: Magnetic versus optical microrobots'. In: *Advanced Materials* 32.20 (2020), p. 1906766 (cit. on p. 20).

[41] Arthur W Mahoney and Jake J Abbott. `Managing magnetic force applied to a magnetic device by a rotating dipole field'. In: *Applied Physics Letters* 99.13 (2011), p. 134103 (cit. on p. 20).

[42] Jake J Abbott, Olgaç Ergeneman, Michael P Kummer, Ann M Hirt and Bradley J Nelson. `Modeling magnetic torque and force for controlled manipulation of soft-magnetic bodies'. In: *IEEE Transactions on Robotics* 23.6 (2007), pp. 1247–1252 (cit. on p. 20).

[43] Jürgen Rahmer, Christian Stehning and Bernhard Gleich. `Remote magnetic actuation using a clinical scale system'. In: *PlOS ONE* 13.3 (2018), e0193546 (cit. on p. 21).

[44] Zheng Zhang, Xianghao Li, Xiaochen Yu et al. `Magnetic actuation bionic robotic gripper with bistable morphing structure'. In: *Composite Structures* 229 (2019), p. 111422 (cit. on p. 21).

[45] Jiong Zhang, Julian Hu, Hao Wang, A Senthil Kumar and Akshay Chaudhari. `A novel magnetically driven polishing technique for internal surface finishing'. In: *Precision Engineering* 54 (2018), pp. 222–232 (cit. on p. 21).

[46] Donghoon Son, Musab Cagri Ugurlu and Metin Sitti. 'Permanent magnet array–driven navigation of wireless millirobots inside soft tissues'. In: *Science Advances* 7.43 (2021), eabi8932 (cit. on p. 21).

[47] Frédéric Rochat, Patrick Schoeneich, Michael Bonani et al. 'Design of magnetic switchable device (MSD) and applications in climbing robot'. In: *Emerging trends in mobile robotics*. World Scientific, 2010, pp. 375–382 (cit. on p. 22).

[48] Eric Diller, Joshua Giltinan, Guo Zhan Lum, Zhou Ye and Metin Sitti. 'Six-degree-of-freedom magnetic actuation for wireless microrobotics'. In: *The International Journal of Robotics Research* 35.1-3 (2016), pp. 114–128 (cit. on pp. 22, 61).

[49] H Markides, Michael Rotherham and Alicia El Haj. 'Biocompatibility and toxicity of magnetic nanoparticles in regenerative medicine'. In: *Journal of Nanomaterials* 2012 (2012) (cit. on p. 22).

[50] Chong Hong, Ziyu Ren, Che Wang et al. 'Magnetically actuated gearbox for the wireless control of millimeter-scale robots'. In: *Science Robotics* 7.69 (2022), eabo4401 (cit. on pp. 22, 61, 92, 93, 96, 97, 99).

[51] Wenqi Hu, Guo Zhan Lum, Massimo Mastrangeli and Metin Sitti. 'Small-scale soft-bodied robot with multimodal locomotion'. In: *Nature* 554.7690 (2018), pp. 81–85 (cit. on pp. 23, 30, 43, 103).

[52] Ziyu Ren, Rongjing Zhang, Ren Hao Soon et al. 'Soft-bodied adaptive multimodal locomotion strategies in fluid-filled confined spaces'. In: *Science advances* 7.27 (2021), eabh2022 (cit. on p. 23).

[53] S Sudo, S Segawa and Takashi Honda. 'Magnetic swimming mechanism in a viscous liquid'. In: *Journal of intelligent material systems and structures* 17.8-9 (2006), pp. 729–736 (cit. on p. 23).

[54] Yoonho Kim, Hyunwoo Yuk, Ruike Zhao, Shawn A Chester and Xuanhe Zhao. 'Printing ferromagnetic domains for untethered fast-transforming soft materials'. In: *Nature* 558.7709 (2018), pp. 274–279 (cit. on p. 23).

[55] Guo Zhan Lum, Zhou Ye, Xiaoguang Dong et al. 'Shape-programmable magnetic soft matter'. In: *Proceedings of the National Academy of Sciences* 113.41 (2016), E6007–E6015 (cit. on pp. 24, 43).

[56] Stefano Fusco, Hen-Wei Huang, Kathrin E Peyer et al. 'Shape-switching microrobots for medical applications: The influence of shape in drug delivery and locomotion'. In: *ACS applied materials & interfaces* 7.12 (2015), pp. 6803–6811 (cit. on p. 24).

[57] Connor Watson and Tania K Morimoto. 'Permanent magnet-based localization for growing robots in medical applications'. In: *IEEE Robotics and Automation Letters* 5.2 (2020), pp. 2666–2673 (cit. on p. 24).

[58] Jialun Liu, Hironari Sugiyama, Tadachika Nakayama and Shuhei Miyashita. 'Magnetic Sensor Based Topographic Localization for Automatic Dislocation of Ingested Button Battery'. In: *2020 IEEE International Conference on Robotics and Automation* (*ICRA*). IEEE. 2020, pp. 5488–5494 (cit. on pp. 25, 42, 45).

[59] Mehmet Efe Tiryaki and Metin Sitti. 'Magnetic Resonance Imaging-Based Tracking and Navigation of Submillimeter-Scale Wireless Magnetic Robots'. In: *Advanced Intelligent Systems* 4.4 (2022), p. 2100178 (cit. on p. 25).

[60] Chytra Pawashe, Steven Floyd and Metin Sitti. 'Magnetic mobile micro-robots'. In: *7ème Journées Nationales de la Recherche en Robotique* (2009) (cit. on p. 26).

[61] Eric Diller, Steven Floyd, Chytra Pawashe and Metin Sitti. 'Control of multiple heterogeneous magnetic micro-robots on non-specialized surfaces'. In: *2011 IEEE International Conference on Robotics and Automation*. IEEE. 2011, pp. 115–120 (cit. on pp. 26, 90).

[62] Steven Floyd, Eric Diller, Chytra Pawashe and Metin Sitti. 'Control methodologies for a heterogeneous group of untethered magnetic micro-robots'. In: *The International Journal of Robotics Research* 30.13 (2011), pp. 1553–1565 (cit. on p. 26).

[63] Eric Diller, Joshua Giltinan and Metin Sitti. 'Independent control of multiple magnetic microrobots in three dimensions'. In: *The International Journal of Robotics Research* 32.5 (2013), pp. 614–631 (cit. on p. 26).

[64] Mohammad Salehizadeh and Eric Diller. 'Two-agent formation control of magnetic microrobots'. In: *2016 International Conference on Manipulation, Automation and Robotics at Small Scales* (*MARSS*). IEEE. 2016, pp. 1–6 (cit. on p. 27).

[65] Dana D Damian, Karl Price, Slava Arabagi et al. `In vivo tissue regeneration with robotic implants'. In: *Science Robotics* 3.14 (2018), eaaq0018 (cit. on p. 30).

[66] Eduardo Perez-Guagnelli, Joanna Jones, Ahmet H Tokel et al. `Characterization, simulation and control of a soft helical pneumatic implantable robot for tissue regeneration'. In: *IEEE Transactions on Medical Robotics and Bionics* 2.1 (2020), pp. 94–103 (cit. on p. 30).

[67] Bradley J Nelson, Ioannis K Kaliakatsos and Jake J Abbott. `Microrobots for minimally invasive medicine'. In: *Annual review of biomedical engineering* 12 (2010), pp. 55–85 (cit. on pp. 42, 61).

[68] Christos Bergeles and Guang-Zhong Yang. `From passive tool holders to microsurgeons: safer, smaller, smarter surgical robots'. In: *IEEE Transactions on Biomedical Engineering* 61.5 (2013), pp. 1565–1576 (cit. on p. 42).

[69] N Peter Wiklund. `Technology Insight: surgical robots—expensive toys or the future of urologic surgery?' In: *Nature Clinical Practice Urology* 1.2 (2004), pp. 97–102 (cit. on p. 42).

[70] Maria C Carrozza, L Lencioni, B Magnani et al. `A microrobot for colonoscopy'. In: *MHS'96 Proceedings of the Seventh International Symposium on Micro Machine and Human Science*. IEEE. 1996, pp. 223–228 (cit. on p. 42).

[71] Gastone Ciuti, Pietro Valdastri, Arianna Menciassi and Paolo Dario. `Robotic magnetic steering and locomotion of capsule endoscope for diagnostic and surgical endoluminal procedures'. In: *Robotica* 28.2 (2010), pp. 199–207 (cit. on p. 42).

[72] Sehyuk Yim, Kartik Goyal and Metin Sitti. `Magnetically actuated soft capsule with the multimodal drug release function'. In: *IEEE/ASME Transactions on Mechatronics* 18.4 (2013), pp. 1413–1418 (cit. on p. 42).

[73] Makoto Nokata, Satoshi Kitamura, Toshihiro Nakagi, Toshiro Inubushi and Shigeki Morikawa. `Capsule type medical robot with magnetic drive in abdominal cavity'. In: *2008 2nd IEEE RAS & EMBS International Conference on Biomedical Robotics and Biomechatronics*. IEEE. 2008, pp. 348–353 (cit. on p. 42).

[74] Shuhei Miyashita, Steven Guitron, Kazuhiro Yoshida et al. `Ingestible, controllable, and degradable origami robot for patching stomach wounds'. In: *2016 IEEE international conference on robotics and automation (ICRA)*. IEEE. 2016, pp. 909–916 (cit. on p. 42).

[75] Brian P. Timko, Tal Dvir and Daniel S. Kohane. `Remotely Triggerable Drug Delivery Systems'. In: *Advanced Materials* 22.44 (2010), pp. 4925–4943 (cit. on p. 42).

[76] Michael P Kummer, Jake J Abbott, Bradley E Kratochvil et al. `OctoMag: An electromagnetic system for 5-DOF wireless micromanipulation'. In: *IEEE Transactions on Robotics* 26.6 (2010), pp. 1006–1017 (cit. on p. 42).

[77] Ellen T Roche, Markus A Horvath, Isaac Wamala et al. `Soft robotic sleeve supports heart function'. In: *Science translational medicine* 9.373 (2017) (cit. on p. 42).

[78] Veronica Iacovacci, Izadyar Tamadon, Emanuele Federico Kauffmann et al. `A fully implantable device for intraperitoneal drug delivery refilled by ingestible capsules'. In: *Science Robotics* 6.57 (2021), eabh3328 (cit. on p. 43).

[79] Dana D Damian, Karl Price, Slava Arabagi et al. `In vivo tissue regeneration with robotic implants'. In: *Science robotics* 3.14 (2018), eaaq0018 (cit. on pp. 43, 44).

[80] Guang-Zhong Yang, Jim Bellingham, Pierre E. Dupont et al. `The grand challenges of Science Robotics'. In: *Science Robotics* 3.14 (2018) (cit. on p. 43).

[81] DongDong Jin, JiangFan Yu, TianYun Huang, HuiLing Duan and Li Zhang. `Magnetic micro-/nanoscale swimmers: Current status and potential applications'. In: *Chinese Science Bulletin* 62.2-3 (2016), pp. 136–151 (cit. on p. 43).

[82] Jake J Abbott, Zoltan Nagy, Felix Beyeler and Bradley J Nelson. `Robotics in the small, part I: microbotics'. In: *IEEE Robotics & Automation Magazine* 14.2 (2007), pp. 92–103 (cit. on pp. 43, 61).

[83] Shuhei Miyashita, Steven Guitron, Shuguang Li and Daniela Rus. `Robotic metamorphosis by origami exoskeletons'. In: *Science Robotics* 2.10 (2017) (cit. on p. 43).

[84] K Ishiyama, M Sendoh, A Yamazaki and KI Arai. `Swimming micro-machine driven by magnetic torque'. In: *Sensors and Actuators A: Physical* 91.1-2 (2001), pp. 141–144 (cit. on pp. 43, 61).

[85] Li Zhang, Jake J Abbott, Lixin Dong et al. `Artificial bacterial flagella: Fabrication and magnetic control'. In: *Applied Physics Letters* 94.6 (2009), p. 064107 (cit. on pp. 43, 61).

[86] Arthur W Mahoney, Nathan D Nelson, Kathrin E Peyer, Bradley J Nelson and Jake J Abbott. `Behavior of rotating magnetic microrobots above the step-out frequency with application to control of multi-microrobot systems'. In: *Applied Physics Letters* 104.14 (2014), p. 144101 (cit. on p. 44).

[87] Dana D Damian, Slava Arabagi, Assunta Fabozzo et al. `Robotic implant to apply tissue traction forces in the treatment of esophageal atresia'. In: *2014 IEEE International Conference on Robotics and Automation* (*ICRA*). IEEE. 2014, pp. 786–792 (cit. on pp. 44, 97).

[88] Taylor A Howell, Braxton Osting and Jake J Abbott. `Sorting rotating micromachines by variations in their magnetic properties'. In: *Physical Review Applied* 9.5 (2018), p. 054021 (cit. on pp. 49, 73).

[89] Konstantin I Morozov and Alexander M Leshansky. `The chiral magnetic nanomotors'. In: *Nanoscale* 6.3 (2014), pp. 1580–1588 (cit. on pp. 49, 73).

[90] Frank G Shellock. `Magnetic resonance safety update 2002: implants and devices'. In: *Journal of Magnetic Resonance Imaging: An Official Journal of the International Society for Magnetic Resonance in Medicine* 16.5 (2002), pp. 485–496 (cit. on pp. 50, 75, 98).

[91] Hyunjun Park, Sungjin Park, Euisung Yoon et al. `Paddling based microrobot for capsule endoscopes'. In: *Proceedings 2007 IEEE International Conference on Robotics and Automation*. IEEE. 2007, pp. 3377–3382 (cit. on p. 61).

[92] Yongju Kim, Jeong Eun Park, Jeong Jae Wie et al. `Effects of helix geometry on magnetic guiding of helical polymer composites on a gastric cancer model: A feasibility study'. In: *Materials* 13.4 (2020), p. 1014 (cit. on p. 61).

[93] Amirhossein Hajiaghajani, Dongwook Kim, Ali Abdolali and Seungyoung Ahn. `Patterned magnetic fields for remote steering and wireless powering to a swimming microrobot'. In: *IEEE/ASME Transactions on Mechatronics* 25.1 (2019), pp. 207–216 (cit. on p. 61).

[94] Metin Sitti, Hakan Ceylan, Wenqi Hu et al. `Biomedical applications of untethered mobile milli/microrobots'. In: *Proceedings of the IEEE* 103.2 (2015), pp. 205–224 (cit. on p. 61).

[95] Sylvain Martel. `Beyond imaging: Macro-and microscale medical robots actuated by clinical MRI scanners'. In: *Science Robotics* 2.3 (2017), eaam8119 (cit. on p. 61).

[96] Pietro Valdastri, Edoardo Sinibaldi, Sebastiano Caccavaro et al. `A novel magnetic actuation system for miniature swimming robots'. In: *IEEE Transactions on Robotics* 27.4 (2011), pp. 769–779 (cit. on p. 61).

[97] Jiyuan Tian, Kenneth Omokhagbo Afebu, Zepeng Wang, Yang Liu and Shyam Prasad. `Dynamic analysis of a soft capsule robot self-propelling in the small intestine via finite element method'. In: *Nonlinear Dynamics* (2023), pp. 1–22 (cit. on p. 61).

[98] Zhibin Song, Zhongru Fu, Donato Romano, Paolo Dario and Jian S Dai. `A novel biomimetic compliant structural skin based on composite materials for biorobotics applications'. In: *Soft Robotics* 9.3 (2022), pp. 440–450 (cit. on p. 61).

[99] Sehyuk Yim, Kartik Goyal and Metin Sitti. `Magnetically actuated soft capsule with the multimodal drug release function'. In: *IEEE/ASME Transactions on Mechatronics* 18.4 (2013), pp. 1413–1418 (cit. on p. 61).

[100] Jiaen Wu, Bumjin Jang, Yuval Harduf et al. `Helical Klinotactic Locomotion of Two-Link Nanoswimmers with Dual-Function Drug-Loaded Soft Polysaccharide Hinges'. In: *Advanced Science* 8.8 (2021), p. 2004458 (cit. on p. 61).

[101] Jürgen Rahmer, Christian Stehning and Bernhard Gleich. `Spatially selective remote magnetic actuation of identical helical micromachines'. In: *Science Robotics* 2.3 (2017), eaal2845 (cit. on pp. 61, 89).

[102] Hen-Wei Huang, Mark W Tibbitt, Tian-Yun Huang and Bradley J Nelson. `Matryoshka-inspired micro-origami capsules to enhance loading, encapsulation, and transport of drugs'. In: *Soft robotics* 6.1 (2019), pp. 150–159 (cit. on p. 61).

[103] Zhuo Fan Bao and Eric Diller. 'Evaluating Miniature Robot Surgical Scissors'. In: *2022 International Conference on Manipulation, Automation and Robotics at Small Scales* (*MARSS*). IEEE. 2022, pp. 1–6 (cit. on p. 61).

[104] Mengmeng Sun, Chenyao Tian, Liyang Mao et al. 'Reconfigurable magnetic slime robot: deformation, adaptability, and multifunction'. In: *Advanced Functional Materials* 32.26 (2022), p. 2112508 (cit. on p. 61).

[105] Aaron T Becker, Ouajdi Felfoul and Pierre E Dupont. 'Toward tissue penetration by MRI-powered millirobots using a self-assembled Gauss gun'. In: *2015 IEEE International Conference on Robotics and Automation* (*ICRA*). IEEE. 2015, pp. 1184–1189 (cit. on p. 61).

[106] Michael P Kummer, Jake J Abbott, Bradley E Kratochvil et al. 'OctoMag: An electromagnetic system for 5-DOF wireless micromanipulation'. In: *IEEE Transactions on Robotics* 26.6 (2010), pp. 1006–1017 (cit. on p. 61).

[107] Sehyuk Yim and Metin Sitti. 'Design and rolling locomotion of a magnetically actuated soft capsule endoscope'. In: *IEEE Transactions on Robotics* 28.1 (2011), pp. 183–194 (cit. on pp. 61, 83).

[108] D Yardeni, H Yardeni, AGI Coran and Eustace S Golladay. 'Severe esophageal damage due to button battery ingestion: can it be prevented?' In: *Pediatric surgery international* 20.7 (2004), pp. 496–501 (cit. on p. 64).

[109] Joshua M Hamilton, Scott A Schraff and David M Notrica. 'Severe injuries from coin cell battery ingestions: 2 case reports'. In: *Journal of Pediatric Surgery* 44.3 (2009), pp. 644–647 (cit. on p. 64).

[110] Shohei Honda, Masato Shinkai, Yoshiko Usui et al. 'Severe gastric damage caused by button battery ingestion in a 3-month-old infant'. In: *Journal of pediatric surgery* 45.9 (2010), e23–e26 (cit. on p. 64).

[111] Anette Mortensen, Nikolaj Friis Hansen and Ole Mikael Schiødt. 'Fatal aortoesophageal fistula caused by button battery ingestion in a 1-year-old child'. In: *American Journal of Emergency Medicine* 8.28 (2010), 984–e5 (cit. on p. 64).

[112] V Soerdjbalie-Maikoe and RR Van Rijn. 'A case of fatal coin battery ingestion in a 2-year-old child'. In: *Forensic Science International* 198.1-3 (2010), e19–e22 (cit. on p. 64).

[113] *Swallowed a Button Battery? National Capital Poison Center*. URL: https://www.poison.org/battery. (accessed: 22.08.2022) (cit. on p. 64).

[114] Jun Hee Lee, Jee Hoo Lee, Jung Ok Shim et al. 'Foreign body ingestion in children: should button batteries in the stomach be urgently removed?' In: *Pediatric gastroenterology, hepatology & nutrition* 19.1 (2016), pp. 20–28 (cit. on p. 64).

[115] Bryan Laulicht, Giovanni Traverso, Vikram Deshpande, Robert Langer and Jeffrey M Karp. 'Simple battery armor to protect against gastrointestinal injury from accidental ingestion'. In: *Proceedings of the National Academy of Sciences* 111.46 (2014), pp. 16490–16495 (cit. on p. 64).

[116] Haruna Iwasaki, Flavien Lefevre, Dana D Damian, Eiji Iwase and Shuhei Miyashita. 'Autonomous and reversible adhesion using elastomeric suction cups for in-vivo medical treatments'. In: *IEEE Robotics and Automation Letters* 5.2 (2020), pp. 2015–2022 (cit. on p. 64).

[117] Jialun Liu, Hironari Sugiyama, Tadachika Nakayama and Shuhei Miyashita. 'Magnetic Sensor Based Topographic Localization for Automatic Dislocation of Ingested Button Battery'. In: *2020 IEEE International Conference on Robotics and Automation (ICRA)*. 2020, pp. 5488–5494 (cit. on pp. 64, 76, 77).

[118] Kira Seleznyova, Mark Strugatsky and Janis Kliava. 'Modelling the magnetic dipole'. In: *European Journal of Physics* 37.2 (2016), p. 025203 (cit. on p. 69).

[119] Eric Diller, Chytra Pawashe, Steven Floyd and Metin Sitti. 'Assembly and disassembly of magnetic mobile micro-robots towards deterministic 2-D reconfigurable micro-systems'. In: *The International Journal of Robotics Research* 30.14 (2011), pp. 1667–1680 (cit. on p. 89).

[120] Zicheng Bi, Lingjun Song, Robert De Kleine, Chunting Chris Mi and Gregory A Keoleian. 'Plug-in vs. wireless charging: Life cycle energy and greenhouse gas emissions for an electric bus system'. In: *Applied Energy* 146 (2015), pp. 11–19 (cit. on p. 98).

[121] Andreas Berger, Matteo Agostinelli, Sanna Vesti et al. `A wireless charging system applying phase-shift and amplitude control to maximize efficiency and extractable power'. In: *IEEE Transactions on Power Electronics* 30.11 (2015), pp. 6338–6348 (cit. on p. 98).

Appendix A

Magnetic Force Driven Wireless Motor

Cameron Duffield and Shuhei Miyashita, `Magnetic Force Driven Wireless Motor, In: Annual Conference Towards Autonomous Robotic Systems, published [2020], [Springer] [1]

Magnetic Force Driven Wireless Motor*

Cameron Duffield and Shuhei Miyashita[0000−0002−9795−9247]

Automatic Control and Systems Engineering, The University of Sheffield,
Portobello Ln, Sheffield, S1 3JD, UK
{cduffield1 | shuhei.miyashita}@sheffield.ac.uk
https://sites.google.com/site/shuheidotnet/

Abstract. A wirelessly actuated motor has wide potential application in in-vivo mechatronic devices, due to the absence of power and control cables from outside the device. This paper presents a magnetically actuated wireless motor with no net force acting on the device. The developed motor has a double crank; each connecting rod accommodates a 5mm neodymium magnet, actuated using a magnetic field produced by an electromagnetic coil system located nearby. The magnetic field aligned parallel to the direction of the magnet produces a magnetic force. The magnets are oppositely oriented, so experience attraction and repulsion forces, the crank converts this into a rotational motion. By altering the direction of the magnetic field, these forces are switched, and by using a ratchet a rotational motion in a single direction is produced.

Keywords: Magnetic control · Wireless motor · Dual-crank mechanism.

1 Introduction

Recent advances have been made with implantable medical robots. These implants often have electrical connections to the outside of the body [2], or in the case of soft robots pneumatic or hydraulic connections are used [6]. Magnetic induction based wireless power transmission is a promising approach, however, it necessitates the presence of electronics and a receiver coil within the device [1]. Magnetic direct drive mechanisms, where magnetic force or torque are transmitted in a non-contact manner, offer an alternative to on-board energy source or tethers. Small magnet on-board microrobots are one of the examples, where a magnetic field provided by an electromagnetic coil system directly actuates the robot [5]. Locomotion of magnetically controlled robots involves the entire body moving. Hu et. al. developed a soft robot that exploits multiple modes of actuation including, rolling, walking, and swimming [3]. The method removes the energy source from the robot, allowing them to be smaller and lighter. However, this approach does not allow for the driving of mechanisms within the robot as a net torque is applied to the robot body, causing it to rotate [4].

* Supported by the Department of Automatic Control and Systems Engineering, The University of Sheffield.

This paper presents a novel magnetic drive mechanism using a double crank. A magnet in each connecting rod is directly actuated by a magnetic field, producing a rotational motion. Thanks to the opposed directions of magnetic forces, the motor experiences zero net force, thus minimising the impact on the local environment where it is situated.

2 Method

The developed motor consists of two counterweighting cranks, with 180° phase difference, on each of which is a 5 mm cubic neodymium iron boron (NdFeB) magnet at the end (Fig. 1).

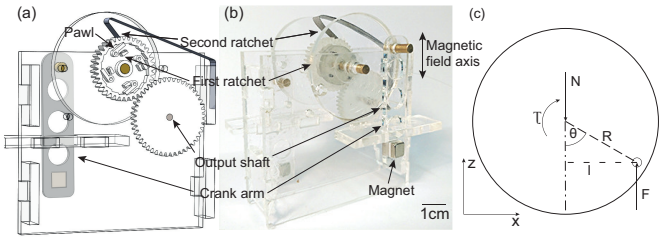

Fig. 1: The developed magnetic force driven wireless motor. (a) CAD section view and (b) Photograph. (c) Force analysis.

The magnets are vertical, with opposite orientation, this ensures there is no net magnetic force acting on the motor from the external magnetic field. The magnetic field gradient ($0.14\,\mathrm{T\ m^{-1}}$) is applied vertically from a 200 mm diameter electromagnetic coil embedded 40 mm below the workspace, and can periodically switch the orientation. A crank converts the linear motion of the crank arm to rotary motion. To remove the singularity at top dead centre the crank is designed to oscillate 45° either side of horizontal. A double ratchet mechanism is used to convert this oscillating rotation to rotation in a single direction and prevent the load back-driving the motor. The first ratchet consists of four pawls within a saw-tooth ring gear. The second ratchet uses a combined pawl and pawl spring against the involute tooth driving gear.

For the driving stroke the magnetic field gradient is applied in the negative z direction, moving the crank clockwise. The geometry of the design prevents the crank from rotating past $\theta = 135°$. The field gradient is then reversed, the first ratchet disengages and the crank moves counter-clockwise for the recoil stroke. The maximum torque is given when the crank is horizontal ($\theta = 90°$) and the minimum is at the two extremes of motion ($\theta = 45°$, $\theta = 135°$). The control of the magnetic field is open loop. The angular position of the output shaft can be calculated for open-loop position control from the number of driving strokes performed.

The magnetic force on a magnet with moment $\vec{m}$, $\vec{F}_m$, in a magnetic field $\vec{B}$ is given by

$$\begin{aligned}\vec{F}_m &= (\vec{m} \cdot \nabla)\, \vec{B} \\ &= \left(\frac{\partial \vec{B}}{\partial x} \frac{\partial \vec{B}}{\partial y} \frac{\partial \vec{B}}{\partial z} \right)^T \vec{m}. \end{aligned} \tag{1}$$

Referring to Fig.1 (c) which shows the relation of a free body diagram of the system, with (1), The producible torque about the output shaft, τ, is

$$\tau = 2\, n\, \frac{\partial \vec{B}}{\partial z}\, \vec{m}\, R\, \sin\theta - Fr, \tag{2}$$

where the coefficient 2 represents the use of two magnets, n is the used gear ratio, R is the crank radius, and Fr is torque loss to friction in the mechanism.

The housing parts were laser cut from 3 mm, and the connecting rods from 2 mm, sheet acrylic using a CO_2 laser cutter. The gears and ratchet parts were manufactured from Formlabs clear resin using a Form 2 SLA printer. The 3mm diameter shafts were cut from brass (CZ121/CW614N) rod and 2mm diameter stainless steel rod. Small pieces of Ecoflex 00-10 were used for the pawl springs in the ratchet mechanism. The second ratchet was cut from a 0.1 mm thick steel sheet (full hard, cold rolled, low carbon 1008-1010) and bent to shape. The mechanism was assembled using acrylic adhesive and cyano acrylate.

3 Results

The experimental setup for the measurement of torque is shown in Fig. 2 (a).

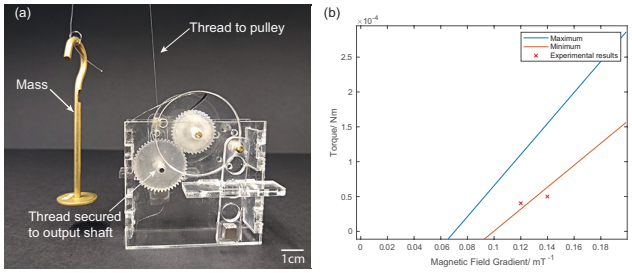

Fig. 2: Measurement of torque. (a) The experimental setup, (b) Theoretical and experimental plot of torque τ.

The output torque of the motor was measured using a simple hoist mechanism. A length of mono-filament nylon thread was secured to the shaft, passed up over a pulley, and down to a known mass to provide the load. The friction in

the mechanism was measured by removing the crank arms, winding the thread around the output shaft and adding mass until the mechanism rotates. This gave $Fr = 0.15 \times 10^{-3} \pm 0.01 \times 10^{-3}$ Nm. Fig.2 (b) shows the measured and calculated motor torque for a given magnetic field gradient. The maximum line represents the point when the crank is horizontal and torque is greatest, while the minimum line shows where the crank is at its lowest or highest point (45° from horizontal) and the torque is at its minimum. The experimentally measured values are the greatest load at which the motor could complete the full cycle, so correspond to the minimum torque line. The provisional experimental results in Fig. 2 (b) show the model being a reasonable fit for the data.

4 Conclusion

A magnetically actuated wireless motor driven by a magnetic force has been presented. Because of the force and weight countering mechanism, the device experiences net zero force and thus exhibits stability in operation. Initial values for output torque were measured. Future work includes further data collection and improvement of the design to reduce the torque lost to friction.

References

1. Boyvat, M., Koh, J.S., Wood, R.J.: Addressable wireless actuation for multijoint folding robots and devices. Science Robotics **2**(8), eaan1544 (2017)
2. Damian, D.D., Price, K., Arabagi, S., Berra, I., Machaidze, Z., Manjila, S., Shimada, S., Fabozzo, A., Arnal, G., Van Story, D., et al.: In vivo tissue regeneration with robotic implants. Science Robotics **3**(14), eaaq0018 (2018)
3. Hu, W., Lum, G.Z., Mastrangeli, M., Sitti, M.: Small-scale soft-bodied robot with multimodal locomotion. Nature **554**(7690), 81–85 (2018)
4. Lien, G.S., Liu, C.W., Jiang, J.A., Chuang, C.L., Teng, M.T.: Magnetic control system targeted for capsule endoscopic operations in the stomach—design, fabrication, and in vitro and ex vivo evaluations. IEEE Transactions on Biomedical Engineering **59**(7), 2068–2079 (2012)
5. Miyashita, S., Guitron, S., Ludersdorfer, M., Sung, C.R., Rus, D.: An untethered miniature origami robot that self-folds, walks, swims, and degrades. In: 2015 IEEE International Conference on Robotics and Automation (ICRA). pp. 1490–1496. IEEE (2015)
6. Perez-Guagnelli, E., Jones, J., Tokel, A.H., Herzig, N., Jones, B., Miyashita, S., Damian, D.D.: Characterization, simulation and control of a soft helical pneumatic implantable robot for tissue regeneration. IEEE Transactions on Medical Robotics and Bionics **2**(1), 94–103 (Feb 2020). https://doi.org/10.1109/TMRB.2020.2970308

Appendix B

Wirelessly Magnetically Actuated Motor for Tissue Regeneration Robotic Implant

Wirelessly Magnetically Actuated Motor for Tissue Regeneration Robotic Implant

Cameron Duffield[1], Abigail F Smith[1], Daniela Rus[2], Dana Damian[1,3], and Shuhei Miyashita[1,3]

***Abstract*— In biomedical engineering, robotic implants provide new methods to restore and improve bodily function, and regenerate tissue. A significant challenge with the design of these devices is to safely actuate them for weeks or months, while they are residing in a patient's body. Magnetic, and other force-at-distance actuation methods, allow mechanisms to be controlled remotely and without contact or line of sight to the device. In this paper, we present a novel magnetic field driven wireless motor. The motor drives a robotic implant for the treatment of long gap esophageal atresia and short bowel syndrome. The motor is equipped with two oppositely oriented permanent magnets which experience forces in opposite directions when a magnetic field is applied tangential to the magnets' directions. The implant can produce a force of 2 N. It is demonstrated with an ex vivo porcine esophagus.**

I. Introduction

Wirelessly controlled robots show great potential to be used for biomedical applications [1]. Telesurgery robots are widely clinically approved and are used to improve the outcomes of surgical interventions [2], [3]. Tethered crawlers have been shown to improve the effectiveness of certain medical procedures, such as colonoscopies [4], [5]. Untethered robots [6], [7] provide a new solution to gastrointestinal (GI) diseases, incorporating drug release and wireless actuation techniques. Medical robots in vivo have also shown promise in foreign matter retrieval [8], [9], targeted drug delivery [10] and ophthalmologic procedures [11]. Another area of interest is the implementation of robotic implants for long-term therapies. Such devices are able to reside in the body and achieve effective functions and therapies. Examples include supporting heart function [12], performing as an artificial pancreas [13] and tissue regeneration [14].

One of the significant challenges with designing robotic implants is power delivery and control [15]. Conventional motors require a source of electricity to run which could be provided by wires passing into the body or batteries. Alternatively, magnetic control can be used as a form of force-at-distance actuation. Magnetic fields are used to apply forces and torques to a magnetized robot [16], [17], [18], [19], [20]. Using magnetic fields to control devices wirelessly has been shown to be a plausible solution [21]. Magnetic fields are able to pass through common materials, including biological tissue, making magnetic actuation a suitable method for robots purposed for biomedical applications as magnetic fields of up to 7 T are approved for use in MRI machines with no adverse effects on a patient.

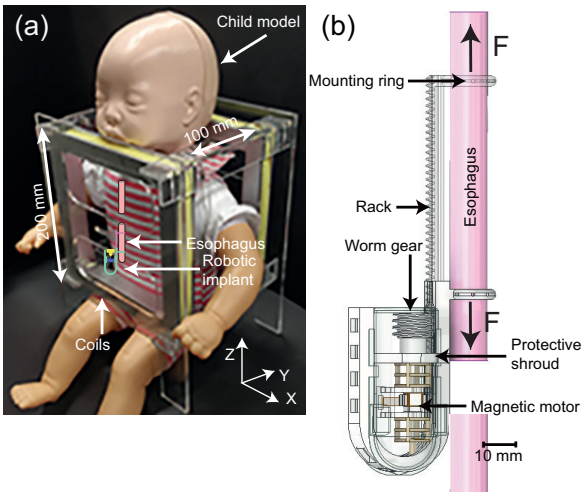

Fig. 1. The developed wirelessly powered robotic implant. (a) Shows the control coils and where the device would be positioned in a patient. (b) Shows details of parts of the robotic implant

Existing robots using magnetic control move the entire robot as a solid body by changing the orientation of the magnetic field [22] [23]. One of the recognized approaches is to apply a continuously rotating magnetic field, requiring a complex arrangement of coils that are capable of creating a magnetic field of any orientation [24].

This paper continues on our previous work [25] to present a magnetic wireless motor that produces zero net torque and net force powered by electromagnetic field from a pair of coils. As extension of our previous work, this paper introduces a motor with improved torque, more than a 60% reduction in body size and integrated in a robotic implant capable of stimulating tissue growth through mechanical therapy. The single pair of coils used to drive the motor greatly simplifies the equipment required and control of the robot compared to the existing magnetic control approaches.

This motor is incorporated into a device to lengthen tubular organs by applying a uniaxial force, advancing previous work [26]. The device could be used to improve the treatment of esophageal atresia or short bowel syndrome. The treatment of esophageal atresia traditionally requires multi-week sedation and ventilation. Sutures attached to the esophagus are manually pulled from outside

[1]Automatic Control and Systems Engineering Department, University of Sheffield, Sheffield S1 3JD, UK. cduffield1@sheffield.ac.uk
[2]Computer Science and Artificial Intelligence Laboratory, Massachusetts Institute of Technology, 32 Vassar Street, Cambridge, MA 02139, USA.
[3]Insigneo Institute for *in silico* Medicine, University of Sheffield, UK.
*Supported by the Department of Automatic Control and Systems Engineering, The University of Sheffield.

II. Methods

A. Robotic implant

The implant (Fig. 1) consists of two rings sutured to the esophagus. The first ring is connected to the main housing, while the second is connected to a rack. The rack is driven by the magnetic motor with a worm gear with a 2mm pitch. All moving parts are contained within a shroud to prevent damage to surrounding tissue. The rack has a travel of 45mm with the force being unaffected by the extension. A force of 2N has been shown to stimulate growth in porcine esophagus in vivo. The 20mm length of tissue grew an average of 2.5mm per day [14]. Magnetic control makes the implant design inherently safe. Magnetic control is forced based; unlike position based control it is impossible to apply greater force than intended, reducing the risk of damage to the tissue. The elongation of the implant can be detected using an array of hall effect sensors outside the body, as demonstrated in Liu et al. [9], to allow the position to be detected without any electronics being in the implant, or wires passing through the body.

B. Wireless motor

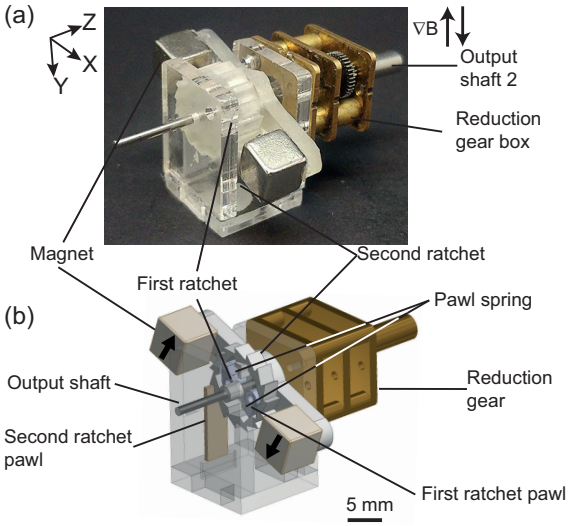

Fig. 2. The developed magnetic force driven wireless motor showing the double ratchet mechanism. (a) Photograph and (b) CAD section view.

For a magnetic motor to convert a magnetic field into rotary motions about a different axis, a magnetic field gradient that periodically reverses direction was chosen as the control power input. This allows for a reduction of net torque of the device or operation of multiple motors. This applies a force to any magnet in the field. A crank mechanism is used to convert this force to a torque. The developed motor uses two counter-weighting cranks, with 180° phase difference. At the end of each cranks is a magnet, the two magnets face in opposite directions (Fig. 2). This ensures that the system is balanced, and gravity does not affect the operation. This means when one has an upwards force from the magnetic field, the second has a downwards force, ensuring there is no net force acting on the motor.

A crank converts the force acting on the magnet to rotary motion. When the cranks are vertical (top dead center), the magnets are perpendicular to the magnetic field. This means there is no magnetic force, leading to a singularity. To remove this singularity the cranks' oscillation is limited to 45° either side of horizontal, this also keeps the motor near the maximum torque region where the cranks are horizontal. A double ratchet mechanism converts this oscillating rotation to rotation in a single direction and prevents the load back-driving the motor. The output torque is increased by a 1:290 reduction gear box.

The first ratchet consists of two pawls within a saw-tooth ring gear, Fig. 2 (b). The pawl carrier is free to rotate on the shaft, while the output gear is fixed to the shaft to transfer the torque. The two pawls are offset by half a tooth, meaning only one engages at any one time. This doubles the number of engagement point to 20, reducing the backlash. The second ratchet uses a combined pawl and pawl spring against the external saw tooth gear required to prevent back-driving, this has 15 engagement points. This means the motor only rotates in a single direction and can hold an unlimited load even without any magnetic field.

Fig. 3 shows the main stages of the motion of the motor. The cycle begins with the cranks inclined by 45° ($\theta = 45°$) (Fig. 3 (a)). A downwards magnetic field is applied, applying opposing forces to the two magnets, rotating the cranks clockwise. This engages the first ratchet, rotating the shaft and disengaging the second ratchet. When the cranks is horizontal (Fig. 3 (b)) the magnets are aligned with the magnetic field, giving the motor the maximum torque. When the cranks are declined by 45° ($\theta = 45°$) the magnet hits the end-stop, ending the driving stroke. When a magnetic field is then applied upwards this applies an opposite force to the magnets, causing the cranks to rotate anticlockwise (Fig. 3 (c)). The first ratchet disengages, disconnecting the cranks from the output shaft, while the second ratchet engages to prevent the load from back-driving the motor. This recoil stroke returns the cranks to the starting position, completing the cycle.

C. Model

To understand the properties of the motor, a model is presented for the output torque and speed of the motor. The motor is driven by the force of a magnetic field on the magnet at each end of the crank. The magnetic force on a magnet with magnetic moment $\vec{m}$, $\vec{F}_m$, in a magnetic field $\vec{B}$ is given by

$$\begin{aligned} \vec{F}_m &= (\vec{m} \cdot \nabla)\, \vec{B} \\ &= \left(\frac{\partial \vec{B}}{\partial x} \frac{\partial \vec{B}}{\partial y} \frac{\partial \vec{B}}{\partial z} \right)^T \vec{m}. \end{aligned} \tag{1}$$

When the magnet is out of alignment with the magnetic field gradient, the force is reduced. To calculate this reduced force the vector component of the magnetic field gradient

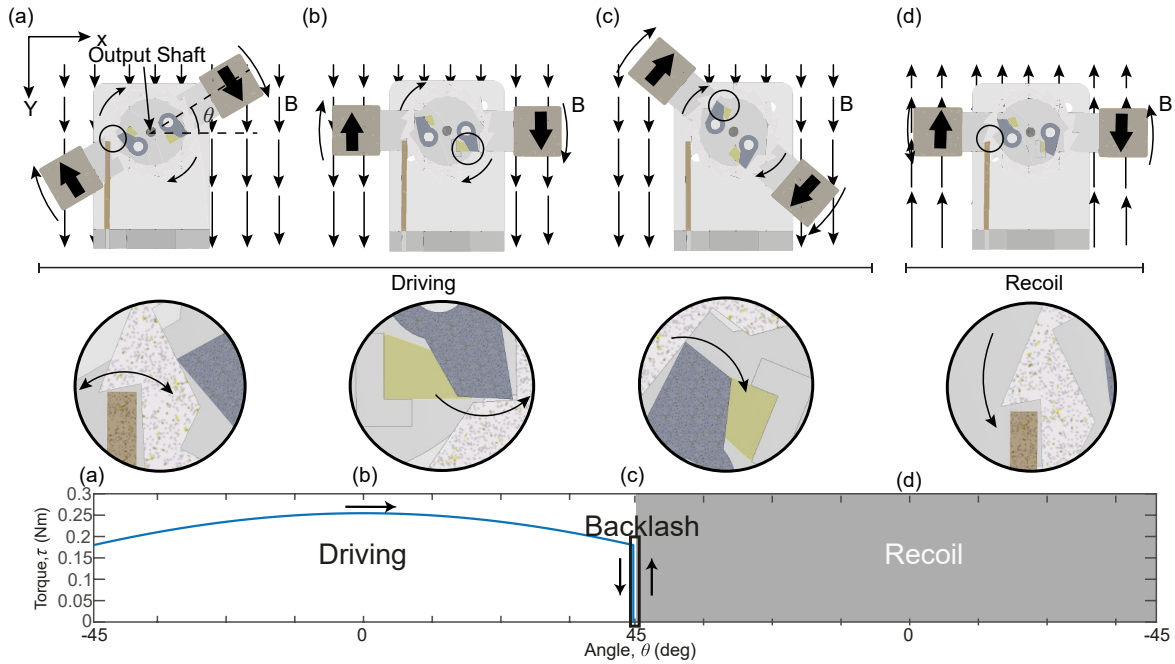

Fig. 3. The motion of the motor. (a) The driving stroke with the cranks at the highest point, and minimum torque, inset showing the disengaged second ratchet; (b) horizontal cranks giving the greatest torque, inset showing the engaged first ratchet pawl and decompressed Ecoflex™ pawl-spring; (c) the cranks at the end of the driving stroke, minimum torque, insert showing the second pawl with compressed pawl-spring; (d) the field gradient is reversed for the cranks to move back for the recoil stroke, inset showing the engaged second ratchet.

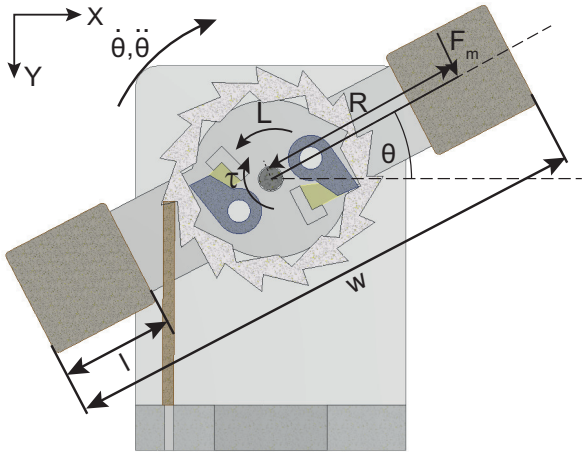

Fig. 4. A simplified free body diagram of the crank, showing the principle dimensions, forces and torques about the output shaft while the magnetic field is applied.

parallel to the magnetic moment is taken. Using the free body diagram of the system, shown in Fig. 4 with Eq. (1), the torque produced about the output shaft, τ, is

$$\tau = 2\,n \left\| \frac{\partial \vec{B}}{\partial z} \right\| \|\vec{m}\|\, R\, \cos\theta - F_r, \tag{2}$$

where the coefficient 2 represents the use of two magnets; it is assumed that the magnetic field gradient is constant across the work space and so both magnets experience a force of equal magnitude. n is the ratio of the gear box, R is the crank radius, and $F_r$is an empirical friction term. As there are two magnets of equal mass, the system is balanced and so weight does not affect torque.

The force from the robotic implant is given by:

$$F = \eta \frac{2\,\tau\,\pi}{P} \tag{3}$$

where P is the worm screw pitch, and η is an empirical efficiency term.

The implant extension velocity, v, is given by

$$v = \frac{\alpha}{2\pi n} p f, \tag{4}$$

where v is the rack speed, p is the pitch of the rack, n is the ratio of the gearbox, f is the magnetic field frequency, and α is the angle the crank passes through each driving stroke. For the motor presented $\alpha = \frac{\pi}{2}$ radians.

This is based on the assumption that the motor completes a full cycle is with each cycle of the magnetic field. If the actuation frequency, or load, is high then the motor will "step out" in a similar manner to a stepper motor.

When the motor is not subject to any load, the frequency is limited by the angular velocity. The time taken to reach angle θ from the initial position is given by:

$$T = \sqrt{\frac{2I(\theta - c)}{K\ I\ \cos(\theta) - 2L}}, \tag{5}$$

where c is the initial angle of the crank, L is the load on the motor, $K = \frac{2\ \frac{\partial \vec{B}}{\partial z}\ ||\vec{m}||\ R}{I}$ and I is the moment of inertia of the rotating parts,

$$I = 2\rho V R^2, \tag{6}$$

where ρ is the density of the magnet ($\rho = 7516$ kg m^{-3}) V is the volume of the magnets (125 mm^3), and R is the radius of the crank (10 mm). This assumes the mass of the crank arm is low compared to the mass of the magnets.

By making θ equal to $\alpha/2$, to give the time for the crank to travel a full stroke, the step out frequency can be found using,

$$f_{so} = \frac{1}{2T}, \tag{7}$$

for the motor demonstrated, the model gives a no-load step-out frequency of 13.15 Hz.

Above the step-out frequency, the motor speed decreases with increasing actuation frequency. For both rolling [27] and swimming [28] robots, the velocity of the rack for the implant is given by:

$$v = \frac{\alpha}{2\pi n} p(f_a - \sqrt{f_a^2 - f_{so}^2}), \tag{8}$$

where f_a is the actuation frequency, and f_{so} is the step-out frequency. The net torque acting on the system is given by:

$$\Sigma\tau = \Sigma\ \vec{F_m}\ \vec{P}, \tag{9}$$

where $\vec{F_m}$ is the force from a magnet, and $\vec{P}$ is the position vector for where the force is acting, perpendicular to the force. All forces are parallel to the magnetic field, meaning all position vectors are in the xy plane. This shows that for a single motor, a net torque will act on the system, if two motors are used, with opposite orientation, there will be no net torque acting on the system.

D. Motor fabrication and electromagnetic coil system

The robot body was cut from 2 mm cast acrylic sheet. Ratchet parts were manufactured using Form 2 SLA printer using clear resin (Formlabs), clear resin was chosen as it exhibits similar material properties to other resins produced by Formlabs which are certified for medical use. Small pieces of Ecoflex™ 00-10 (Smooth-On) were used for the pawl springs in the ratchet mechanism. The second ratchet was cut from a 0.5 mm thick low density polythene and bent to shape. The magnets used were 5 mm cubic neodymium iron boron (NdFeB) (Supermagnete). The reduction gear box is a commercially available unit with 1:290 reduction (Pololu). The mechanism was assembled using an acrylic adhesive (RS) and cyanoacrylate adhesive (Loctite). The worm gear was FDM printed (Mojo) using ABS, using a different material to the rack reduces friction compared with manufacturing both parts from the same material. All components are contained within a protective shroud made from photo-curable resin (Formlabs) meaning the device can be made bio-compatible.

Two electromagnetic coil systems were used. Magnetic field gradients of up to 0.37 Tm^{-1} were applied vertically from two square coils of 200 mm side length. For tests requiring a greater magnetic field gradient a Helmholtz coil of 180 mm diameter was used to provide a magnetic field gradient of up to 0.37 Tm^{-1} and a field strength of up to 15 mT. This is well below the static magnetic field strength of $0.046 - 8$ T of MRI machines [29].

E. Scalability

In this section, we investigate the impact of scaling down the motor on the output torque. Eq. 2 shows how the torque is proportional to the magnetic moment (m); this is given by $m = \frac{1}{\mu_0} B_r V$ where μ_0 is vacuum permeability ($4\pi \times 10^{-7}$ Hm^{-1}), B_r is the residual flux density (1.2 T), and V is the volume of the magnet. For a cubic magnet this means the magnetic moment, and motor torque, are proportional to the edge length cubed, as shown in Fig. 5.

Scaling down the device is also limited by the practical minimum feature resolution which can be made by a given manufacturing technique. The smallest components are the pawl springs in the first ratchet, and the finest details are the gear teeth. These components could be made half the current size without significantly changing manufacturing techniques. The maximum size of the motor may be limited for in vivo applications. The equivalent magnetic dipole for a cubic magnet passes through its center, meaning as the magnet size is increased the dipole moves closer to the center of the crank, reducing its effective radius. This leads to a compromise between maximizing the volume of the magnet and the crank radius. Eq. 5 gives the torque of the motor of width w and a cubic magnet of edge length l

$$\tau = \frac{\partial \vec{B}}{\partial z}\ \frac{1}{\mu_0} B_r\ l^3\ (w - l)\ \cos\theta. \tag{10}$$

Fig. 5 shows the affect of increasing the magnet size for both a fixed overall width of the motor, and for a fixed crank length. The plot shows that the magnet size greatly influences the output torque of the motor, meaning that the largest magnets possible should be used. For experiments in this paper the width was fixed at 25 mm and 5 mm cubic magnets were used as these are the greatest stock size of magnet that clears the ratchet mechanism.

III. Experimental Results

A. System characterization

Experiments were conducted to characterize the performance of the magnetic motor. A hoist mechanism was used for the experimental torque measurement. A length of monofilament nylon thread was attached to the shaft, passed up over a pulley, and down to a load. A known mass (± 0.001 g) was used for the load, and the magnetic field gradient gradually increased until the motor was able to lift the mass.

Fig. 6 shows the measured and calculated motor torque for a given magnetic field gradient. The experimentally

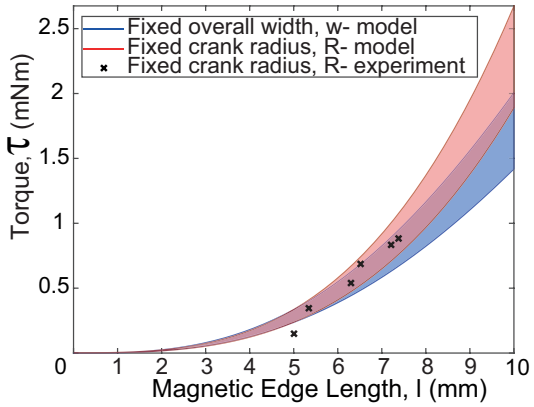

Fig. 5. The effect of increasing the size of the magnets used where first the overall width (w) is fixed, then the crank radius is fixed (R). The shaded region is the range between the peak and minimum torque without the reduction gearbox.

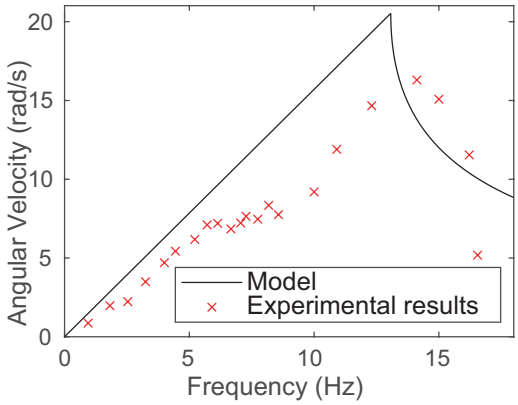

Fig. 7. The angular velocity of the motor without the reduction gearbox against the input frequency. It can be seen that at frequencies over the step-out frequency of 14 Hz the speed reduces, this is close to the modeled step-out frequency of 13.2 Hz.

measured values shown in the graph are the greatest load at which the motor could complete the full cycle, meaning they represent the minimum torque at any point in the cycle, which occurs where the crank is at $\pm 45°$. From these results it was determined that the friction term for the motor is $F_r = 0.03$ Nm.

The model for the motor torque is proportional to the magnetic field gradient (Eq. 2) with a peak torque where the cranks are horizontal, and a minimum torque where they are inclined at $45°$. Fig. 7 Shows how the angular velocity of the motor increases proportionally to the input magnetic field frequency, up until the step-out frequency where the angular velocity rapidly decays. It can be seen that at 6 Hz the angular velocity briefly decays before again becoming proportional to the input frequency.

1) Robotic implant characterization: The force from the implant was characterized using a similar method to torque, by hanging calibrated weights from the mounting ring ad reducing the magnetic field until it was unable to lift the mass. The modeled and predicted values for the force are shown in Fig. 8. The efficiency term was determined to be $\eta = 0.2$.

When implanted it is possible the robotic implant won't be perfectly positioned within the coil system. It is necessary that this does not pose any risk to the patient. The implant continues to operate when rotated $30°$ horizontally and $43°$ vertically from the ideal position. If the implant is moved from the center position, the force from the implant is reduced, making it a fail safe system.

The force from the implant on a phantom esophagus (made from Ecoflex™ $00-30$, Smooth-On) was measured using

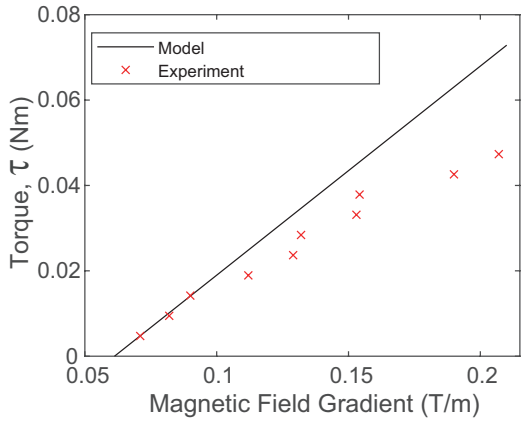

Fig. 6. Plot showing the output torque of the motor, both experimentally and modeled. It can be seen that the model is initially a good fit for the data, before diverging for greater magnetic field gradients.

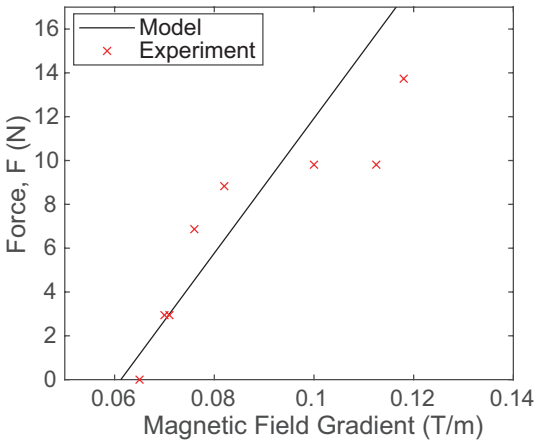

Fig. 8. Plot showing the implant force against magnetic field gradient.

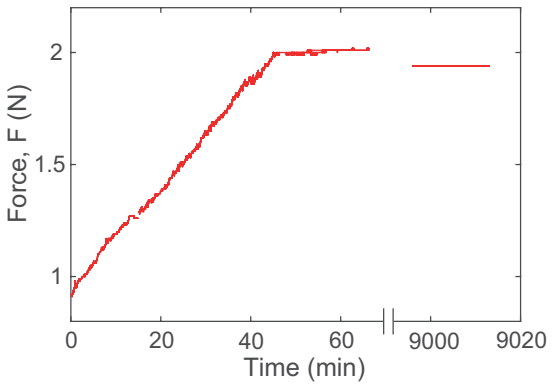

Fig. 9. The force from the implant on a phantom esophagus against time, showing how once the input power is stopped the implant maintains a near-constant force, for multiple days if required, due to the mechanism being non-backdriveable. The coils were turned off after 40 minutes, once the implant reached the target force demonstrating the force holding capability of the implant. 2N of force has previously been shown to stimulate tissue growth.

a compression force sensor (Fig 9). The coils were activated until the target force was reached after 40 minutes, before being turned off. The implant can continue to hold the desired force for extended periods of time without requiring any energy input, as the mechanism is non-backdrivable. For the clinical application the magnetic field would only need to be applied for short periods at regular intervals with no no nead for the patient to remain in the coil system between these. To prevent to coils overheating, the data was collected across multiple runs.

The implant was demonstrated using an ex vivo porcine esophagus. The esophagus was sutured, with simple interrupted sutures, to the attachment rings of the implant Fig. 10. The esophagus measured 11 mm in diameter when relaxed. The distance between the two attachment rings was 75 mm before stretching. The implant was able to stretch the tissue 5 mm in 10 minutes 42 seconds (6% extension) with a force of 2 N. These results show that the robotic implant is able to successfully apply the forces required to stimulate tissue regeneration to ex vivo esophageal tissue.

IV. Discussion and Conclusions

This paper presents a wirelessly actuated robotic implant for tissue regeneration. The implant has been demonstrated to produce 2N of force and hold the force without continued energy input. This has been demonstrated with both phantom and ex vivo porcine esophagi. 2 N of force have previously been shown to stimulate tissue growth, during animal trials.

The implant shown is driven by a novel magnetically actuated motor. The magnetic motor is driven by an externally applied uni-axial magnetic field gradient, and has been characterized for torque and speed. The motor experiences net zero force due to the magnetic force and weight countering mechanism, which was difficult to achieve with conventional approaches with magnetic field. The uni-axial magnetic field application means the direction of torque producible from the motor depends on its orientation, hence versatile combinations of multiple motors in a single body are possible. The presented mechanics showed a promising scalability in the motor size down by 15% keeping the output torque above 1 mNm, and also showed a tolerance to water given there are no electronic parts.

The motor is operational when fully submerged in water due to the absence of any electrical components which is ideal for operation within the body. Future work aims to scale down the body size using photo lithography methods. Alternating magnetic field could be used to allow multiple motors to operate with different orientations.

Future work includes implementing position detection using hall effect sensors and scaling down the device by half.

V. Acknowledgment

The authors thank Jack GS Davies, Marco Pontin, Quentin MP Lahondes, Sokratis Dimitriadis, and Joanna Jones for valuable comments and assistance with the project.

References

[1] B. J. Nelson, I. K. Kaliakatsos, and J. J. Abbott, "Microrobots for minimally invasive medicine," *Annual review of biomedical engineering*, vol. 12, pp. 55–85, 2010.

[2] C. Bergeles and G.-Z. Yang, "From passive tool holders to microsurgeons: safer, smaller, smarter surgical robots," *IEEE Transactions on Biomedical Engineering*, vol. 61, no. 5, pp. 1565–1576, 2013.

[3] N. P. Wiklund, "Technology insight: surgical robots—expensive toys or the future of urologic surgery?," *Nature Clinical Practice Urology*, vol. 1, no. 2, pp. 97–102, 2004.

[4] M. C. Carrozza, L. Lencioni, B. Magnani, P. Dario, D. Reynaerts, M. G. Trivella, and A. Pietrabissa, "A microrobot for colonoscopy," in *MHS'96 Proceedings of the Seventh International Symposium on Micro Machine and Human Science*, pp. 223–228, 1996.

[5] G. Ciuti, P. Valdastri, A. Menciassi, and P. Dario, "Robotic magnetic steering and locomotion of capsule endoscope for diagnostic and surgical endoluminal procedures," *Robotica*, vol. 28, no. 2, pp. 199–207, 2010.

[6] S. Yim, K. Goyal, and M. Sitti, "Magnetically actuated soft capsule with the multimodal drug release function," *IEEE/ASME Transactions on Mechatronics*, vol. 18, no. 4, pp. 1413–1418, 2013.

[7] M. Nokata, S. Kitamura, T. Nakagi, T. Inubushi, and S. Morikawa, "Capsule type medical robot with magnetic drive in abdominal cavity," in *2008 2nd IEEE RAS EMBS International Conference on Biomedical Robotics and Biomechatronics*, pp. 348–353, 2008.

[8] S. Miyashita, S. Guitron, K. Yoshida, Shuguang Li, D. D. Damian, and D. Rus, "Ingestible, controllable, and degradable origami robot for patching stomach wounds," in *2016 IEEE International Conference on Robotics and Automation (ICRA)*, pp. 909–916, 2016.

[9] J. Liu, H. Sugiyama, T. Nakayama, and S. Miyashita, "Magnetic sensor based topographic localization for automatic dislocation of ingested button battery," in *2020 IEEE International Conference on Robotics and Automation (ICRA)*, pp. 5488–5494, 2020.

[10] B. P. Timko, T. Dvir, and D. S. Kohane, "Remotely triggerable drug delivery systems," *Advanced Materials*, vol. 22, no. 44, pp. 4925–4943, 2010.

[11] M. P. Kummer, J. J. Abbott, B. E. Kratochvil, R. Borer, A. Sengul, and B. J. Nelson, "Octomag: An electromagnetic system for 5-DOF wireless micromanipulation," *IEEE Transactions on Robotics*, vol. 26, no. 6, pp. 1006–1017, 2010.

[12] E. T. Roche, M. A. Horvath, I. Wamala, A. Alazmani, S.-E. Song, W. Whyte, Z. Machaidze, C. J. Payne, J. C. Weaver, and G. Fishbein, "Soft robotic sleeve supports heart function," *Science translational medicine*, vol. 9, no. 373, 2017.

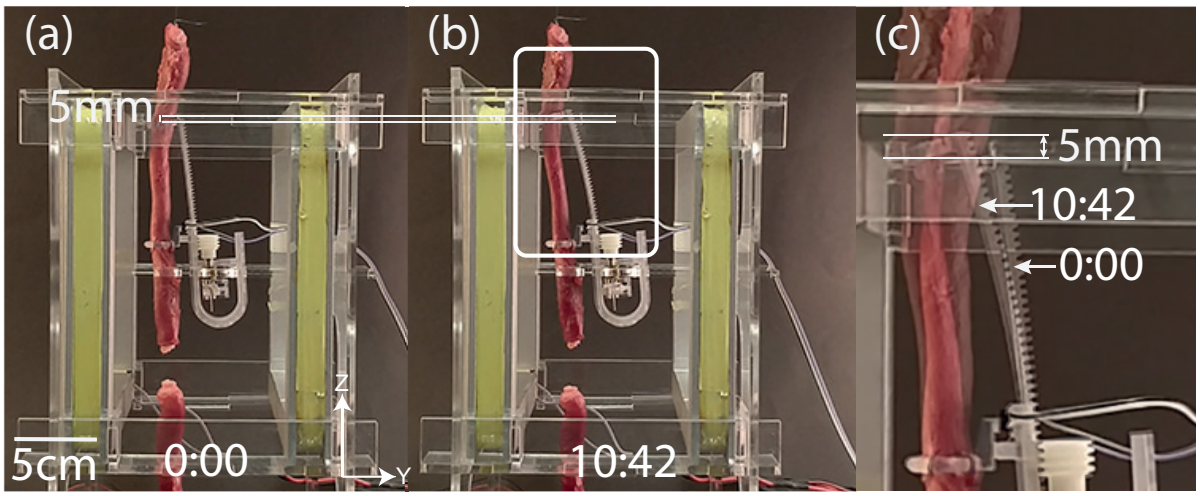

Fig. 10. Implant stretching an ex vivo porcine esophagus by 5 mm over 10 minutes and 42 seconds. (a) The initial position at 0 seconds, showing the esophagus in its relaxed position. (b) The esophagus after 10 minutes and 42 seconds, the esophagus has elongated by 5 mm. (c) Enlarged view showing the elongation of the esophagus. See video 1 for more detail.

[13] V. Iacovacci, I. Tamadon, E. F. Kauffmann, S. Pane, V. Simoni, L. Marziale, M. Aragona, L. Cobuccio, M. Chiarugi, P. Dario, *et al.*, "A fully implantable device for intraperitoneal drug delivery refilled by ingestible capsules," *Science Robotics*, vol. 6, no. 57, p. eabh3328, 2021.

[14] D. D. Damian, K. Price, S. Arabagi, I. Berra, Z. Machaidze, S. Manjila, S. Shimada, A. Fabozzo, G. Arnal, D. Van Story, J. D. Goldsmith, A. T. Agoston, C. Kim, R. W. Jennings, P. D. Ngo, M. Manfredi, and P. E. Dupont, "In vivo tissue regeneration with robotic implants," *Science Robotics*, vol. 3, no. 14, 2018.

[15] G.-Z. Yang, J. Bellingham, P. E. Dupont, P. Fischer, L. Floridi, R. Full, N. Jacobstein, V. Kumar, M. McNutt, R. Merrifield, B. J. Nelson, B. Scassellati, M. Taddeo, R. Taylor, M. Veloso, Z. L. Wang, and R. Wood, "The grand challenges of science robotics," *Science Robotics*, vol. 3, no. 14, 2018.

[16] D. Jin, J. Yu, T. Huang, H. Duan, and L. Zhang, "Magnetic micro-/nanoscale swimmers: Current status and potential applications," *Chinese Science Bulletin*, vol. 62, no. 2-3, pp. 136–151, 2016.

[17] J. J. Abbott, Z. Nagy, F. Beyeler, and B. J. Nelson, "Robotics in the small, part i: microbotics," *IEEE Robotics & Automation Magazine*, vol. 14, no. 2, pp. 92–103, 2007.

[18] G. Z. Lum, Z. Ye, X. Dong, H. Marvi, O. Erin, W. Hu, and M. Sitti, "Shape-programmable magnetic soft matter," *Proceedings of the National Academy of Sciences*, vol. 113, no. 41, pp. E6007–E6015, 2016.

[19] S. Miyashita, S. Guitron, M. Ludersdorfer, C. R. Sung, and D. Rus, "An untethered miniature origami robot that self-folds, walks, swims, and degrades," in *2015 IEEE International Conference on Robotics and Automation (ICRA)*, pp. 1490–1496, IEEE, 2015.

[20] W. Hu, G. Z. Lum, M. Mastrangeli, and M. Sitti, "Small-scale soft-bodied robot with multimodal locomotion," *Nature*, vol. 554, no. 7690, pp. 81–85, 2018.

[21] S. Miyashita, S. Guitron, S. Li, and D. Rus, "Robotic metamorphosis by origami exoskeletons," *Science Robotics*, vol. 2, no. 10, 2017.

[22] K. Ishiyama, M. Sendoh, A. Yamazaki, and K. Arai, "Swimming micro-machine driven by magnetic torque," *Sensors and Actuators A: Physical*, vol. 91, no. 1-2, pp. 141–144, 2001.

[23] L. Zhang, J. J. Abbott, L. Dong, B. E. Kratochvil, D. Bell, and B. J. Nelson, "Artificial bacterial flagella: Fabrication and magnetic control," *Applied Physics Letters*, vol. 94, no. 6, p. 064107, 2009.

[24] A. W. Mahoney, N. D. Nelson, K. E. Peyer, B. J. Nelson, and J. J. Abbott, "Behavior of rotating magnetic microrobots above the step-out frequency with application to control of multi-microrobot systems," *Applied Physics Letters*, vol. 104, no. 14, p. 144101, 2014.

[25] C. Duffield and S. Miyashita, "Magnetic force driven wireless motor," in *Annual Conference Towards Autonomous Robotic Systems*, pp. 409–412, Springer, 2020.

[26] D. D. Damian, S. Arabagi, A. Fabozzo, P. Ngo, R. Jennings, M. Manfredi, and P. E. Dupont, "Robotic implant to apply tissue traction forces in the treatment of esophageal atresia," in *2014 IEEE International Conference on Robotics and Automation (ICRA)*, pp. 786–792, 2014.

[27] T. A. Howell, B. Osting, and J. J. Abbott, "Sorting rotating micromachines by variations in their magnetic properties," *Physical Review Applied*, vol. 9, no. 5, p. 054021, 2018.

[28] K. I. Morozov and A. M. Leshansky, "The chiral magnetic nanomotors," *Nanoscale*, vol. 6, no. 3, pp. 1580–1588, 2014.

[29] F. G. Shellock, "Magnetic resonance safety update 2002: implants and devices," *Journal of Magnetic Resonance Imaging: An Official Journal of the International Society for Magnetic Resonance in Medicine*, vol. 16, no. 5, pp. 485–496, 2002.

Appendix C

Remotely Actuated Magnetic Motor for Unconstrained Robotic Capsule

Journal submission under review, submitted 26 May 2023.

Remotely Actuated Magnetic Motor for Unconstrained Robotic Capsule

Cameron Duffield[1], Jialun Liu[1], Yuqi Zhang[1,2], George Ashton[1]
Daniela Rus[3], Dana D. Damian[1,4] and Shuhei Miyashita[1,4]

***Abstract*— The realization of ingestible robots for use inside the body, has long been hampered by the limitations of mechatronic components, including battery life, motor power and computational power. With the advent of capsule endoscopes guided by an external magnetic field, it is expected that an ingested mechanical capsule, will be able to perform clinical treatments utilizing magnetically actuated motors. However, the conventional method of transferring magnetic torque to a remotely located magnetic body, by applying a rotating magnetic field, merely results in rotating the entire body, not the desired mechanism. In this study, we solved this problem by applying a magnetic field to a newly developed magnetic motor with a special magnet arrangement, allowing the body of the motor to remain stationary, while the output shaft rotates. The magnetic motor is lightweight (3.7 g) and has two magnets. When an external magnetic field is applied, the magnets rotate and align with it, before continuing to rotate, and aligning, due to their interaction with each other, to achieve a half rotation. A further half rotation is achieved by the magnetic field being applied in the opposite direction and the magnets' interaction, resulting in continuous drive of the motor. We investigated the characteristics of this motor and integrated it in a capsule that retrieves an accidentally ingested button battery from the stomach. The entire robotic capsule does not rotate due to this motor's characteristic of zero net torque. Instead, it's able to extend its arm, and sweeps it around itself, successfully retrieving a button battery under certain conditions. This study demonstrates how a capsule without electronics could achieve a series of mechanical functions within the body, opening up new possibilities for small-sized battery-less robots, together with the possibility of their further miniaturization and the use of biodegradable materials.**

I. Introduction

Despite the recent advancements towards the realization of a small autonomous robots that can move inside the human body for non-invasive medical treatments, various technical obstacles must still be overcome to ensure their clinical viability. One of the most notable issues is the limited battery capacity due to the small size of the robot, which rules out the use of conventional electric motors. The alternative to using such motors is the use of external magnetic fields to directly apply torque to a ferromagnetic material in the robot. Such a driving magnetic field is either produced by electromagnetic coils [1]–[3] or permanent magnets [4] positioned outside the body. This method provides a means of wirelessly supplying power to the robot while inside the body and removes the necessity for electronics within the robot [5]–[11]. The targeted applications include capsule endoscopes navigating using either rolling [12], swimming [13], or self propelling using vibro-impact [14], [15], and used for biopsy [16], [17] and drug delivery [18], [19], medical implants [20], encapsulation and transportation [21], cutting with scissors [22], accessing constrained environments [23], and tissue penetration [24].

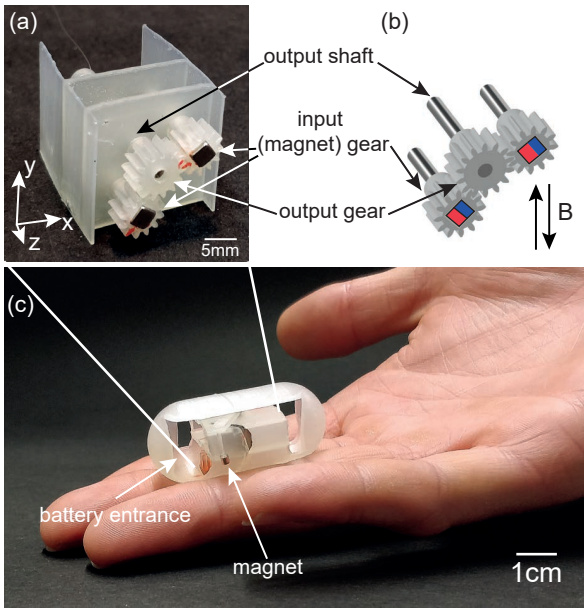

Fig. 1. Arrangement of the magnetic motor, (a) photograph, and (b) CAD model. (c) Capsule incorporating the motor.

While a free-floating rigid object has six degrees of freedom (DOF), three translational and three rotational; five navigational DOF of a magnet have been achieved with eight electromagnetic coils to enable any magnetic field or field gradient to be produced in the workspace, allowing for translation in three axes and rotation in two [25], and a sixth DOF have been achieved by having a non-uniform magnetization to act as a moment arm on the micro robot [26]. If further DOF are required on a free-floating (or an unconstrained) body beyond the navigational function, a method of applying a further mode of magnetic field and an additional mechanism that can be driven by this field must be devised. For example, in [16], [27], a technique is used

* This work has been supported by the EPSRC ERC DTP Scholarship. [1]Automatic Control and Systems Engineering Department, University of Sheffield, Sheffield S1 3JD, UK. shuhei.miyashita@sheffield.ac.uk +44 (0) 114 222 5662 [2]Faculty of Robot Science and Engineering, Northeastern University, Shenyang, China. [3]Computer Science and Artificial Intelligence Laboratory, Massachusetts Institute of Technology, Cambridge, MA, USA. [4]Insigneo Institute for *in silico* Medicine, University of Sheffield, UK.

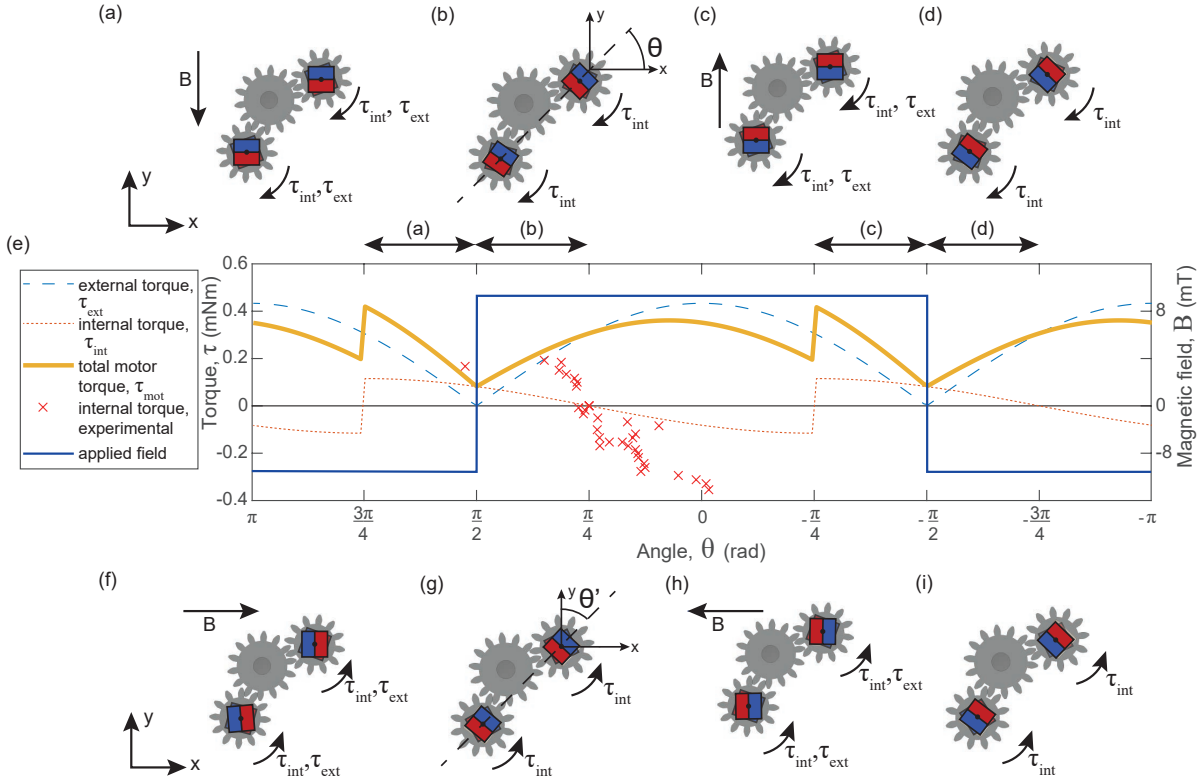

Fig. 2. Diagram showing the operation of the motor. (a) First, the magnets align with the magnetic field in the negative Y direction. (b) next, as the magnetic field is reversed, the internal torque causes the magnets to align with each other. (c) then the magnets align with the magnetic field in the positive Y direction. (d) finally, as the field is again reversed, and the magnets align with each other. (e) A graph of the motor torque through the operating cycle, showing internal, external, and total torque, both modeled and experimental values. (f)-(i) The motion of the motor running in reverse; by applying the magnetic field from the side the motor can be made to run in reverse.

in which a permanent magnet in the capsule is moved using the gradient of the magnetic field. In [28], the extra DOF is achieved passively by the chemically-induced deployability of an origami structure in the presence of surrounding fluids. The previously developed magnetically actuated motors such as the device in [4], however, experience a net torque on the whole motor from the external magnetic field, resulting in the motor's posture being unstable without the robot being secured by reaction forces from its surroundings [29], [30]. It is therefore required that a robot using this motor is either fixed in its environment or has a wide enough base to provide stability; in the case of [30] it is possible to use two counter-rotating motors to balance the torque and provide stability.

Taking these challenges into consideration, in this paper, we present a centimeter-scale magnetically-actuated motor to enable extra degrees of freedom in an unconstrained capsule. The motor, shown in Fig. 1 (a) in a photo and (b) in a CAD model, utilizes a periodically reversing external magnetic field to apply torque to a pair of permanent magnets. The motor consists of three meshing gears, the outer two of which have identical shapes and incorporate cubic permanent magnets (3 mm NdFeB) in specific orientations, called input gears. The output (central) gear is connected to the output shaft, delivering the total output torque to the desired load. The motor primarily rotates due to the torque applied by the external magnetic field, with the interaction between the two magnets In our system, the endoscopic capsule shown in Fig. 1 (c) is equipped with a ferro magnetic steel sheet that is magnetized by the applied magnetic field. As a rotating magnetic field is not being used to induce rotational motion, a ferromagnetic body can be integrated to align to the external magnetic field and stabilize the posture. When at an angle to the external magnetic field a torque acts on it, acting to align it with the magnetic field. This cancels the external torque acting on the motor, thereby achieving zero net torque applied to the capsule. This results in the capsule remaining stationary while the motor shaft is rotating.

As a proof of concept, we chose to use this motor to actuate an arm coming out of the endoscopic capsule to "grab" and retrieve an accidentally ingested button battery inside the body. Accidental ingestion of button batteries can be highly harmful, as short circuits through the tissue can lead to chemical burns in the GI tract from hydroxides formed [31]. Over 3,000 people in the US alone accidentally ingest button batteries every year, requiring medical imaging techniques such as x-rays to identify the location [32] and

potentially requiring endoscopy to remove the battery [33]. Alternatively systems for coating batteries with waterproof quantum tunneling composite coatings to prevent them from conducting when ingested have been developed [34], however, this has seen little uptake. Previous work has been done to develop magnetically actuated robots for the removal of ingested button batteries; however, these do not encapsulate the battery, leaving the terminals exposed to potentially cause further damage during removal [35], or focus on dressing the wounds caused by the battery [36]. The proposed capsule, alongside a method of remotely localizing a button battery and identifying its type using an array of Hall-effect sensors, building on the work presented in [37], acts as a first-of-a-kind concept that would be able to augment the arsenal of treatments available for this scenario.

II. Methods

This section first details the mechanics of the motor, followed by the mechanics of the capsule that houses the motor and retrieves a battery. Since there is a limit to the size of the button batteries that can be retrieved due to the limited size of the capsule, a wireless identification method for the type of button battery is subsequently presented.

A. Motor Design and Operation

The motor consists of two input (magnet) gears each containing a 3 mm cube magnet, these magnets sit on a line at $\frac{\pi}{4}$ rad to the axis of the magnetic field (Fig. 1). The magnet gears have 12 teeth of 0.5 mm modulus. These gears mesh with a central gear connected to the output shaft, allowing the torque from both magnets to be transmitted to the load. The center gear has 14 teeth, giving a gear ratio of 1:1.6667, the non-integer ratio helps to reduce hunting by ensuring even wear on the gear teeth. By changing the gear ratio of the input gears and the output gear, it is possible to change the output torque (or angular velocity) of the output shaft. All results are shown as for a 1:1 gear ratio.

Fig. 2 (a)-(d) shows the operating cycle of the motor in the forward (clockwise) direction. Initially the magnets are aligned with each other due to the interaction of their magnetic fields. Applying the magnetic field exerts a torque on the two magnets, resulting in a rotation of $\frac{3}{4}\pi$ radians to align with the external magnetic field (Fig. 2 (a), $\theta = \frac{\pi}{4}$ rad). This is denoted as the "external torque" (τ_{ext}). The interaction of the magnetic fields from the two magnets apply a further "internal torque" (τ_{int}) as the magnets move to align with each other, resulting in an additional rotation of $\frac{1}{4}\pi$ radians (Fig. 2 (b), $\theta = \frac{\pi}{4}$ rad). Applying the magnetic field in reverse then results in the magnets rotating a further $\frac{3}{4}\pi$ radians in the same direction (Fig. 2 (c), $\theta = -\frac{\pi}{2}$ rad). The magnets align with each other, completing the last $\frac{\pi}{4}$ radians and achieving a full revolution (Fig. 2 (d), $\theta = -\frac{3\pi}{4}$ rad), and are ready for the cycle to restart. Repeating this alternating external magnetic field results in a continuous rotation of the output shaft.

Fig. 2 (e) shows the torques of the motor through the cycle. The internal torque is the torque of the magnets acting on each other, while the external torque is the torque from the external magnetic field acting on the magnets. The two of these sum to give the total output torque of the motor. It can be seen how the internal torque reverses as the magnets pass through parallel at $\frac{3\pi}{4}$ rad and $-\frac{\pi}{4}$ rad, and how the negative internal torque, from $\frac{\pi}{4}$ rad to $-\frac{\pi}{4}$ rad and from $-\frac{3\pi}{4}$ rad to $-\pi$ rad and π rad to $\frac{3\pi}{4}$ rad, reduces the total motor torque compared with the external torque.

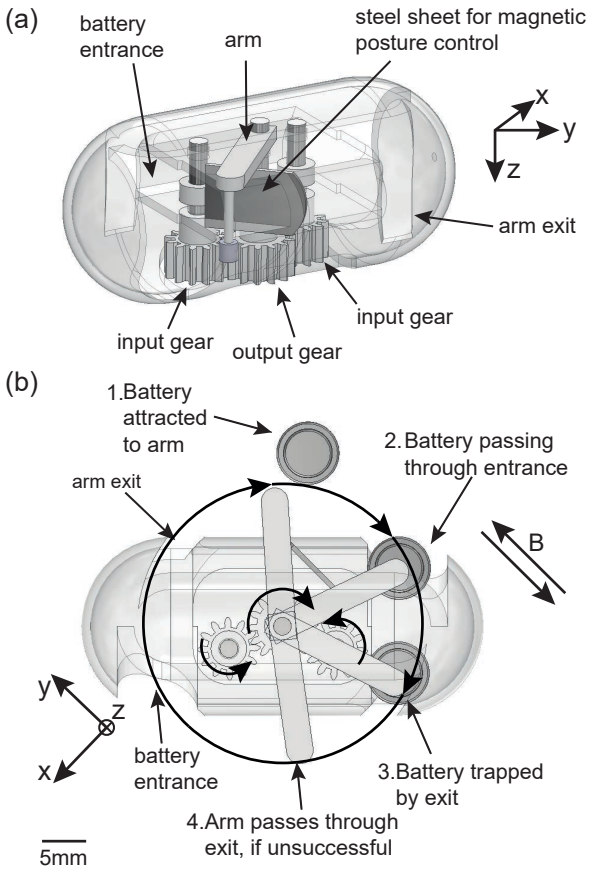

Fig. 3. Details of the parts of the capsule (a) CAD model. (b) Diagram showing the region swept by the arm, illustrating an LR261 battery passing through the entrance and being trapped by the narrow exit from the capsule.

Fig. 2 (f)-(i) show how the motor can be reversed by applying the alternating magnetic field from the side. θ is transposed to become θ' which is clockwise from the positive y axis to keep the angles consistent with the forwards rotation. The magnets are initially aligned with each other due to the internal torque (Fig. 2 (i)). The magnets align with the external magnetic field due to the external torque (Fig. 2 (h)). Internal torque makes the magnets align with each other (Fig. 2 (g)). The magnets align with the external magnetic field, ready to restart the cycle (Fig. 2 (f)).

B. Capsule Design

We present a two-step approach consisting of battery type identification and battery retrieval and encapsulation using the capsule. An array of Hall-effect sensors are used to determine the type and location of an ingested battery, and thus confirm if it is a size that the capsule is able to encapsulate. The capsule, powered by the novel magnetic motor, is then used to encapsulate the button battery for safe removal from the body. Fig. 3 shows the capsule for the retrieval of ingested button batteries from the stomach with Fig. 3 (a) an overview of the design and Fig. 3 (b) a top view showing the area swept by the arm. The capsule is 45 mm long and 20 mm in diameter, and the arm is 15 mm from the center-line of the capsule. The capsule has a motor in the base to keep the weight low and help the capsule naturally sit in an upright position. The output shaft of the motor is connected to an arm, initially within the capsule, with a 2 mm cylindrical magnet on the end. When the motor is actuated the arm rotates, sweeping a circular area. When the magnet is close to a button battery it attracts the battery, connecting it to the arm. The arm continues on its circular trajectory, pulling the button battery in through the capsule entrance. The button battery is captive in the capsule, as it is too large to fit out through the arm exit from the capsule, while the arm is able to pass through the exit if it is not connected to a battery.

The capsule also incorporates the magnetic posture control system for the capsule to rotate to the correct orientation. This is achieved by two low carbon steel sheets, each measuring $10 \times 5 \times 0.127$ mm. Being a ferromagnetic material, when in a magnetic field the sheet becomes temporarily magnetized, causing a torque to act on the steel sheet, thus making the entire capsule align with the magnetic field. This generates a torque that cancels the external torque, thereby achieving zero net torque applied to the capsule. This results in the unconstrained ("free-floating") capsule remaining stationary while the motor shaft is rotating. When the magnetic field reverses the magnetization of the steel also reverses. This ensures the capsule remains in the same orientation as the magnetic field alternates. Due to the symmetry of the capsule there are two possible orientations. The steel is positioned $\frac{\pi}{4}$ rad to the axis of the capsule to correctly orientate the motor relative to the magnetic field, while also maximizing the space within the capsule by allowing the motor to be along the center-line of the capsule. In Fig. 4 it can be seen that within 2 s of the alternating magnetic field being applied the capsule is correctly orientated relative to the magnetic field. This is shown in Supplementary Video 1. When the posture of the capsule is disturbed, it again returns to the correct orientation and remains there until the magnetic field is switched off. There is a small steady state error in the angle of the capsule, well within what is acceptable for the operation of the motor. This is caused by the torque of the motor being applied to the capsule, the steel sheet needs to be at an angle to the magnetic field to experience a torque to balance this.

C. Model

A mathematical model was made to describe the torque produced by the motor at a given angle and external magnetic field. The external torque (τ_{ext}) is the torque from the external magnetic field acting on the magnets in the motor, the internal torque (τ_{int}) is the torque from the two magnets acting on each other, and the motor torque (τ_{mot}) is the sum of the two to give the total output from the motor. The magnetic torque ($\vec{\tau}$) on a magnetic dipole in a magnetic field is given by:

$$\vec{\tau} = \vec{m} \times \vec{B} \tag{1}$$

where $\vec{m}$ is the magnetic moment, and $\vec{B}$ is the magnetic flux density. Eq. (1) is used to find the torque applied to the motor by the external magnetic field (τ_{ext}), given by:

$$\tau_{ext} = 2\|\vec{m}\|\left\|\vec{B}\right\|\cos\theta, \tag{2}$$

where θ is the angle of the magnet counter-clockwise from the positive x-axis as defined in Fig 2. The 2 term comes from the two magnets, with equal magnetic moments, being subject to the same magnetic field.

The motor also has an internal torque from the interaction between the two magnets. The magnetic flux density ($\vec{B}$) from a dipole using the Ampère model [38] is given by:

$$\vec{B}(\vec{m},\vec{p}) = \frac{\mu_0}{4\pi\|\vec{p}\|^3}\left(3(\vec{m}\cdot\hat{p})\hat{p} - \vec{m}\right) + \frac{2\mu_0}{3}\vec{m}\delta^3(\vec{p}), \tag{3}$$

where $\vec{m}$ is the magnetic moment ($0.0258\,\mathrm{Am}^2$ for the magnets used), μ_0 is the permeability of free space ($1.256 \times 10^{-6}\,\mathrm{NA}^{-2}$), p is the distance from the magnetic dipole, $\vec{p}$ is the position vector, and $\delta^3(\vec{p})$ is the three dimensional dirac delta function. The Ampère model assumes a perfect magnetic dipole, and can be used to approximate the field of a permanent magnet at distances sufficient that the size and shape of the magnet are not significant. This can be simplified to give the magnetic field parallel (B_z) and perpendicular (B_x) to the axis of the magnetic dipole:

$$B_x(\vec{p}) = \frac{\mu_0}{4\pi}\|\vec{m}\|\left(\frac{3\cos\beta\sin\beta}{\|\vec{p}\|^3}\right), \tag{4}$$

$$B_z(\vec{p}) = \frac{\mu_0}{4\pi}\|\vec{m}\|\left(\frac{3\cos^2\beta - 1}{\|\vec{p}\|^3}\right), \tag{5}$$

where β is the angle from the axis of magnetic dipole. Using Eq. (1) and the geometry of the system we can get the torque between the two magnets (τ_{int}) for a given angle of rotation:

$$\tau_{int} = \begin{cases} 2\dfrac{3\mu_0\|\vec{m}\|^2}{8\pi r^3}\cos\left(\theta - \dfrac{3\pi}{4}\right), & \sin\left(\theta + \dfrac{\pi}{4}\right) > 0 \\ 2\dfrac{3\mu_0\|\vec{m}\|^2}{8\pi r^3}\cos\left(\theta + \dfrac{\pi}{4}\right), & \sin\left(\theta + \dfrac{\pi}{4}\right) < 0, \end{cases} \tag{6}$$

where r is the distance between the centers of the magnets. When $\sin(\theta + \frac{\pi}{4}) = 0$, τ_{int} is undefined due to the discontinuity as the magnets are parallel to each other.

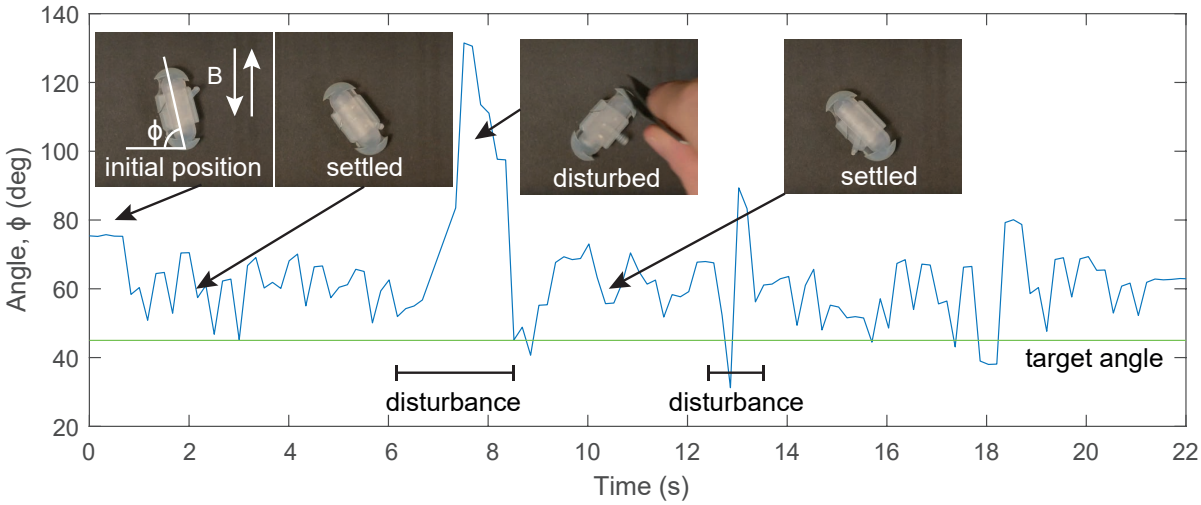

Fig. 4. Demonstration of the magnetic posture control, with a plot showing angle of the capsule to the horizontal, and disturbances at 7 s and 13 s and the capsule returning to the correct orientation. The capsule is initially at the wrong angle to the magnetic field to operate correctly. After 6 s the capsule experiences a disturbance, forcing it away from the correct angle. The capsule then returns to the correct orientation close to $\frac{\pi}{4}$ rad to the magnetic field, allowing the motor to operate well. The capsule then remains in the desired position as the motor continues to run. There is some steady state error in the angle of the capsule, this is small enough it doesn't impact the operation.

To get the total torque output from the motor (τ_{mot}) Eq. (2) is added to Eq. (6) giving:

$$\begin{aligned}\tau_{mot} &= \tau_{int} + \tau_{ext} \\ &= \begin{cases} 2\frac{3\mu_0\|\vec{m}\|^2}{8\pi r^3}\cos\left(\theta - \frac{3\pi}{4}\right) + 2\|\vec{m}\|\left\|\vec{B}\right\|\cos\theta, \\ \qquad\qquad \sin\left(\theta + \frac{\pi}{4}\right) > 0 \\ 2\frac{3\mu_0\|\vec{m}\|^2}{8\pi r^3}\cos\left(\theta + \frac{\pi}{4}\right) + 2\|\vec{m}\|\left\|\vec{B}\right\|\cos\theta, \\ \qquad\qquad \sin\left(\theta + \frac{\pi}{4}\right) < 0\,. \end{cases} \end{aligned} \tag{7}$$

The torque output from the motor is shown in Fig. 2 (e) alongside the corresponding positions of the gears. This shows the repeating pattern of the internal and external torques and the internal torque reversal at the point where the magnets are parallel ($\theta = \frac{3\pi}{4}$ rad and $\theta = -\frac{\pi}{4}$ rad).

This model can be used to optimize the design parameters of the motor for the intended application. The main parameter to change is the distance between the two magnets; this is a compromise between having close magnets to maximize internal torque, but not so close that the internal torque is too great for the external torque to overcome. Fig. 5 shows the effect of changing the magnet spacing. Fig. 5 (a) shows how the torque profile of the motor changes with the magnet spacing, for a magnetic field of 7 mT. It can be seen that, if the magnets are too close together, the torque can go negative, meaning the internal torque is opposing motion and is too great to be overcome by the external torque. Conversely, if the magnets are too far apart, the total torque becomes very low at angles were there is little external torque being applied. Fig. 5 (b) shows the effect of changing the magnet spacing on the minimum torque produced by the motor at any point in the cycle, for a range of applied magnetic fields. This shows how, by increasing the magnetic field, the magnets can be placed closer together to increase the output torque. Fig. 5 (c) shows the optimum magnet spacing to maximize output torque for an applied magnetic field. This is found by taking the magnet spacing at peak of each curve in Fig. 5 (b) and plotting this against the magnetic field strength.

To operate the motor effectively, it is essential that the motor is correctly orientated relative to the magnetic field. To achieve this, a system of magnetic posture control has been developed using a sheet steel in the capsule which acts as a soft magnet, aligning with the magnetic field. When in a magnetic field the steel is magnetized with the magnetic moment (m) proportional to the applied magnetic field (B). Using Eq. (1) the torque acting on a soft magnet (τ_{soft}) in a magnetic field can be given by:

$$\tau_{soft} = k\left\|\vec{B}\right\|^3 sin\alpha, \tag{8}$$

where k is an empirical constant specific to the shape and material used, and α is the angle between the major axis of the soft magnet and the magnetic field. For the sheet used in this study k was found to be 380×10^3 Nm T^{-3} by placing it on a torsional spring in a known magnetic field and comparing the deflection with that of a known magnet. Supplementary Material IV-A shows the details of the experimental setup.

Fig. 6 shows the output torque (τ_{mot}) against magnetic field strength. The output torque is considered to be the least torque produced at any point in the cycle, Supplementary Material IV-B shows the experimental setup. There is no torque below the field strength required to overcome the internal torque of the motor. It then increases with the field

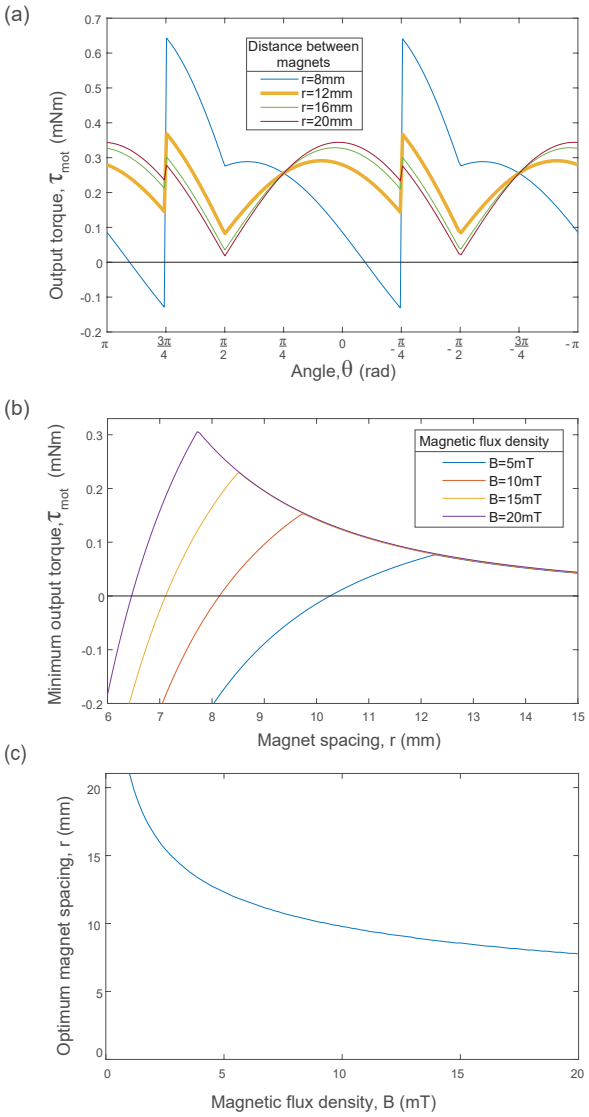

Fig. 5. The effect of magnet spacing on the torque output of a motor using 3 mm cubic magnets. (a) The effect of magnet spacing on the torque profile of the motor for a 7 mT magnetic field, the spacing of 12 mm used in this article is shown in yellow. (b) The output torque of the motor against the spacing between the magnets for a range of magnetic fields. This is the minimum output torque from any point in the cycle. (c) the optimum magnet spacing to maximize output torque for a given magnetic field flux density.

strength up until the point where the internal torque becomes the limiting factor. From then on, the output torque remains constant. The model is a good fit for the experimental data where the magnetic flux density is low. There is, however, some discrepancy between the model and the experimental data around the region where the motor transitions from being limited by the external torque (τ_{ext}) to the internal torque (τ_{int}) being the limiting factor.

The angular velocity of the motor (ω) is proportional to

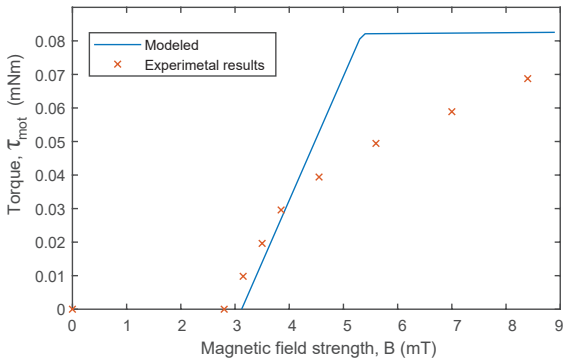

Fig. 6. Torque of the motor against magnetic field strength, experimental and modeled. There is no torque below the field strength required to overcome the internal torque. It then increases with field strength up until the point where internal torque is the limiting factor, then it remains constant with increasing field strength

the actuation frequency (f_a), up to the step-out frequency (f_{so}):

$$\omega = 2\pi f_a. \tag{9}$$

When the actuation frequency exceeds the step-out frequency the motor speed decreases as the actuation frequency, further increases. This has been shown for both swimming [39] and rolling robots [40] and is given by:

$$\omega = 2\pi(f_a - \sqrt{f_a^2 - f_{so}^2}). \tag{10}$$

Fig. 7 shows the angular velocity increasing proportionally to the actuation frequency, the model shows a good fit to the data. It can be seen that there is no stepping out within the frequency range of the coil system used.

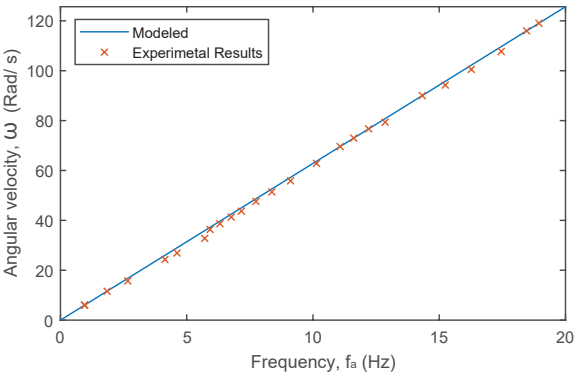

Fig. 7. Angular velocity of the motor against actuation frequency, experimental and modeled. The figure shows the speed increasing proportionally to the actuation frequency. The motor does not step out within the frequency range of the coil system.

D. Fabrication

The main components of the capsule were manufactured with Form3 SLA printer using durable resin (Formlabs), durable resin was chosen as it exhibits similar material

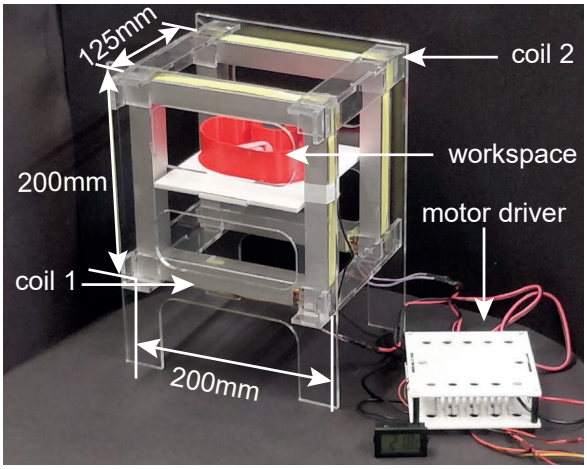

Fig. 8. The coil system used for capsule demonstrations, with stomach model shown on the workspace. Coils 1 and 2 are identical and parallel allowing a near uniform magnetic field to be produced across the entire workspace.

properties to other resins produced by Formlabs which are certified for medical use, but is more transparent, making the capsule mechanism easier to see. The magnets used were 3 mm cubic neodymium iron boron (NdFeB) (Supermagnete). For the steel sheet to control the capsule orientation, two low carbon steel sheets (RS, full hard, cold rolled) were used. The ferromagnetic steel has no permanent magnetism, however, it becomes magnetized when placed within a magnetic field. The capsule developed weighs just 5.13 g and measures 45 mm in length and 20 mm in diameter, and the motor on its own weighs 3.7 g, measuring 20 mm by 20 mm by 20 mm.

E. Capsule actuation by the electromagnetic coil system.

For the capsule demonstration, a horizontal magnetic field is required, to extend the workspace, a pair of coils were used (Fig. 8). Magnetic fields of up to 14 mT were applied horizontally from two square coils of 200 mm side length and 125 mm apart with a horizontal workspace along the center axis of the coils. The coil system is designed to fit an infant with the stomach within the workspace. The magnetic fields used are well below the static magnetic field strength of 0.046 - 8 T of MRI machines [41], this shows that these magnetic field can safely be used in a medical setting. All coils were controlled using Sabertooth 2x32 motor drivers (Dimension Engineering).

F. Battery type detection

The localization and detection of the type of button battery are based on the trilateration method, a common method for localization [37]. An array of Hall-effect sensors and a magnetic coil are placed below the workspace where a button battery is placed. For button battery detection tests, we additionally used, a single 200 mm diameter electromagnetic coil embedded 40 mm below the workspace, capable of

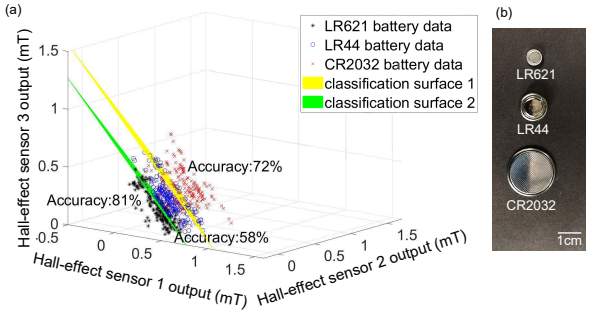

Fig. 9. (a) The dataset for SVM classification algorithm and the classification surfaces. (b) The batteries used for the tests.

magnetic fields of up to 9 mT, as used in [37]. The magnetic coil produces vertical magnetic field to magnetize the button battery. The hall-effect sensors read the magnetic flux density of the magnetized button battery and then classify the type of the button battery using the sensor readings. The Hall-effect sensors used in this setup are A1389 analog linear Hall-effect sensors (Allegro Inc.). These sensors are arranged in an array on a printed circuit board (PCB) which is positioned on a 2D plane. The total sensing area provided by the PCB is 32.15 cm^2, allowing for accurate detection and measurement of magnetic fields in the surrounding environment. Three neighboring sensors are arranged in an equilateral triangle with a side length of 15 mm. The magnetic field strengths read by the three sensors are converted to distances to run the classification algorithm for determining the button battery type.

Among the commonly used button batteries, three representative sizes of batteries, LR621 ($\varnothing 7 \times 2.2$ mm), LR44 ($\varnothing 11.4 \times 5$ mm), and CR2032 ($\varnothing 19 \times 3$ mm) (Fig. 9 (b)) were selected. When a button battery is placed in the working area above the Hall-effect sensor array, the magnetic coil produces vertical magnetic fields to magnetize the button battery, and then the magnetic flux density of the magnetized button battery is read by the three nearest Hall-effect sensors. The nearest Hall-effect sensors receive higher magnetic flux densities than the rest of the sensors, therefore by finding the largest three sensor readings, the nearest three sensors can be determined. By using the data reading from the nearest three sensors, the location of the button battery can be calculated [37], and the button battery type can be detected. 90 sets of the data from the nearest three sensors were taken by placing three different types of batteries above the sensor array and reading the sensor data. The obtained dataset is the training set for the support vector machine (SVM) classification algorithm which is used to classify the button battery type. The dataset and the two classification surfaces are shown in Fig. 9 (a). It can be seen that the accuracy of classification using the classification surfaces is 81% for LR621, 58% for LR44, and 72% for CR2032.

III. Results

A. Battery detection

For battery classification, three different types of batteries, LR621, LR44, and CR2032 were placed in turn on the workspace and ran the SVM classification algorithm to detect the button battery type. In our setup, there is a 6 mm gap between the workspace and the Hall-effect sensor array. It is possible to increase this distance by generating stronger magnetic fields to magnetize the button battery. However, the strength of the magnetic field that can be produced is limited by the magnetic coil available in our system. In order to improve the accuracy of the classification, the classification algorithm was run five times for each button battery sample. The button battery type which is the most frequent was chosen as the final detection result. The detection results are shown in Fig. 10. The figure depicts the proportion of tests in which the battery was accurately recognized, and in cases where the button battery type was misidentified, the type that was identified instead. The LR621 was correctly identified 93% of the time and it can only be misidentified as LR44; the LR44 was correctly identified 72% with one third of the incorrect identifications being CR2032 and the remainder being LR621; and the CR2032 was correctly identified 89% of the time with 90% of misidentifications being as LR44. This indicates that the average accuracy rate of the proposed classification method is 85% across all battery types. In cases where mistakes occur, the batteries are identified incorrectly as one of similar dimensions.

B. Capsule- encapsulation test

The proposed capsule was tested using an LR621 battery, (Fig. 11) in a model of a child's stomach (PLA). The capsule starts near the battery (Fig. 11 (a)). When the alternating magnetic field is applied the arm begins to rotate (Fig. 11 (b)) while the orientation of the capsule remains stable. It can be seen that when the arm swings over the button battery (Fig. 11 (c)) the button battery is attracted to the magnet and is picked up by the arm. The arm then continues on its path into the body of the capsule, through the battery

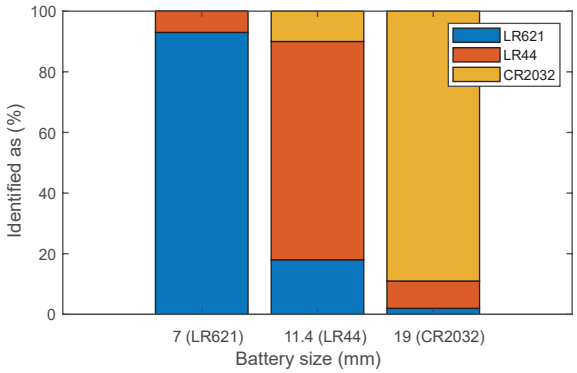

Fig. 10. The accuracy of identifying the button battery type among five trials.

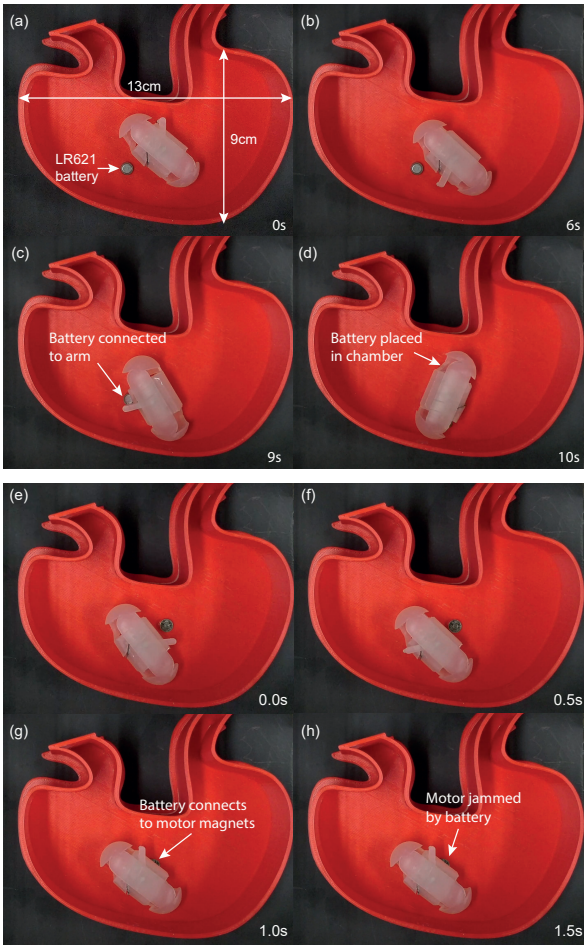

Fig. 11. A demonstration of the capsule encapsulating a button battery in a child-sized stomach model. (a) In position ready to capture the battery. (b) Arm rotating to sweep over the battery. (c) Battery connecting to the magnet on the end of the arm. (d) Placing the battery in the storage area ready for transport out of the body. The failure of the capsule to encapsulate the battery: (e) The capsule in position ready to encapsulate the battery. (f) The capsule arm rotating to pick up the battery, the battery moving towards the motor magnets. (g) The capsule with the battery connected to the motor magnets. (h) The motor jammed by the battery, preventing further motion of the arm.

entrance, with the button battery (Fig. 11 (d)), preventing it from coming into contact with the tissue. The button battery is then trapped by the narrower arm exit, preventing the arm from continuing out of the capsule. In the figure the battery is horizontal, this is the position where the battery sits naturally. If the battery were to be balanced on its edge, the battery would be closer to the magnet as the arm passes over to it, making it easier for the capsule to pick up.

Fig. 11 (e)-(h) show a failed attempt at retrieving the button battery, Fig. 11 (e) the capsule is in position ready to encapsulate the battery, Fig. 11 (f) the capsule arm rotates to pick up the battery, Fig. 11 (g) the battery is attracted to the motor magnets, Fig. 11 (h) the motor is jammed by the

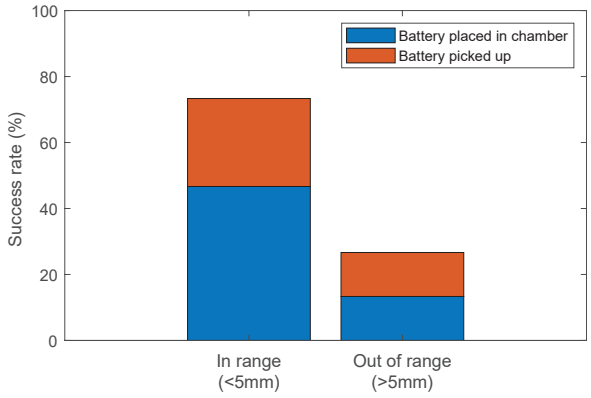

Fig. 12. A summary of the success rate of the capsule at picking up an LR621 button battery.

battery connected to the motor magnets, preventing further operation of the motor and the battery from being correctly encapsulated.

The success rate of the capsule at encasing the button battery is summarized in Fig. 12. Of the trials (15 trials) where the button battery was within 5 mm of the capsule 47% of times the button battery was successfully placed within the capsule and 73% of times it was successfully picked up by the arm. Of the times the battery was outside of the workspace (more than 5 mm from the capsule) (15 trials) the battery was successfully placed within the chamber 13% of times and 27% of times it was picked up by the arm. This shows how the capsule can be highly successful when it is close to the battery, however, the success rate reduces significantly once the battery is outside of the area swept by the arm.

IV. Discussion & Conclusion

In this study, a magnet motor rotated by an external alternating magnetic field was developed, and its effectiveness was demonstrated by the ability of an ingestable capsule to extend its arm and retrieve a button battery. The capsule developed weighs only 5.13 g, as it contains no electronic components. It can turn the motor inside it without being turned by the external magnetic field, due to the motor's characteristic of zero net torque. The motor can also rotate in the opposite direction by applying the magnetic field from a perpendicular direction. As this approach does not rely on transmission gears to minimize the net torque applied, it can be achieved without reducing the speed of the motor, and a transmission gear can be implemented if further torque increase is desired.

The current capsule design needs reducing in size by 50% to fit inside a #000 capsule. #000 is the largest capsule approved by the Food and Drug Administration (FDA) for human consumption, so this is necessary for the capsule to enter clinical trials. The challenge associated with this is that the torque of the motor (τ_{mot}) decrease as the scale of the motor is reduced, necessitating the friction in the mechanism to also be reduced to allow the arm to still rotate freely; the space withing hte capsule available to store batteries would also be reduced.

The posture control system is capable of holding the capsule at an acceptable angle to the magnetic field while the motor is operated, however, there is some steady state error caused by the torque applied to the motor. If desired this could be reduced by increasing the size of the steel sheet, or eliminated by adjusting the angle of the steel sheet to the axis of the capsule.

Larger sizes of battery cannot currently be encapsulated by the capsule, due to the limited space within the capsule. It can, however, connect to the battery with the magnet arm. This problem is likely to be limited, as if a child is unable to swallow a large capsule, they would be unable to swallow the larger sizes of battery. The battery detection and identification makes it possible to determine whether the capsule is appropriate to use for a given patient, or if endoscopic removal is required.

The capsule needs to be near to the battery to retrieve it. This problem could be overcome by using external magnetic fields to navigate the capsule by making it "walk" with a stick-slip motion [42] or roll [16], [27] to a position where the battery can be reached by the arm. This can be achieved by adding additional coils to the control system, to allow magnetic fields to be produced in any direction. Future work includes the development of mechanisms to navigate the capsule to a target location and further miniaturization of the capsule.

Acknowledgment

The authors thank Marco Pontin, Quentin MP Lahondes, Xiao Chen, Xuanni Luo, Joanna Jones and Junyi Han for valuable comments and assistance with the project.

References

[1] H. Park, S. Park, E. Yoon, B. Kim, J. Park, and S. Park, "Paddling based microrobot for capsule endoscopes," in *Proceedings 2007 IEEE International Conference on Robotics and Automation*. IEEE, 2007, pp. 3377–3382.

[2] Y. Kim, J. E. Park, J. J. Wie, S. G. Yang, D. H. Lee, and Y.-J. Jin, "Effects of helix geometry on magnetic guiding of helical polymer composites on a gastric cancer model: A feasibility study," *Materials*, vol. 13, no. 4, p. 1014, 2020.

[3] A. Hajiaghajani, D. Kim, A. Abdolali, and S. Ahn, "Patterned magnetic fields for remote steering and wireless powering to a swimming microrobot," *IEEE/ASME Transactions on Mechatronics*, vol. 25, no. 1, pp. 207–216, 2019.

[4] C. Hong, Z. Ren, C. Wang, M. Li, Y. Wu, D. Tang, W. Hu, and M. Sitti, "Magnetically actuated gearbox for the wireless control of millimeter-scale robots," *Science Robotics*, vol. 7, no. 69, p. eabo4401, 2022.

[5] K. Ishiyama, M. Sendoh, A. Yamazaki, and K. Arai, "Swimming micro-machine driven by magnetic torque," *Sensors and Actuators A: Physical*, vol. 91, no. 1-2, pp. 141–144, 2001.

[6] J. J. Abbott, Z. Nagy, F. Beyeler, and B. J. Nelson, "Robotics in the small, part i: microbotics," *IEEE Robotics & Automation Magazine*, vol. 14, no. 2, pp. 92–103, 2007.

[7] M. Nokata, S. Kitamura, T. Nakagi, T. Inubushi, and S. Morikawa, "Capsule type medical robot with magnetic drive in abdominal cavity," in *2008 2nd IEEE RAS & EMBS International Conference on Biomedical Robotics and Biomechatronics*. IEEE, 2008, pp. 348–353.

[8] L. Zhang, J. J. Abbott, L. Dong, B. E. Kratochvil, D. Bell, and B. J. Nelson, "Artificial bacterial flagella: Fabrication and magnetic control," *Applied Physics Letters*, vol. 94, no. 6, p. 064107, 2009.

[9] B. J. Nelson, I. K. Kaliakatsos, and J. J. Abbott, "Microrobots for minimally invasive medicine," *Annual review of biomedical engineering*, vol. 12, pp. 55–85, 2010.

[10] M. Sitti, H. Ceylan, W. Hu, J. Giltinan, M. Turan, S. Yim, and E. Diller, "Biomedical applications of untethered mobile milli/microrobots," *Proceedings of the IEEE*, vol. 103, no. 2, pp. 205–224, 2015.

[11] S. Martel, "Beyond imaging: Macro-and microscale medical robots actuated by clinical mri scanners," *Science Robotics*, vol. 2, no. 3, p. eaam8119, 2017.

[12] G.-S. Lien, C.-W. Liu, J.-A. Jiang, C.-L. Chuang, and M.-T. Teng, "Magnetic control system targeted for capsule endoscopic operations in the stomach—design, fabrication, and in vitro and ex vivo evaluations," *IEEE Transactions on Biomedical Engineering*, vol. 59, no. 7, pp. 2068–2079, 2012.

[13] P. Valdastri, E. Sinibaldi, S. Caccavaro, G. Tortora, A. Menciassi, and P. Dario, "A novel magnetic actuation system for miniature swimming robots," *IEEE Transactions on Robotics*, vol. 27, no. 4, pp. 769–779, 2011.

[14] Y. Yan, B. Guo, J. Tian, J. Zhang, B. Zhang, E. Ley, Y. Liu, and S. Prasad, "Evaluating the resistant force of an endoscopic capsule self-propelling in the small intestine," *Archive of Applied Mechanics*, vol. 92, no. 12, pp. 3861–3875, 2022.

[15] J. Tian, K. O. Afebu, Z. Wang, Y. Liu, and S. Prasad, "Dynamic analysis of a soft capsule robot self-propelling in the small intestine via finite element method," *Nonlinear Dynamics*, pp. 1–22, 2023.

[16] D. Ye, J. Xue, S. Yuan, F. Zhang, S. Song, J. Wang, and M. Q.-H. Meng, "Design and control of a magnetically-actuated capsule robot with biopsy function," *IEEE Transactions on Biomedical Engineering*, vol. 69, no. 9, pp. 2905–2915, 2022.

[17] Z. Song, Z. Fu, D. Romano, P. Dario, and J. S. Dai, "A novel biomimetic compliant structural skin based on composite materials for biorobotics applications," *Soft Robotics*, vol. 9, no. 3, pp. 440–450, 2022.

[18] S. Yim, K. Goyal, and M. Sitti, "Magnetically actuated soft capsule with the multimodal drug release function," *IEEE/ASME Transactions on Mechatronics*, vol. 18, no. 4, pp. 1413–1418, 2013.

[19] J. Wu, B. Jang, Y. Harduf, Z. Chapnik, Ö. B. Avci, X. Chen, J. Puigmartí-Luis, O. Ergeneman, B. J. Nelson, Y. Or *et al.*, "Helical klinotactic locomotion of two-link nanoswimmers with dual-function drug-loaded soft polysaccharide hinges," *Advanced Science*, vol. 8, no. 8, p. 2004458, 2021.

[20] J. Rahmer, C. Stehning, and B. Gleich, "Spatially selective remote magnetic actuation of identical helical micromachines," *Science Robotics*, vol. 2, no. 3, p. eaal2845, 2017.

[21] H.-W. Huang, M. W. Tibbitt, T.-Y. Huang, and B. J. Nelson, "Matryoshka-inspired micro-origami capsules to enhance loading, encapsulation, and transport of drugs," *Soft robotics*, vol. 6, no. 1, pp. 150–159, 2019.

[22] Z. F. Bao and E. Diller, "Evaluating miniature robot surgical scissors," in *2022 International Conference on Manipulation, Automation and Robotics at Small Scales (MARSS)*. IEEE, 2022, pp. 1–6.

[23] M. Sun, C. Tian, L. Mao, X. Meng, X. Shen, B. Hao, X. Wang, H. Xie, and L. Zhang, "Reconfigurable magnetic slime robot: deformation, adaptability, and multifunction," *Advanced Functional Materials*, vol. 32, no. 26, p. 2112508, 2022.

[24] A. T. Becker, O. Felfoul, and P. E. Dupont, "Toward tissue penetration by mri-powered millirobots using a self-assembled gauss gun," in *2015 IEEE International Conference on Robotics and Automation (ICRA)*. IEEE, 2015, pp. 1184–1189.

[25] M. P. Kummer, J. J. Abbott, B. E. Kratochvil, R. Borer, A. Sengul, and B. J. Nelson, "Octomag: An electromagnetic system for 5-dof wireless micromanipulation," *IEEE Transactions on Robotics*, vol. 26, no. 6, pp. 1006–1017, 2010.

[26] E. Diller, J. Giltinan, G. Z. Lum, Z. Ye, and M. Sitti, "Six-degree-of-freedom magnetic actuation for wireless microrobotics," *The International Journal of Robotics Research*, vol. 35, no. 1-3, pp. 114–128, 2016.

[27] S. Yim and M. Sitti, "Design and rolling locomotion of a magnetically actuated soft capsule endoscope," *IEEE Transactions on Robotics*, vol. 28, no. 1, pp. 183–194, 2011.

[28] A. du Plessis d'Argentré, S. Perry, Y. Iwata, H. Iwasaki, E. Iwase, A. Fabozzo, I. Will, D. Rus, D. D. Damian, and S. Miyashita, "Programmable medicine: autonomous, ingestible, deployable hydrogel patch and plug for stomach ulcer therapy," in *2018 IEEE International Conference on Robotics and Automation (ICRA)*. IEEE, 2018, pp. 1511–1518.

[29] C. Duffield and S. Miyashita, "Magnetic force driven wireless motor," in *Annual Conference Towards Autonomous Robotic Systems*. Springer, 2020, pp. 409–412.

[30] C. Duffield, A. F. Smith, D. Rus, D. Damian, and S. Miyashita, "Wirelessly magnetically actuated motor for tissue regeneration robotic implant(accepted)," in *IEEE International Conference on Intelligent Robots and Systems (IROS)*. IEEE, 2022, pp. 465–471.

[31] D. Yardeni, H. Yardeni, A. Coran, and E. S. Golladay, "Severe esophageal damage due to button battery ingestion: can it be prevented?" *Pediatric surgery international*, vol. 20, no. 7, pp. 496–501, 2004.

[32] Swallowed a button battery? national capital poison center. [Online]. Available: https://www.poison.org/battery

[33] J. H. Lee, J. H. Lee, J. O. Shim, J. H. Lee, B.-L. Eun, and K. H. Yoo, "Foreign body ingestion in children: should button batteries in the stomach be urgently removed?" *Pediatric gastroenterology, hepatology & nutrition*, vol. 19, no. 1, pp. 20–28, 2016.

[34] B. Laulicht, G. Traverso, V. Deshpande, R. Langer, and J. M. Karp, "Simple battery armor to protect against gastrointestinal injury from accidental ingestion," *Proceedings of the National Academy of Sciences*, vol. 111, no. 46, pp. 16 490–16 495, 2014.

[35] S. Miyashita, S. Guitron, K. Yoshida, S. Li, D. D. Damian, and D. Rus, "Ingestible, controllable, and degradable origami robot for patching stomach wounds," in *2016 IEEE international conference on robotics and automation (ICRA)*. IEEE, 2016, pp. 909–916.

[36] H. Iwasaki, F. Lefevre, D. D. Damian, E. Iwase, and S. Miyashita, "Autonomous and reversible adhesion using elastomeric suction cups for in-vivo medical treatments," *IEEE Robotics and Automation Letters*, vol. 5, no. 2, pp. 2015–2022, 2020.

[37] J. Liu, H. Sugiyama, T. Nakayama, and S. Miyashita, "Magnetic sensor based topographic localization for automatic dislocation of ingested button battery," in *2020 IEEE International Conference on Robotics and Automation (ICRA)*, 2020, pp. 5488–5494.

[38] K. Seleznyova, M. Strugatsky, and J. Kliava, "Modelling the magnetic dipole," *European Journal of Physics*, vol. 37, no. 2, p. 025203, 2016.

[39] K. I. Morozov and A. M. Leshansky, "The chiral magnetic nanomotors," *Nanoscale*, vol. 6, no. 3, pp. 1580–1588, 2014.

[40] T. A. Howell, B. Osting, and J. J. Abbott, "Sorting rotating micromachines by variations in their magnetic properties," *Physical Review Applied*, vol. 9, no. 5, p. 054021, 2018.

[41] F. G. Shellock, "Magnetic resonance safety update 2002: implants and devices," *Journal of Magnetic Resonance Imaging: An Official Journal of the International Society for Magnetic Resonance in Medicine*, vol. 16, no. 5, pp. 485–496, 2002.

[42] S. Miyashita, S. Guitron, S. Li, and D. Rus, "Robotic metamorphosis by origami exoskeletons," *Science Robotics*, vol. 2, no. 10, p. eaao4369, 2017.

Supplementary Material

A. Magnetic moment of a soft magnet

To find the constant of magnetism, k, in Eq.(8) torque acting on a representative sample of steel sheet of the same dimensions as that used in the capsule was experimentally measured.

The torque acting on the material for a given magnetic field and angle were found by measuring the angular deflection of an elastomeric (Ecoflex 00-10, Smooth-on) torsional spring. The properties of the spring were found by applying a known torque using a known magnet in a known magnetic field. The experimental setup is shown in Fig.13.

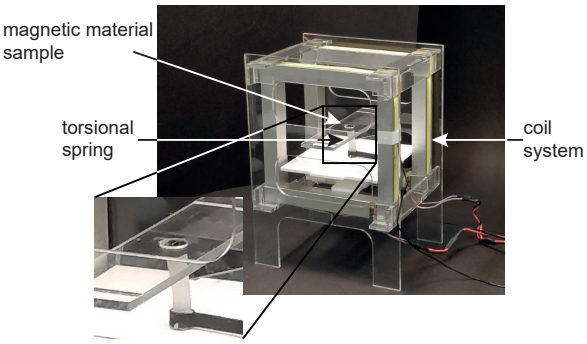

Fig. 13. Figure of the experimental setup used to measure the torque acting on a piece of magnetic material, showing details of the elastomeric torsional spring used to measure torque.

B. Torque measurements

The output torque of the motor was measured by winding a mono-filament thread around the output shaft, passing it over a pulley, and down to a known mass (Fig. 14). This applies a known torque as a load to the motor. The mass was increased until the motor was unable to turn to get the stall torque for an applied magnetic field. The internal torque was measured using the same set up, but without applying an external magnetic field and measuring the angle of the magnets.

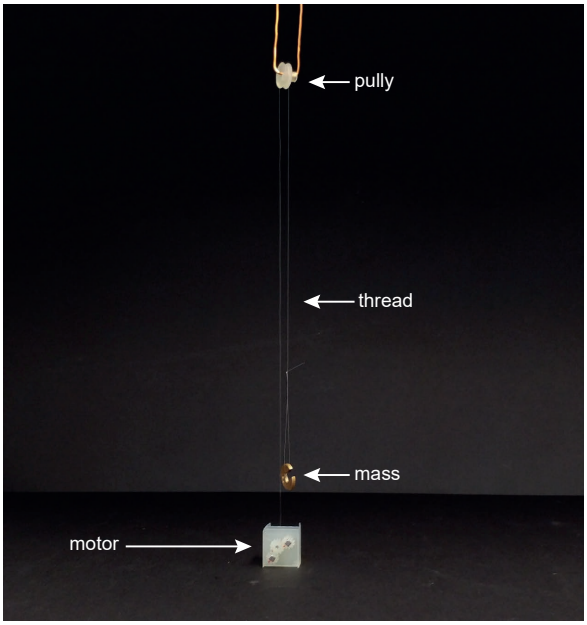

Fig. 14. Figure of the setup for measuring the torque of the motor showing the known mass used to apply a load via a mono-filament thread. The coil is below the work-surface